

SKB

**TECHNICAL
REPORT**

87-31

**Rheological properties of a calcium
smectite**

Lennart Börgesson, Roland Pusch

Swedish Geological Co, Lund

December 1987

RHEOLOGICAL PROPERTIES OF A CALCIUM SMECTITE

Lennart Börgesson, Roland Pusch

Swedish Geological Co, Lund

1987-12-31

This report concerns a study which was conducted for SKB. The conclusions and viewpoints presented in the report are those of the author(s) and do not necessarily coincide with those of the client.

Information on KBS technical reports from 1977-1978 (TR 121), 1979 (TR 79-28), 1980 (TR 80-26), 1981 (TR 81-17), 1982 (TR 82-28), 1983 (TR 83-77), 1984 (TR 85-01), 1985 (TR 85-20) and 1986 (TR 86-31) is available through SKB.

SWEDISH GEOLOGICAL
Div Engineering Geology
Lennart Börgesson/JS

ID-no: IRAP87 513
Date: 1987- 12- 31

RHEOLOGICAL PROPERTIES OF A CALCIUM SMECTITE

Lennart Börgesson
Roland Pusch
Swedish Geological Co
Lund, Sweden

Keywords: Clay, smectite, Ca-smectite, rheology, triaxial tests, shear tests,
creep tests, swelling, permeability

CONTENTS

SUMMARY	I
PREFACE	II
SYMBOLS	1
1 INTRODUCTION	2
1.1 General	2
1.2 Scenarios and properties of interest	2
1.3 Investigated properties	5
2 GENERAL DESCRIPTION OF THE CLAY	6
3 TESTS AND TEST RESULTS	8
3.1 General	8
3.2 Hydraulic conductivity. Saturated flow	8
3.3 Water uptake properties. Non-saturated flow	10
3.4 Swelling ability	11
3.5 Swelling pressure	15
3.6 Stress-strain-strength relations measured by triaxial tests	17
3.6.1 General	17
3.6.2 Testing procedures	18
3.6.3 Saturation process	19
3.6.4 Equilibrium process	19
3.6.5 Heating process	19
3.6.6 Testing process	20
3.6.7 Results	22
3.6.8 Pore pressure change	28
3.6.9 Influence of strain rate	31
3.7 Shear tests	32
3.7.1 Testing procedures	32
3.7.2 Results	32
3.7.3 Test on a natural clay	36
3.7.4 Strain rate dependence	36

3.8	Creep tests using the direct shear apparatus (shear box)	39
3.8.1	General	39
3.8.2	Performed tests	41
3.8.3	Creep results	42
3.8.4	Long time creep tests	54
4	CONCLUSIONS AND REMARKS	59
4.1	General	59
4.2	Permeability	59
4.3	Non-saturated flow	59
4.4	Swelling potential	59
4.5	Swelling pressure	59
4.6	Stress-strain properties	60
4.7	Strength properties	60
4.8	Influence of strain-rate on the strength	61
4.9	Creep tests	61
5	REFERENCES	63

APPENDIX A Triaxial tests

APPENDIX B Simple shear tests

APPENDIX C Creep tests

SUMMARY

The rheological and mechanical properties of a Ca-smectite have been investigated by different laboratory tests. By these tests the permeability, the water uptake properties, the swelling properties, the swelling pressure, the stress-strain properties, the strength and the creep properties have been determined. The influence of density, temperature, time and stress level have been considered.

Mathematical models of the measured properties and behavior of the clay have been suggested so that calculations involving mechanical and rheological scenarios can be made.

The behavior of the clay have been discussed with reference to the microstructure and comparisons between the investigated Ca-smectite and a Na-smectite (Mx-80) have been made.

One main conclusion is that the difference between the properties and behavior of Ca-smectite and Na-smectite is small at densities $\rho_m > 2.0 \text{ t/m}^3$. At densities $\rho_m < 2.0 \text{ t/m}^3$ the difference is increasing with decreasing density.

PREFACE

This investigation is a part of the nuclear waste research cooperation between Sweden and France and has been financed by SKB. It has been carried through thanks to the involvement of several persons whose contributions are gratefully acknowledged.

Most laboratory work, including the computer plotted diagrams, was made by Harald Hökmark and Ola Karnland at the geotechnical laboratory in Lund. The manuscript was given its computer-aided printable form by Jeanette Stenelo. All man-made figures were drawn by Birgitta Hellström.

The support from Anders Bergström, SKB with whom we have had many fruitful discussions is also highly appreciated.

SYMBOLS

A	pore pressure parameter
A_c	activity
c	cohesion
C_s	swelling capacity
D	deviator stress
D_w	coefficient of water diffusion
i	hydraulic gradient
I_p	plasticity index
k	hydraulic conductivity
l_c	clay content
S_r	degree of saturation
T	absolute temperature
t	time
u	pore pressure
V	volume
w	water ratio
w_L	liquid limit
w_p	plasticity limit
ε	strain
$\dot{\varepsilon}$	rate of strain
ϕ	angle of friction
γ	shear strain
$\dot{\gamma}$	rate of shear strain
σ_o	reference pressure
$\sigma_1; \sigma_3$	principal stresses
σ_N	normal stress
σ_s	swelling pressure
τ	shear stress
ρ_o	reference density
ρ_m	density at saturation

1 INTRODUCTION

1.1 General

The rheological and physical properties of the clay-based buffer material surrounding the canisters at the disposal of high level radioactive wastes, are of vital importance for the functioning of the barrier. Such properties of interest are the hydraulic conductivity, the water uptake ability, the swelling ability, the swelling pressure, the stress-strain-strength properties and the creep properties. Of interest are also the influence of secondary effects such as the rate of strain during shear, the temperature, the density of the clay, and the external pressure.

The knowledge of those properties and the understanding of different behaviors are necessary to be able to make proper optimizations of the geometry and the initial density and composition of the buffer material. A major conclusion is that the density should be as high as possible in order to retard water flow and ion diffusion to and from the canister and to minimize the settlement of the canister, while the density should be as low as possible in order to offer a soft protection and cause as little damage as possible in the case of rock movements along joints intersecting deposition holes.

1.2 Scenarios and properties of interest

Investigations of the rheological and physical properties by necessity include determination of a number of parameters which can be used for the definition and calculations, thus predicting and describing the consequences of different scenarios. Important scenarios and necessary parameters are the following:

- a) Ability of the clay to absorb water. This property is most easily expressed by the liquid limit (w_L), which is the water content at which the clay turns from plastic to liquid. It is easily determined by using either the cone apparatus or the technique by Casagrande.
- b) Bearing capacity of the clay. Calculation of the load-induced failure of the clay. This calculation requires the knowledge of the swelling pressure (σ_s) of the clay and the relation between the external pressure and the shear

strength (e.g. expressed by the parameters: cohesion (c) and angle of friction (ϕ)).

- c) Settlement of the canister. Calculation of the consolidation and creep settlements caused by the own weight of the canister. These calculations require knowledge of the swelling pressure, the drained and undrained stress strain relations and the stress-strain-time relation (the creep behavior at different applied stress).

These properties can be expressed by different parameters depending upon what theory is used. The creep behavior requires several parameters to be accurately modelled. A general expression is

$$\frac{d\varepsilon}{dt} = AT^a D^b (t+t_0)^n \quad (1)$$

where ε = strain

A = constant

D = deviator type of stress

T = absolute temperature

a, b, n = exponents

t_0 = structure-related constant

t = time after onset of creep

The influence of the deviator stress D in Eqn (1) can also be expressed as e^{bD} according to Singh & Mitchel, as to fit the behavior of illitic clays.

- d) The ability to fill up voids by swelling. This is a vital function, particularly in the initial phase of water saturation or after rock movement. The temperature-induced volume change in the cooling phase is another example when swelling is required. The swelling properties can be expressed through the swelling capacity C_s defined as:

$$C_s = \frac{V_s - V_i}{V_i} \quad (2)$$

V_i is the initial volume and V_s is the volume after swelling when the material is exposed to a specified external pressure (1 kPa).

- e) The rate of saturation after installation. Investigations of various clay materials have shown that the rate of water uptake can be described by applying the general differential equation:

$$\frac{\delta w}{\delta t} = D_w \left(\frac{\delta^2 w}{\delta x^2} + \frac{\delta^2 w}{\delta y^2} + \frac{\delta^2 w}{\delta z^2} \right) \quad (3)$$

where w = water ratio

D_w = coefficient of water diffusion

t = time

The coefficient of water diffusion D_w can be determined by laboratory tests.

- f) The rock-shear case where parts of the rock wall in the deposition hole are displaced thereby shearing the clay barrier and the canister. This scenario can be simulated by three-dimensional non-linear finite element calculations. The stress strain relations under undrained shear for the clay and the canister-material are input data to those calculations.

Since the shear can take place at different rates of strain (rock-creep scenario or earth quake scenario) it is also necessary to know the viscous behavior of the clay (the rate-dependence of the stress-strain relation).

- g) A hydraulic gradient across the deposition hole, which can be simulated using the hydraulic conductivity of the clay as input parameter.
- h) Ion-diffusion from the canister through the clay barrier which is described by the coefficient of diffusion which has to be determined in the laboratory for different ions. The processes related to ion-diffusion are not treated in this investigation.
- i) Temperature increase of canister and clay after deposition. This process is described by the same differential equation as the water-uptake and diffusion processes. The necessary parameters are the thermal conduc-

tivity and the specific heat. Those parameters are not determined in this investigation.

A complete investigation of any presumptive clay barrier should include the above mentioned scenarios and properties, the variation of which should be considered with respect to the following variables:

- * The density of the clay.
- * The temperature of the clay.
- * The salinity of the pore-water.

These properties and variables are the primary ones to be included in a general investigation of the suitability of a clay buffer. They can also be the basis of preliminary optimizations.

1.3 Investigated properties

This project includes investigations on a Ca-smectite of a major part of the properties mentioned in chapter 1.2. Scenarios a-g with the density and the temperature as variables are in most cases considered. The influence of the pore-water salinity is only tested with respect to the liquid limit.

The project is a part of the nuclear waste research cooperation between Sweden and France. The investigated clay is the French main clay barrier candidate A4.

2 GENERAL DESCRIPTION OF THE CLAY

The investigated clay is smectite-rich with calcium as the exchangeable ion. According to French investigations the clay consists of 70 % clay minerals, almost 100% of which are smectitic. Accessory minerals are quartz, goethite and feldspar.

The natural water content in air-dry condition vary between 5% and 10%. The liquid limit is 99% and the plasticity limit is 33%. This means that the activity a_c of the clay is:

$$a_c = I_p/l_c = (w_L - w_p)/l_c = 0.66/0.7 = 0.94$$

where I_p = plasticity index
 w_L = liquid limit
 w_p = plasticity limit
 l_c = clay content

This is a fairly normal activity for a natural Ca-smectite. The activity of a sodium treated Ca-smectite is $a_c \approx 3$ while a natural Na smectite (Mx-80) has $a_c \approx 5$. The activity is a rough measure of the ability of the clay mineral to bind water.

The water content is determined as the loss of weight after drying at 105°C during 24 hours. Illitic clays as well as Na-bentonite do not loose much water at further increase in temperature to about 300 deg. Ca-smectite, however, has an excess amount of loosely bound crystalline water which will be lost at temperatures between 100 and 300 deg. This effect was also measured when drying the clay A4 at higher temperatures as shown below:

Temp	w (%)
105	4.5
160	6.9
250	8.1

The low value at 105°C is probably due to incomplete hydration or to a low RH of the atmosphere in which the clay had been stored. The additional loss of water when heating from 105 to 160°C is mainly caused by dehydration of interlamellar cations, while loss of structural hydroxyls must have been negligible as

manifested by the high water content, i.e. 11.1 %, of samples rehydrated at high RH after heating to 250°C.

The influence of the salt content on the properties of the clay can be roughly reflected by the change in liquid limit. As can be seen in Table I there is a change in liquid limit although it is not very dramatic.

Table I. Relation between salt content and liquid limit

<i>NaCl</i> %	<i>w_L</i> %
0	99
0.1	96
1.0	87
3.5	80

3 TESTS AND TEST RESULTS

3.1 General

The samples have been prepared from a powder which was delivered by C.E.A. This means that the soil was dried and ground in France. All tests have been made using de-aired distilled water.

3.2 Hydraulic conductivity. Saturated flow

The hydraulic conductivity of the clay was measured by use of LuH oedometers (Fig 3:1). Samples, 2 cm high and 50 mm in diameter were obtained by compacting air-dry bentonite powder directly in the apparatus and they were then saturated for at least 10 days by letting in water to the filterstones above and below the sample. All air was evacuated from the sample and filterstones before water was added.

After saturation a water pressure was applied at the bottom of the sample. The magnitude of the pressure varied between 50 kPa and 1100 kPa. The pressure had to be well below the swelling pressure of the clay in order to avoid effects of piping type.

The water flow was continuously measured for about a week and the hydraulic conductivity calculated from the inclination of the flow-time curve. Table II shows the results.

Table II. Results from the permeability measurements

Dens at sat, $\rho_m, \text{t/m}^2$	Hydraul gradient, i	Permeability, k m/s
1.70	250	$2.8 \cdot 10^{-12}$
1.84	500	$8.0 \cdot 10^{-13}$
1.90	5500	$3.6 \cdot 10^{-13}$
2.00	4000	$5.2 \cdot 10^{-14}$
2.10	4000	$1.2 \cdot 10^{-14}$ (uncertain)

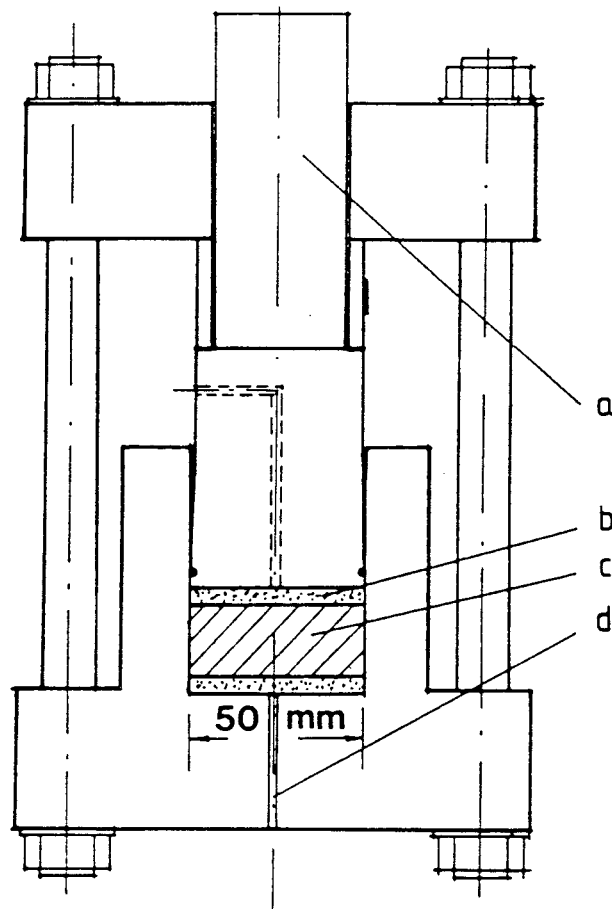


Fig 3.1 The LuH swelling pressure oedometer

- a) Free piston for loading the sample
- b) Filters
- c) Sample
- d) Lower water inlet

The density-permeability relation is also shown in Fig 3:2. The permeability of this clay is about 10 times higher than the permeability of Mx-80 for densities below 2.0 while it seems to be as low as for Mx-80 at densities exceeding 2.0 t/m³.

The similarity in hydraulic behavior between Na- and Ca-smectite at $\rho > 2.0$ t/m³ might be due to that the difference in swelling capacity and in water binding ability do not matter at high densities. The microstructural passages are so small that neither material can fill them.

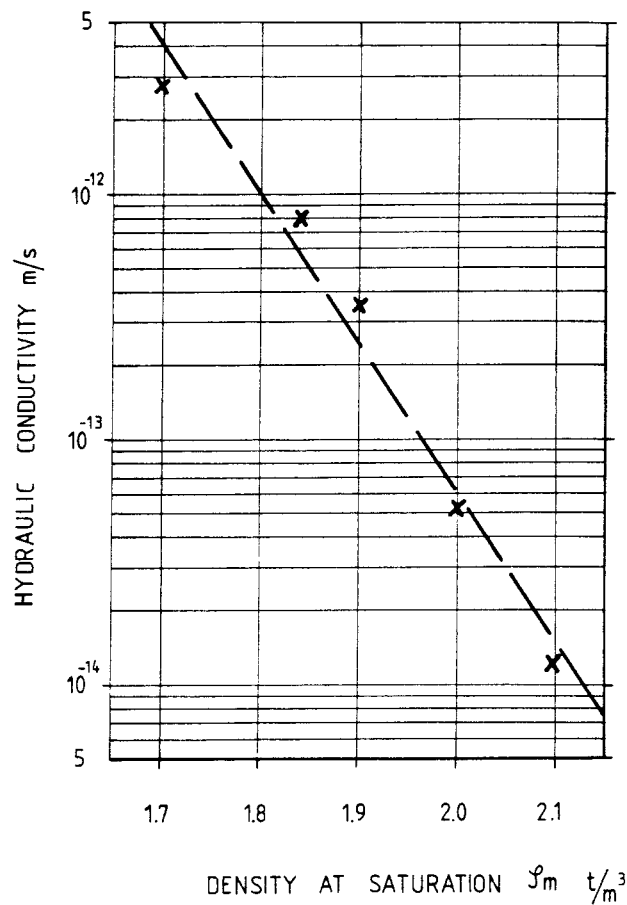


Fig 3.2 Measured hydraulic conductivity as a function of the density

3.3 Water uptake properties. Non-saturated flow

The initial non-saturated flow can be calculated as resulting from the following gradients.

- * A gradient caused by the suction potential of the material. This force is similar to the capillarity.
- * A gradient caused by the external water pressure giving a flow of water according to Darcy's law.
- * A gradient caused by a temperature gradient. A temperature gradient is also causing water transportation in vapour form.

Both laboratory and field tests have shown that the suction potential of the material is the very dominating process as illustrated by the fact that a 1 cm thick confined layer of the clay with $\rho_s = 2.1 \text{ t/m}^3$ is water saturated from one end in about a week. It would require an external hydraulic gradient of 10^6 (or an external water pressure of 100 MPa) to make water penetrate 1 cm of such material in a week. The water uptake process can therefore be accurately modelled by using Eq. (3) in which the parameter D_w must be determined. This can be done by laboratory tests in the following way:

5 cm thick unsaturated samples are compacted to the intended density in LuH oedometers. Water is let through to the lower filter stones. After different times varying between 1 and 20 days the samples are taken out and cut into 5mm thick slices. The water content is then determined for every slice.

In this way the water content can be plotted as a function of the distance from the water inlet. Since the tests are interrupted at different times the influence of the elapsed time will be considered.

From these relations the coefficient of water diffusion D_w can be determined. The technique is described by Börgesson (1985).

The results from two such tests and evaluations are shown in Fig 3:3. The clay was compacted to a density which in a saturated state would correspond to approximately 2.1 t/m^3 . The original water content was 4.6 %. Two calculations using

$$D_w = 0.23 \cdot 10^{-9} \text{ m}^2/\text{s}$$

are also shown in the figure. As can be seen the correspondence between the calculated and measured values are satisfactory. The measured value of D_w agrees very well with the D_w values of compacted Na-bentonite Mx-80 which has been determined to be between $0.2 \cdot 10^{-9}$ and $0.3 \cdot 10^{-9} \text{ m}^2/\text{s}$.

3.4 Swelling ability

The ability and time for the clay to swell can be measured in an oedometer shown in Fig. 3:4. A saturated sample with a height of two cm is placed in the oedometer. A free water level above the sample and water inlet from below certify that the

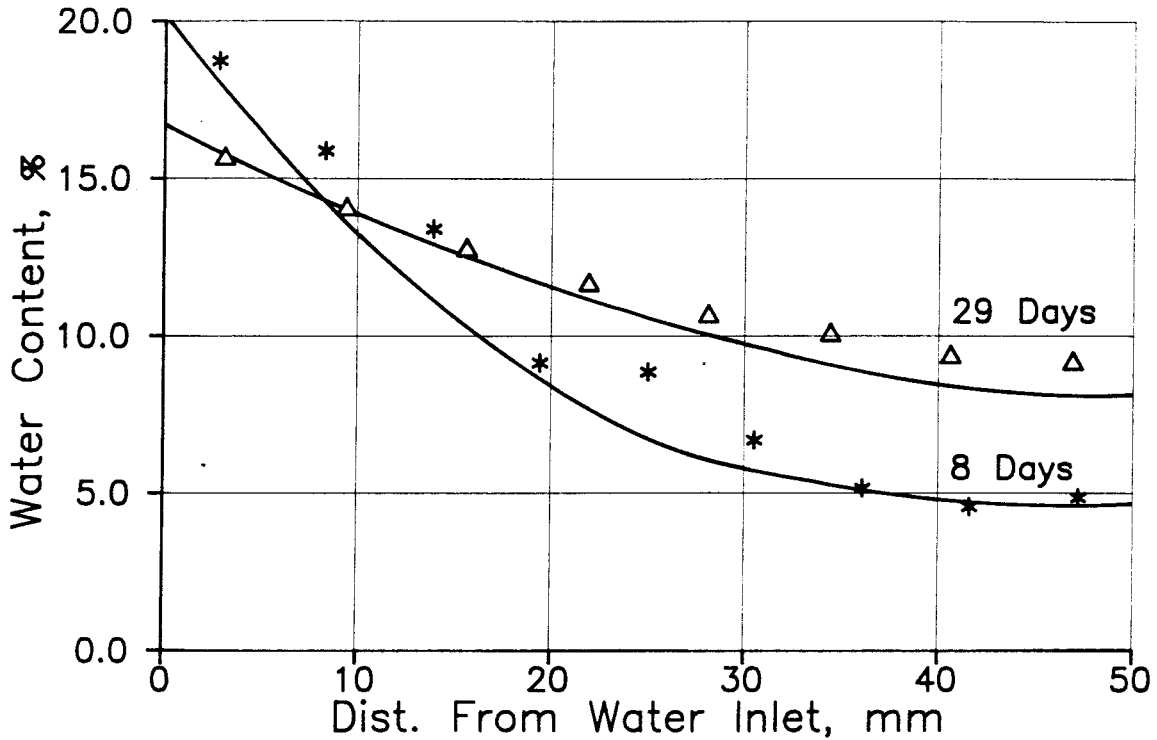


Fig 3.3. Water content distribution 8 and 29 days after start. The solid lines are the calculated distributions using $D_w = 0.23 \cdot 10^{-9} \text{ m}^2/\text{s}$

sample is kept water saturated. The weight of the devices on top of the sample corresponds to an external pressure of approximately 1 kPa.

The swelling of the clay is measured as a function of time by the deformation gauge. It is a very slow process due to the low permeability and the test must continue for 1-3 months.

Fig 3:5 shows the swelling as a function of time for three tests with different densities of the clay. The results are summarized in Table III.

The swelling is considerably lower than for Na-bentonite. Fig. 3.6 shows the swelling as a function of the density. For comparison the swelling of some mixtures of Na-bentonite and ballast material is also plotted (Börgesson & Stenman 1985). The figure shows that the swelling is about the same as would be expected for a mixture of 30% Na-bentonite and 70% ballast material.

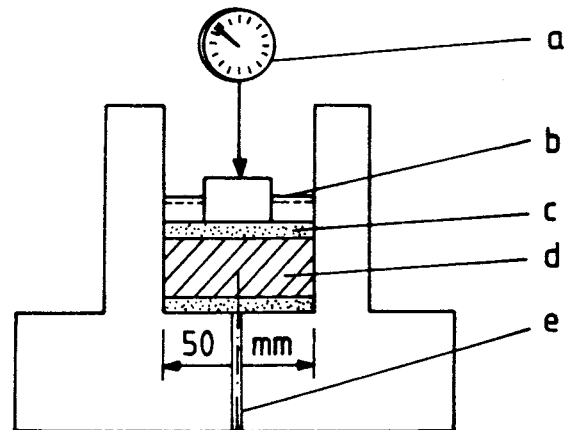


Fig 3.4. Oedometer used for swelling tests

- a) Deformation gauge
- b) Free water level
- c) Filter stones
- d) Sample
- e) Lower water inlet

Table III Results from the swelling tests

Before swelling			After swelling			Swelling %
Dry dens	Sat dens	Water content	Dry dens	Sat dens	Water content	
1.06	1.67	57	1.03	1.65	60	3.2
1.59	2.00	26	1.12	1.70	53	42.3
1.78	2.12	19	1.17	1.74	48	52.0

The tests were finished when the densities were between 1.65 and 1.74 t/m³. As will be shown in the next chapter the swelling pressure at these densities vary between 50 and 150 kPa. This discrepancy depends on a combination of the following factors:

- * The swelling is not completed. There is a very slow continuing swelling which can also be seen in Fig. 3:5.
- * Friction between the clay and the oedometer ring.

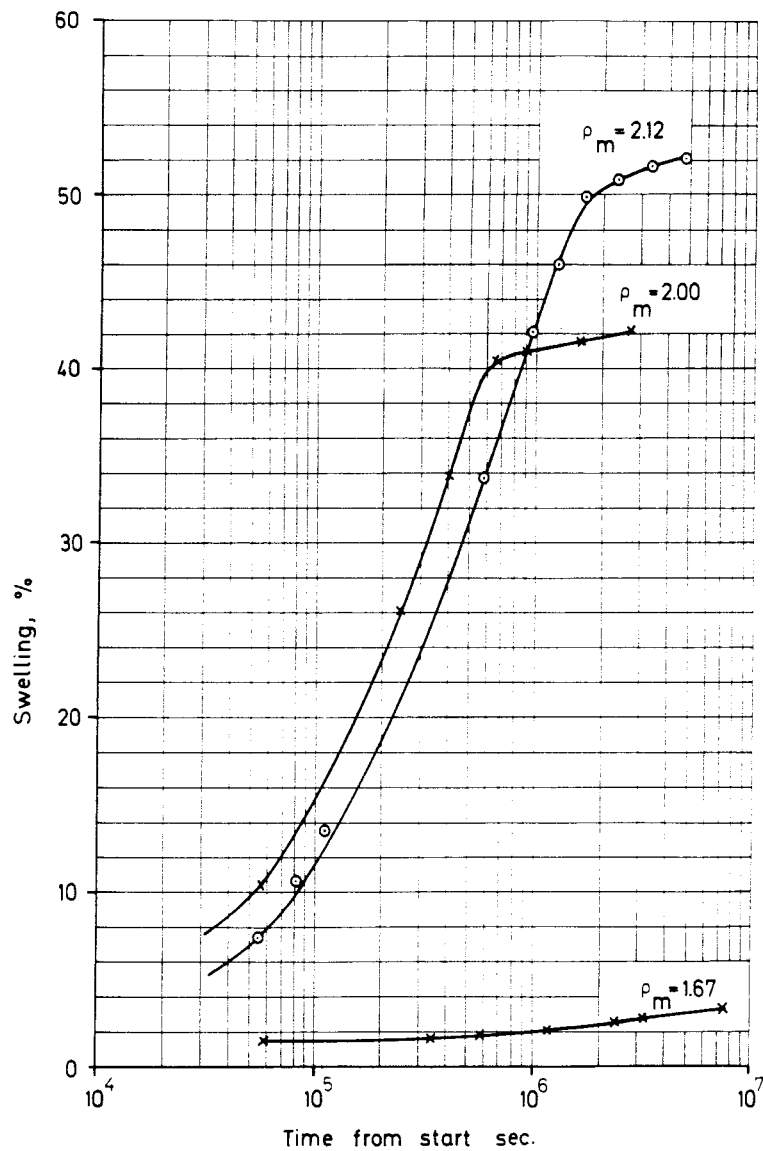


Fig 3.5. Swelling of the clay as a function of time. ρ_m is the initial density of the water saturated sample

- * Some hysteresis effect in the swelling-consolidation process. This effect is not investigated so far.

However the tests of the Na-bentonite mixtures are made in exactly the same way as these tests which means that the results are comparable. The difference in swelling capacity between the materials is probably due to the difference in structure and behavior at low densities.

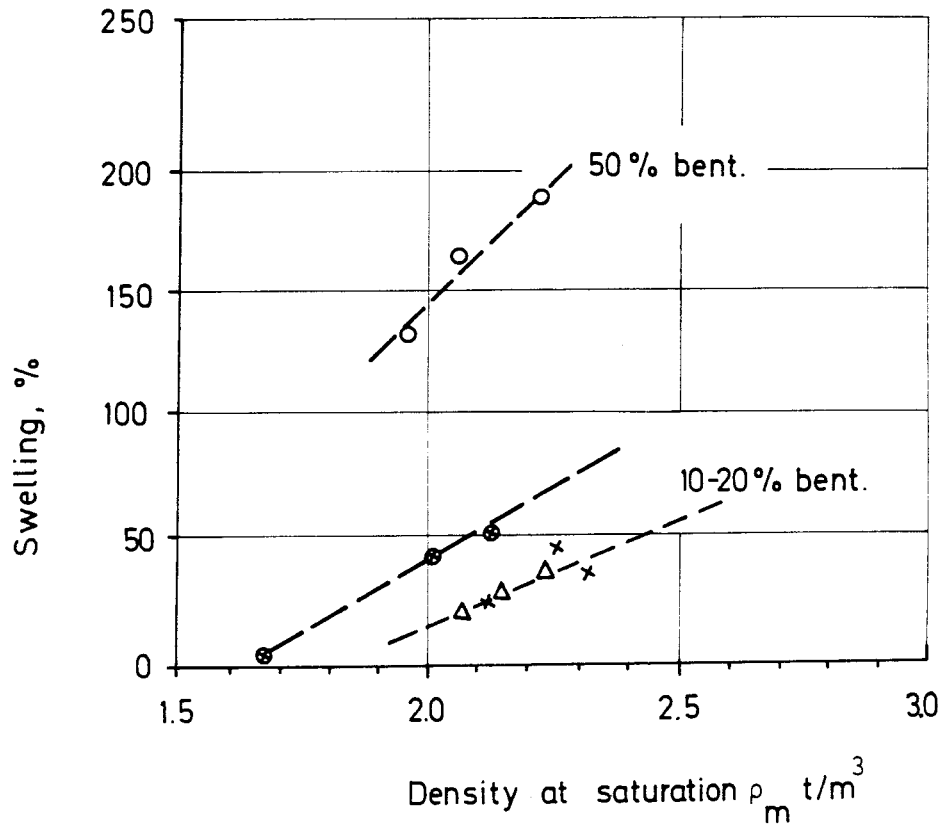


Fig 3.6. Total swelling of the investigated Ca-smectite as a function of the density. The total swelling of Na-bentonite mixed with sand material is plotted for comparison

- x 10 % Na-bentonite
- Δ 20 % Na-bentonite
- O 50 % Na-bentonite
- \otimes 100 % Ca-smectite

3.5 Swelling pressure

The swelling pressure of a clay can be measured in many ways. One way is to adjust the vertical pressure on a sample in an oedometer ring until there is neither swelling nor compression of the clay. This can be done either in an oedometer, in a shear apparatus or in a triaxial cell.

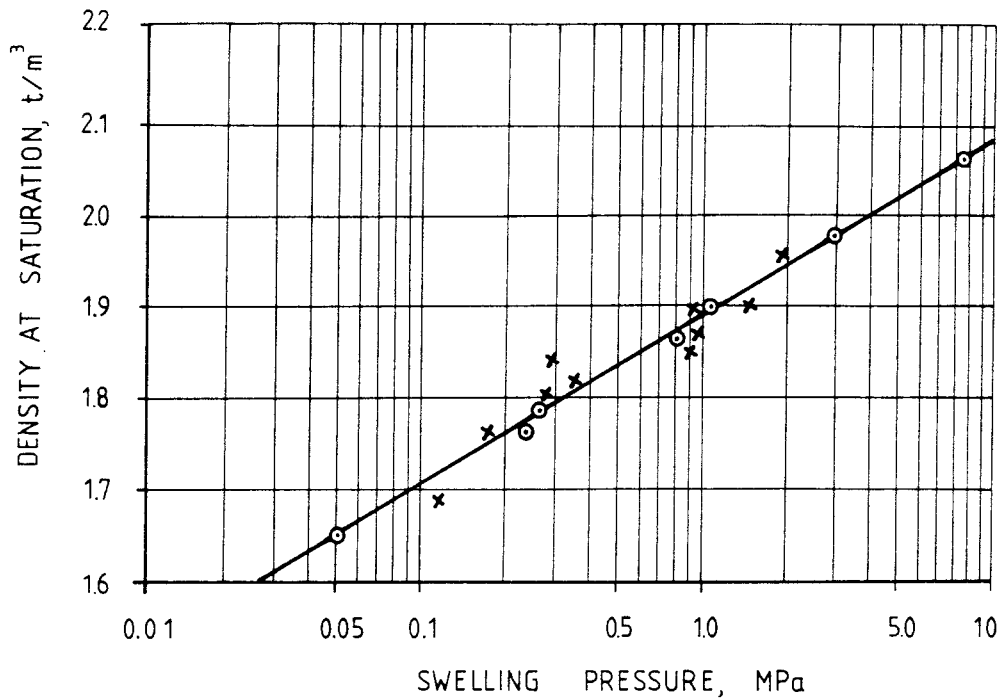


Fig 3.7. Swelling pressure as a function of the density at saturation at 22°C
 o measured in the triaxial cell
 x measured in the shear apparatus

In the triaxial cell the sample, which is surrounded by a rubber membrane, can either be drained or undrained. A drained sample can change its volume by taking up or pressing out water while an undrained sample cannot change its volume. A tendency to change volume in an undrained sample is instead reflected by a change in pore water pressure. Thus the swelling pressure can be measured by adjusting the cell pressure until equilibrium is reached (no change in pore pressure).

Both the above mentioned methods have been used to measure the swelling pressure of the French clay. The tests have been made in connection with the triaxial tests and the shear tests which are described in the next chapters.

The results of the measurements are summarized in Fig. 3:7. The relation between the density at saturation and the swelling pressure forms a straight line

in a semilogarithmic diagram. The values from the measurements in the triaxial cell deviates surprisingly little from the line while the deviation is greater for the other values. It is obvious that the swelling pressure measurements in the triaxial cell are very accurate.

The relation can be mathematically formulated according to Eqn (4):

$$\sigma_s = \sigma_o \cdot e^{\frac{\rho_m - \rho_o}{0.081}} \quad (4)$$

where σ_s = swelling pressure (MPa)

σ_o = reference pressure (MPa)

ρ_m = corresponding density at saturation (t/m³)

ρ_o = corresponding reference density at saturation (t/m³)

If the reference swelling pressure $\sigma_o = 3.7$ Mpa and the corresponding reference density $\rho_o = 2.0$ t/m² are inserted we arrive at Eqn (5):

$$\sigma_s = 3.7 \cdot e^{\frac{\rho_m - 2.0}{0.081}} \quad (5)$$

The swelling pressure does not differ much from the swelling pressure of Na-bentonite Mx-80 at high and medium densities. The pressure is between 75% and 100% of that of Mx-80 at densities exceeding 2.0 t/m² and between 50% and 75% of that of Mx-80 at densities between 2.0 and 1.65 t/m².

3.6 Stress-strain-strength relations measured by triaxial tests

3.6.1 *General*

The stress-strain-strength properties of the clay have been measured by triaxial tests at different densities, temperatures and rates of strain. The tested densities have ranged from 1.64 t/m³ to 2.14 t/m³. Two different temperatures 22 and 60°C and shear rates between 0.06 and 60 percent per hour have been used.

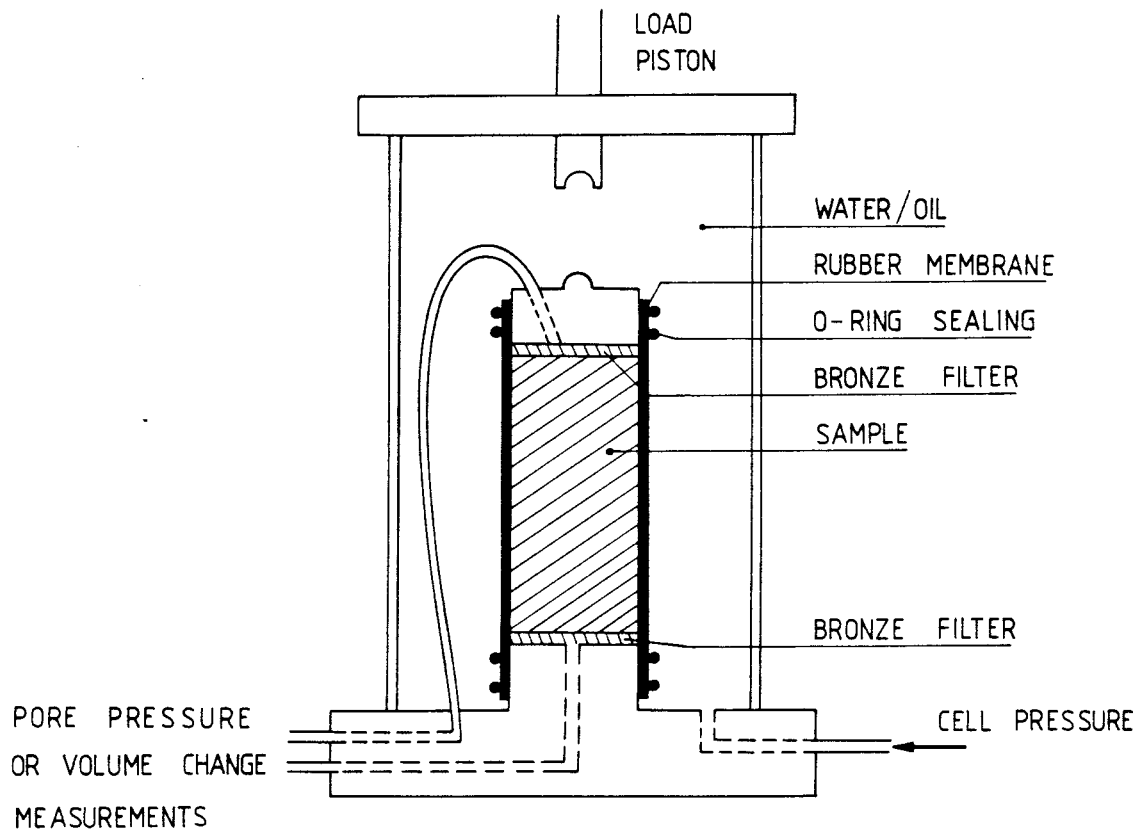


Fig 3.8. Schematic drawing of the triaxial cell

A schematic drawing of a triaxial cell is shown in Fig. 3:8. Two types of experiments have been used, low-pressure cells for samples with a swelling pressure below 1.8 MPa and high-pressure cells for higher swelling pressures. The cell pressure is produced either by compressed air (low pressure cells) or by oil in a high pressure system.

3.6.2 Testing procedures

Triaxial testing of smectite-rich clay is a time consuming process which can be divided into three main steps:

- * Sample preparation and saturation
- * Establishment of equilibrium conditions in the cell (cell pressure = swelling pressure).
- * Stress-strain-strength testing.

The two first steps are necessary because the ordinary tests aimed at finding the friction angle and cohesion from effective-stresses must be performed on saturated samples using a cell pressure equal to the swelling pressure. If the sample is non-saturated we will have an unknown negative pore-pressure in the sample. If the cell-pressure deviates from the swelling pressure we will have non-equilibrium conditions which also results in an unknown pore-pressure situation.

3.6.3 *Saturation process*

The very slow process of saturation and the successively increasing swelling pressure makes it impossible to use the cell for saturating the sample. Instead a specially made saturation device was used. The device consists of a 10 cm long cylindrical bronze filter surrounded by a thick cylinder made of acid-proof stainless steel. The cylinder is attached to a thick bottom steel plate with a filter stone fitting to the end of the filter cylinder. The sample is compacted directly in the device after which the same type of steel plate is attached to the top. The end plates are kept in place by strong bars. By this device the sample 100 mm high and 55 mm in diameter is saturated within 3 weeks and can then be trimmed to the diameter 50 mm.

3.6.4 *Equilibrium process*

After trimming the sample is mounted in the triaxial cell with de-aired water in the filter stones and the pore pressure system. A cell pressure is applied and the pore pressure system closed, thus bringing the sample in an undrained compressed condition. The pore pressure is then recorded and the cell pressure successively adjusted so as to reach pressure equilibrium, which usually requires one to two weeks.

3.6.5 *Heating process*

If the sample is to be tested in a heated condition a heat wire is attached to the bottom plate of the cell. The water in the cell is thus heated via the bottom plate. A heat regulator is controlling the temperature of the cell. The heating is commenced after reaching equilibrium between the cell pressure and the swelling pressure.

The heating of a saturated clay sample is accompanied by several problems. The increased temperature will increase the volume of the pore water more than the volume of the pores. If the sample is undrained the pore water pressure will therefore be increased and if the sample is drained, a slow outflow of porewater will start. Since a higher temperature means a lower swelling pressure of the clay the sample will either tend to increase its density by consolidation (drained state) or tend to decrease the effective stress by increasing the pore water pressure (undrained state). Since the consolidation process is very slow and an increased density is unwanted the drained state is not suitable. At present it is not known how much of the pore pressure increase that is due to temperature induced reduction of the swelling pressure and how much that is caused by the difference in expansion of the pore water and the clay network.

In the author's heat tests, a mixture between the drained and the undrained methods was used. The sample was drained for about four hours after the temperature increase. During this period the increase in volume of the water in the filters and the channels in the cell were let out as well as some of the volume increase of the pore water. Then the drainage was closed and the pore pressure allowed to be fairly stabilized.

An interesting observation in connection with the pore pressure stabilization was made in those tests where pore pressure was measured in both ends of the sample. A pore pressure difference of more than 50 kPa between the two ends of the sample could arise and remain without tendency to disappear. This suggests that the permeability of the clay at low gradients is even lower than the permeability measured and accounted for in Chapter 3.2 and, thus, that there is a deviation from Darcy's law.

3.6.6 Testing process

After equilibrium in either heated or non-heated conditions, the cell was placed in the press which was run at a constant rate of strain applying the standard procedure in soil mechanics. During the test, the pore pressure, the applied force and the deformation was continuously measured.

Fig 3.9 shows a picture of the set up of a test.

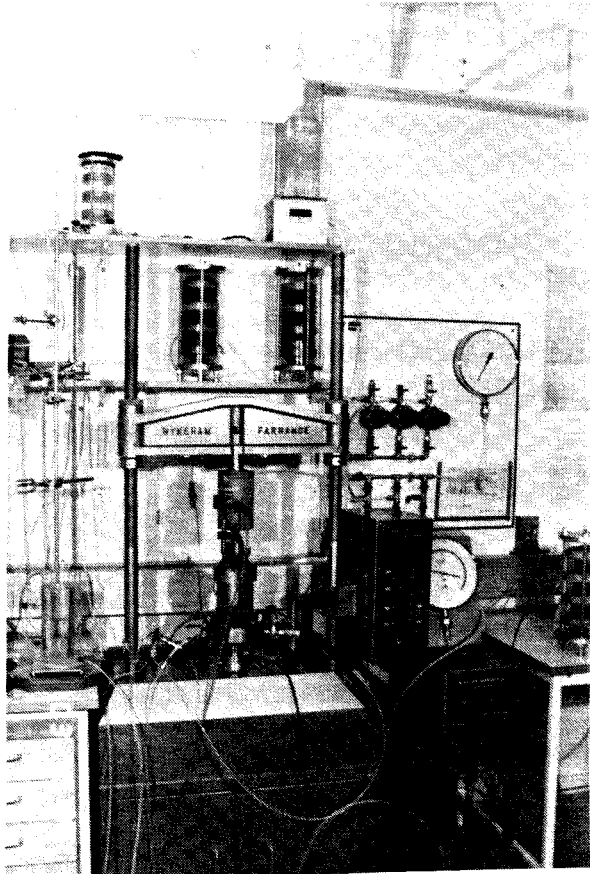


Fig 3.9. Triaxial equipment with the loading machine in the center

The tests were normally conducted at a temperature of 22°C and at a rate of strain of 0.6 % per hour. In tests 6 - 9 the temperature was increased to 60 deg. to study the temperature influence. At tests 11 and 12 the rate of strain was changed and in test 10 the applied cell pressure was only half the expected swelling pressure in order to study the effect of a quick change in confining pressure.

All triaxial tests were performed under undrained conditioned. The influence of the drainage condition was investigated by some drained shear tests.

All stress-strain curves are shown in Appendix A

3.6.7 Results

The triaxial tests are summarized in Table IV.

- * Column 1 shows the test number.
- * Column 2 shows the temperature T of the sample during the test.
- * Column 3 shows the density ρ of the sample.
- * Column 4 shows the calculated degree of saturation S_r .
- * Column 5 shows the effective stress σ'_3 on the sample at the start of the test when the pore pressure is measured in the bottom of the sample.
- * Column 6 shows the pore pressure change Δu_f at the end of the test.
- * Column 7 shows the deviator stress at failure $(\sigma_1 - \sigma_3)_f$.
- * Column 8 shows the residual deviator stress $(\sigma_1 - \sigma_3)_r$ when differing from $(\sigma_1 - \sigma_3)_f$.
- * Column 9 shows the strain at failure ϵ_f .
- * Column 10 shows the applied rate of strain $\dot{\epsilon}$.
- * Column 11 shows the pore pressure parameter at failure A_f . (The pore pressure change divided to the change in deviator stress)
- * Column 12 shows the mobilized friction angle at failure ϕ_f (The friction angle when no cohesion is assumed)

Tabell IV. Data and results from the triaxial tests

1 Test	2 T °C	3 ρ t/m ³	4 S _r %	5 σ'_3 kPa	6 Δu_f kPa	7 $(\sigma_1 - \sigma_3)_f$ kPa	8 $(\sigma_1 - \sigma_3)_r$ kPa	9 ε_f %	10 $\dot{\varepsilon}$ %/h	11 A _f	12 ϕ_f °
T1	22	1.65	94	48	17	39.5	31	3.7	0.6	0.43	22.9
T2	22	1.79	96	266	23	128		9.9	0.6	0.18	12.0
T3	22	1.90	100	1044	29	263		8.9	0.6	0.11	6.6
T4	22	1.98	101	2727	53	530		9.0	0.6	0.10	5.2
T5	22	2.06	100	8227	9	1863	1460	6.1	0.6	0.005	5.8
T6	60	1.64	81	25.6	1.3	52.6	36	1.5	0.6	0.05	31.3
T7	60	1.77	-	71.3	11	101	76	2.6	0.6	0.11	27.1
T8	60	1.89	100	668	10	277	225	6.2	0.6	0.036	10.0
T9	60	2.00	97	4730	40	953	840	9.1	0.6	0.009	
T10	22	2.14	104	7049	3	2339		9.2	0.6	0.001	8.2
T11	22	1.90	99	992	2	307		7.5	60	0.007	7.7
T12	22	1.90	95	1048	37	285		9.4	0.06	0.13	7.1

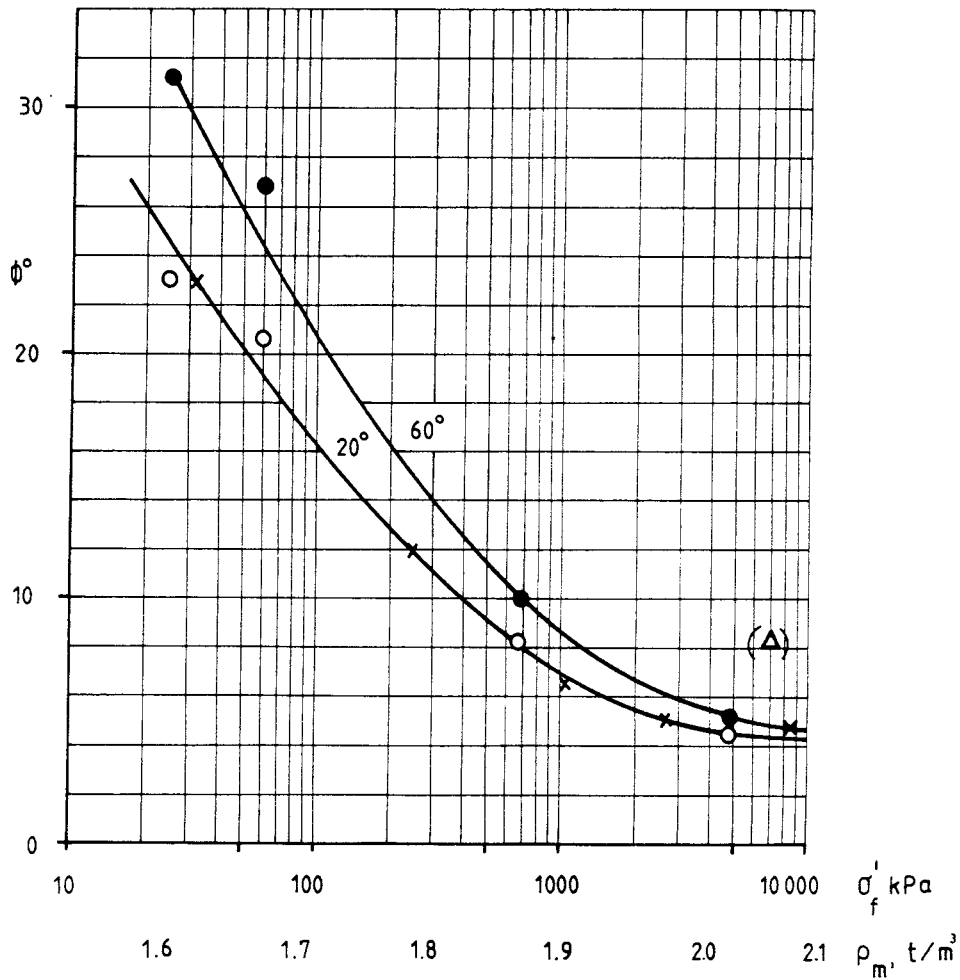


Fig 3.10. The mobilized friction angle ϕ at failure at the triaxial tests as a function of the minor principal effective stress σ_{3f} and the density at saturation ρ_m

The results can be illustrated in several ways. Fig. 3:10 shows the mobilized friction angle at failure as a function of the effective minor principal stress at failure. The approximate corresponding densities are also marked in the figure. The friction angle is obviously no constant material parameter but alters from being very high (20 - 30°C) at low pressures ($\sigma < 50$ kPa) to very low (5°C) at high pressures ($\sigma > 2000$ kPa). Also in this respect an increase in density to about 2.0 t/m³ significantly alters the mechanical behavior of this clay.

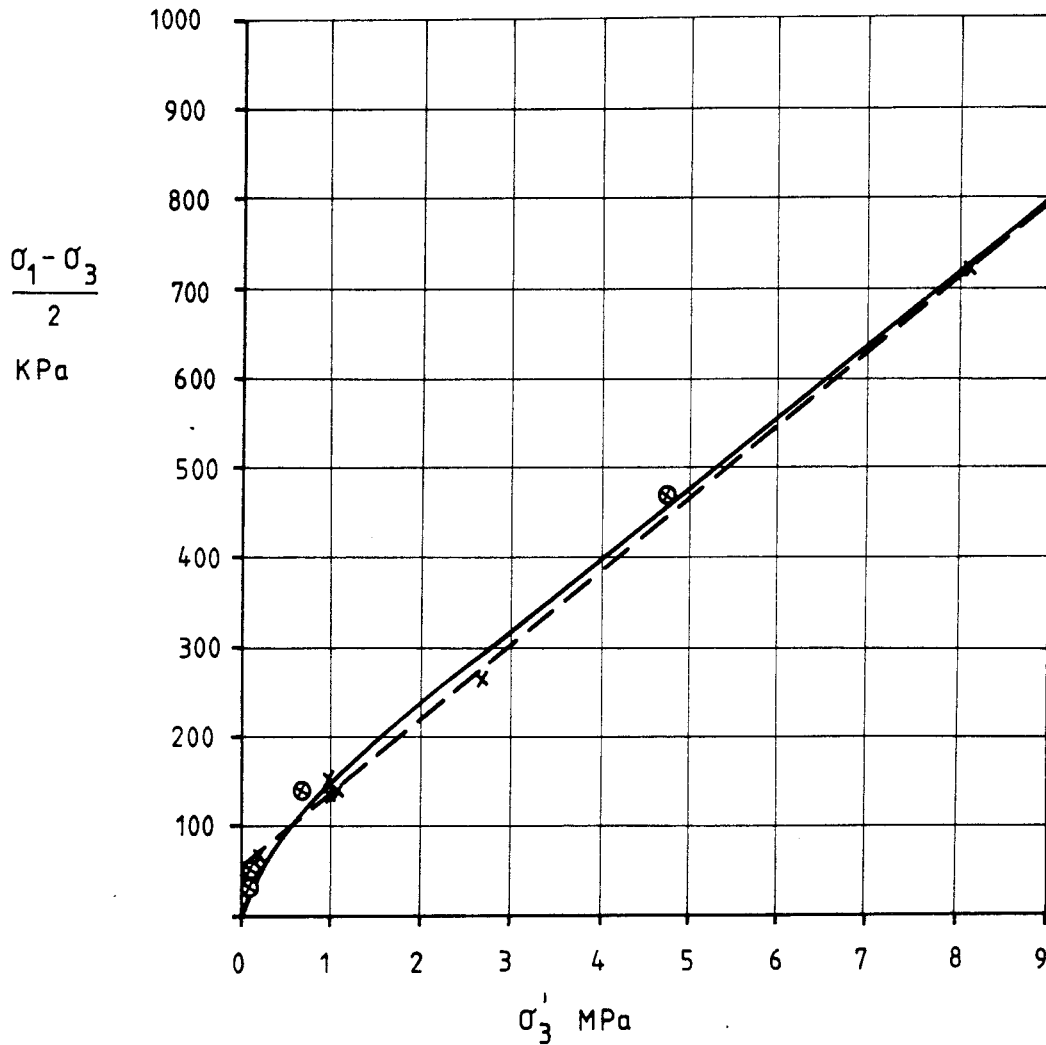


Fig 3:11. Failure stresses in the triaxial tests. Notice the different scales of the axes
 x temperature = 22°C
 ⊗ temperature = 60°C
 — failure envelope
 --- Mohr-Coulomb failure envelope

An increased temperature increases the shear strength at low densities while the influence is very small at higher densities. The influence seems to cease at a density around 2.0 t/m³.

The failure stresses can be plotted in a stress diagram like in Fig. 3:11. Since the difference between the heated and the non-heated samples is significant only at

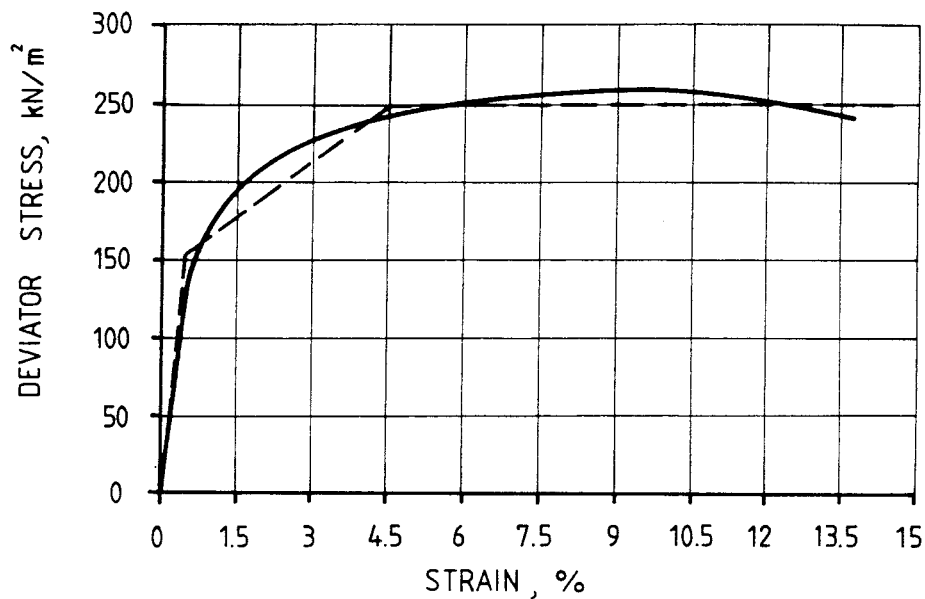


Fig 3.12 Stress/strain relation of test T3. The broken curve represents the idealized elastic-plastic model

low stresses it is not seen as clearly in this figure. A Mohr-Coloumbian evaluation of the cohesion and the angle of friction yields.

cohesion $c = 50$ kPa

angle of friction $\phi = 4.4$ deg

which are only valid at stresses exceeding 200 kPa. A similar evaluation of stresses below 200 kPa yields

cohesion $c = 0$

angle of friction $\phi = 22$ deg

The cohesion intercept is thus fictive and the shear strength is of course zero at zero effective stress. The true failure envelope is curved as shown in the figure.

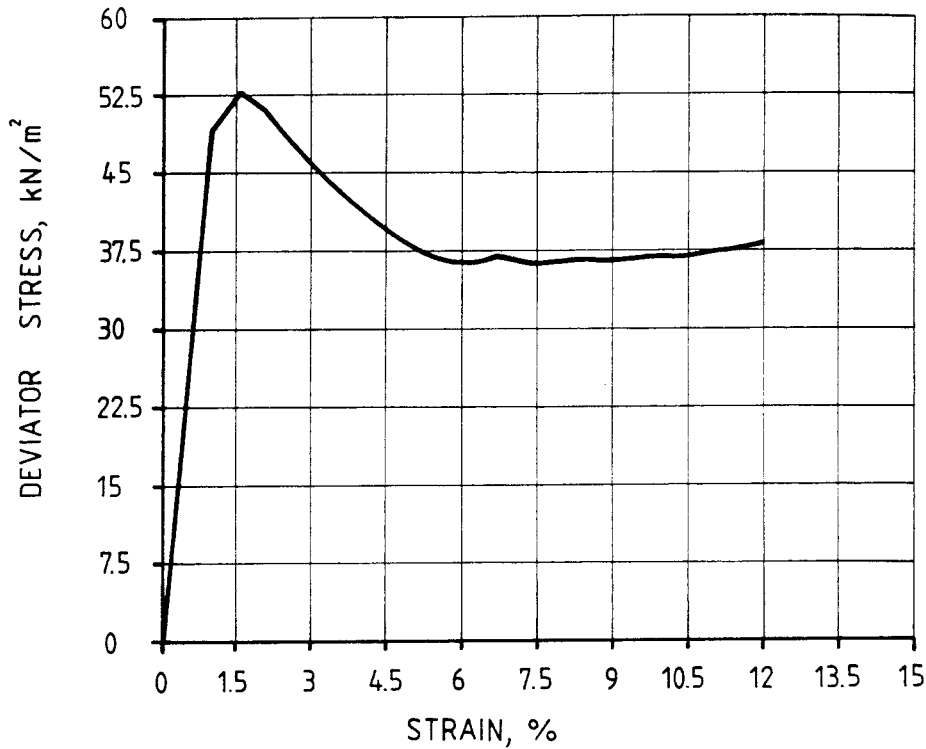


Fig 3.13. Stress/strain curve of test T6 which was conducted at a temperature of 60°C

Most of the recorded stress-strain curves do not show any peak value followed by a low residual strength. Thus, the clay is not brittle. The behavior can be modelled in a simplified way as an elastic-ideally plastic material with initial stiff, linear elastic strain. At about 0.5 % deformation it turns into a strain hardening plastic material which after ~5 % deformation will be ideally plastic. Fig. 3:12 shows a typical stress-strain relation and how it can be idealized.

However, the heated samples with a density below 2.0 t/m³ have a typical brittle behavior. Also the non-heated sample at the low density 1.65 t/m³ exhibits some brittleness. The brittleness is very clear at the high temperature test T6. Fig.3.13 shows the stress-strain curve from that test. It seems as if the residual strength of the heated samples correspond to the real strength of the non-heated samples. This can be seen in Fig 3.10 where the residual strength is plotted as well.

It is very probable that the increased strength of the clay at increased temperatures is caused by the development of additional bonds or true cohesion which might be due to cementation. The following reasons are in support of this explanation:

- * The peak values are not accompanied by a negative pore pressure which would be the case if dilatancy had taken place.
- * A brittle behavior which is not caused by dilatancy is in soil mechanics usually considered to be caused by a true cohesion.
- * The residual strength is equal to the shear strength of the non-heated material which suggests that the heat treatment produces "extra" particle bonds which have been broken.

The difference between the peak value and the residual value is varying between 20 kPa ($\rho = 1.64 \text{ t/m}^3$) and 100 kPa ($\rho = 2.00 \text{ t/m}^3$) or 30 % of the shear strength at the low density and 10 % at the high density. Though the brittleness is not as evident at high densities Fig 3:10 clearly shows the effect of the high temperature on the stress-strain properties which can be related to changes in the clay structure.

The heat-induced strengthening is in agreement with the microstructural reorganization that has been observed in heated smectite clay (Pusch, 1987).

3.6.8 Pore pressure change

The pore pressure in smectitic clays is of special interest. The effective stress theory which is generally applied and known to be valid for sand, silt and illitic clays may not apply to smectitic clays. The theory says that the effective stress σ' is equal to the total stress σ minus the pore pressure u :

$$\sigma' = \sigma - u$$

The stress-strain-strength properties of a soil are entirely depending on the effective stress, such that an increase in total stress does not effect these properties if it is accompanied by an equal change in pore pressure. However this theory

implies that the contact area between the particles is very small compared to the size of the pores and that a pore pressure gradient in the soil dissipates with time. There are many reasons to believe that these requirements are not fully satisfied in smectitic clays, a major one being that the clay particles consist of tiny lamellae separated by strongly adsorbed layers of water molecules. Smectite clays with a density exceeding 1.5 t/m^3 contain at least 20 % adsorbed water that can be considered as belonging to the particles, the particle contact area is significant and the effective stress concept therefore not perfectly applicable. This conclusion is supported by the observed, remaining small hydraulic gradients in some samples. It is also supported by the observations that an applied additional cell pressure does not create an equal increase in pore pressure in completely or almost fully saturated samples.

The pore pressure change during a test is also of interest for the understanding of the mechanical and rheological behavior. The change in pore pressure can be expressed by the pore pressure parameter A :

$$\Delta u = \Delta \sigma_3 + A \cdot \Delta(\sigma_1 - \sigma_3) \quad (6)$$

In the triaxial test where $\Delta \sigma_3 = 0$ A will be the response in pore pressure caused by a change in deviatoric stress

$$A = \frac{\Delta u}{(\sigma_1 - \sigma_3)}$$

A can be considered as a measure of the tendency of the material to change its volume during shear. When the change in pore pressure until failure is considered the pore pressure parameter at failure A_f is studied. If A_f is positive the material is contractant which means that it tends to decrease its volume. If A_f is negative the material is dilatant which means that it tends to increase its volume. If A_f is very small the material can be sheared without volume change. A small value of A_f also means that an undrained test is equal to a drained test.

A_f has been calculated for all the triaxial tests. Fig. 3:14 shows A_f as a function of the effective stress at the beginning of the tests. The figure shows that A_f is quite high at low swelling pressures (low densities) while it decreases with increasing

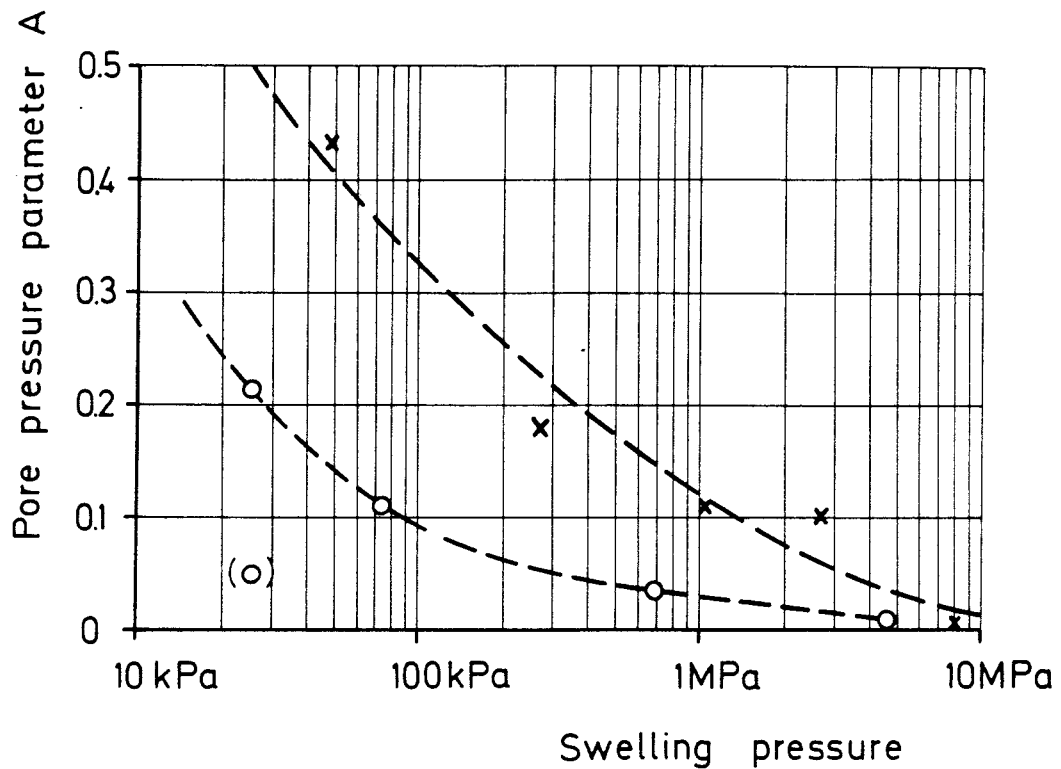


Fig 3.14. Pore pressure parameter evaluated from the triaxial tests as a function of the swelling pressure

x temperature = 22°C
o temperature = 60°C

densities and is very low at swelling pressures above 5 MPa corresponding to densities exceeding 2.0 t/m³.

The figure also shows that the pore pressure parameter is lower at 60°C than at room temperature. This can partly be explained by the heat-induced increase in pore pressure and associated change in microstructure before the start of the test. At test T6 the recorded pore pressure parameter is much smaller and does not fit into the general picture. The reason for this is the very brittle behavior by which failure occurs already at 1.5 % deformation. The pore pressure continues to increase after failure and if the pore pressure at 10 % deformation is used the value of A_f fits better. (Fig. 3:14)

3.6.9 Influence of strain rate

An important question is whether the change in pore pressure in the sample has enough time to be transferred through the sample to the pore pressure gauge. Thus the low permeability of the clay delays the recorded response of quick changes in pore pressure. The three tests run at different rates of strain can be used to answer that question. They were originally made in order to study the effect of the rate of strain on the stress-strain-strength properties. The tests are summarized in Table V, from which the following conclusions can be drawn:

Table V. Results from the strain-rate tests

Test	ρ_m t/m ³	$\dot{\epsilon}$ %/hour	$(\sigma_1 - \sigma_3)_f$ kPa	A_f
T12	1.90	0.06	285	0.13
T3	1.90	0.6	263	0.11
T11	1.90	60	307	0.007

The two tests made at the slow strain-rates have a similar A_f -value but the quick test has a very low A_f -value. This shows that the normal rate of strain 0.6 % per hour is sufficiently slow to yield proper registration of the change in pore pressure, while 60 % per hour is not. If 0.6 % per hour would be too fast, a clear difference in A_f -value between the slow tests would have been noted.

The influence of the rate of strain on the strength properties is more difficult to evaluate from these tests. The influence of the strain rate is so small that the inevitable variation of other factors as the density and the heterogeneity of the clay (variation in smectite content) has a greater effect on the properties. It is thus obvious that it is not possible to use different samples when studying the effect of the strain rate. It is necessary to use the same sample subjected to non-destructive testing. Such a test by which the strain rate dependence is evaluated is shown in Chapter 3.7.

However, it is obvious that the influence of the strain rate is very small. A change in density from 1.90 to 1.91 is increasing the deviator stress at failure about 15 %

which is the same order of magnitude as the maximum difference in failure stresses at the three tests using strain rates between 0.06 and 60 % per hour. This matter is further analysed in Chapter 3.7.

3.7 Shear tests

3.7.1 *Testing procedures*

The triaxial tests have been supplemented by simple shear tests. The shear apparatus is illustrated in Fig 3.15. This figure shows both a picture of the apparatus and a drawing of the sheared sample. The samples are 50 mm in diameter with a height of about 15 mm. The sample has filterstones on the top and in the bottom and is surrounded by a cylindrical rubber membrane. The rubber membrane is supported by cylindrical ring-shaped plates in order to keep the sectional area constant. When the sample is sheared the shearing will take place in the whole sample (simple shear) and the shear deformation is easily calculated as the horizontal deformation divided to the height of the sample. The vertical and horizontal deformations and forces are measured during the test and the change in volume vary equal to the change in height multiplied by the horizontal area. The sample is first compacted and saturated in an oedometer (Fig 3:1) and then transferred to the shear apparatus. A normal pressure is applied to balance the swelling pressure of the clay, the external pressure being carefully adjusted so that neither swelling nor compression is observed.

The necessary procedure described here will take about two weeks. When the sample is in equilibrium the test is started implying that constant rate of strain is applied.

3.7.2 *Results*

The tests and the test results are shown in Table VI.

The first two columns show the test number and the density. The following columns show:

* Column 3: The degree of saturation S_r .

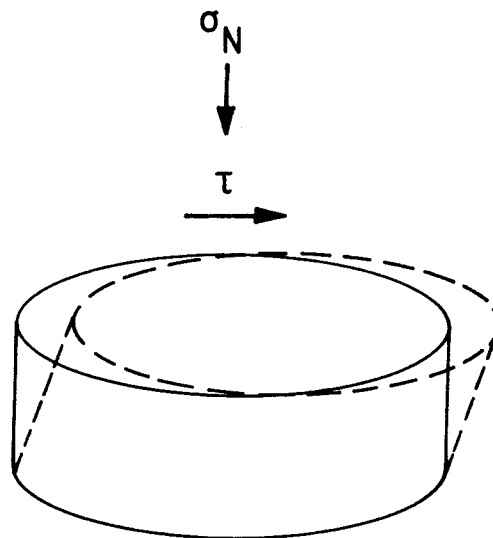
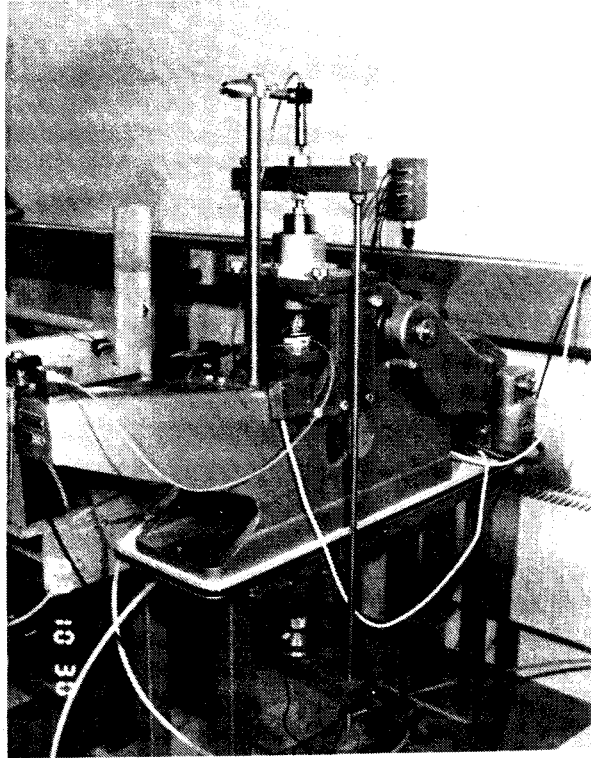


Fig 3.15. Appearance and function of the apparatus for simple shear

- * Column 4: The normal stress σ_N . This stress is applied using dead loads and is kept constant during the test.
- * Column 5: The shear stress at failure τ_f .

Table VI. Data and results from the simple shear tests

1 Test	2 ρ t/m	3 Sr %	4 σ_N kPa	5 τ_f kPa	6 γ_f %	7 $\dot{\gamma}$ %/h	8 ϕ'_f °
S1	1.76	92	172	52.5	12.2	0.6	17.2
S2	1.81	100	304	78.4	11.3	0.6	14.3
S3	1.90	98	1312	103	3.7	0.6	4.5
S4	1.95	96	1775	211	11.8	0.6	6.8
S5	1.87	104	856	133	16.0	0.6	8.8
S6 ¹⁾	1.85	97	811	116	10.7	0.6	8.1
S7	1.69	96	117	42.0	12.0	0.06	20.7
S8	1.80	100	245	69.5	11.0	0.06	15.8
S9	1.90	93	875	126	10.0	0.06	8.2
S10 ²⁾	1.84	99	272	-	-	0.005- -500	

- 1) Natural clay
2) Varying $\dot{\gamma}$

- * Column 6: The shear deformation until failure γ_f .
* Column 7: The shear rate $\dot{\gamma}$.
* Column 8: The friction angle at failure ϕ_f evaluated as $\arctan(\tau_f/\sigma_N)$.

The stress-strain relations in the shear tests are all shown in Appendix B.

The pore pressure was measured in tests S1-S6, which were ran as undrained tests. It turned out however that the change in pore pressure was not measurable. For that reason, the evaluation of these tests was made in terms of total stresses. However, no big difference between the total and the effective stresses was expected since the pore pressures measured at the triaxial tests were very small. This was also confirmed by the drained tests S7-S9, which was conducted at a strain-rate of 0.06 %/hour that is slow enough to yield more than 95% degree of pore-pressure dissipation. No clear difference in stress-strain-strength behavior between the drained and the undrained tests could accordingly be observed.

The shear stresses at failure are shown in Fig. 3:16 as a function of the total normal stress. The failure stresses form a curved failure envelope as in the triaxial tests and a Mohr-Coloumb evaluation of the results appears as a straight

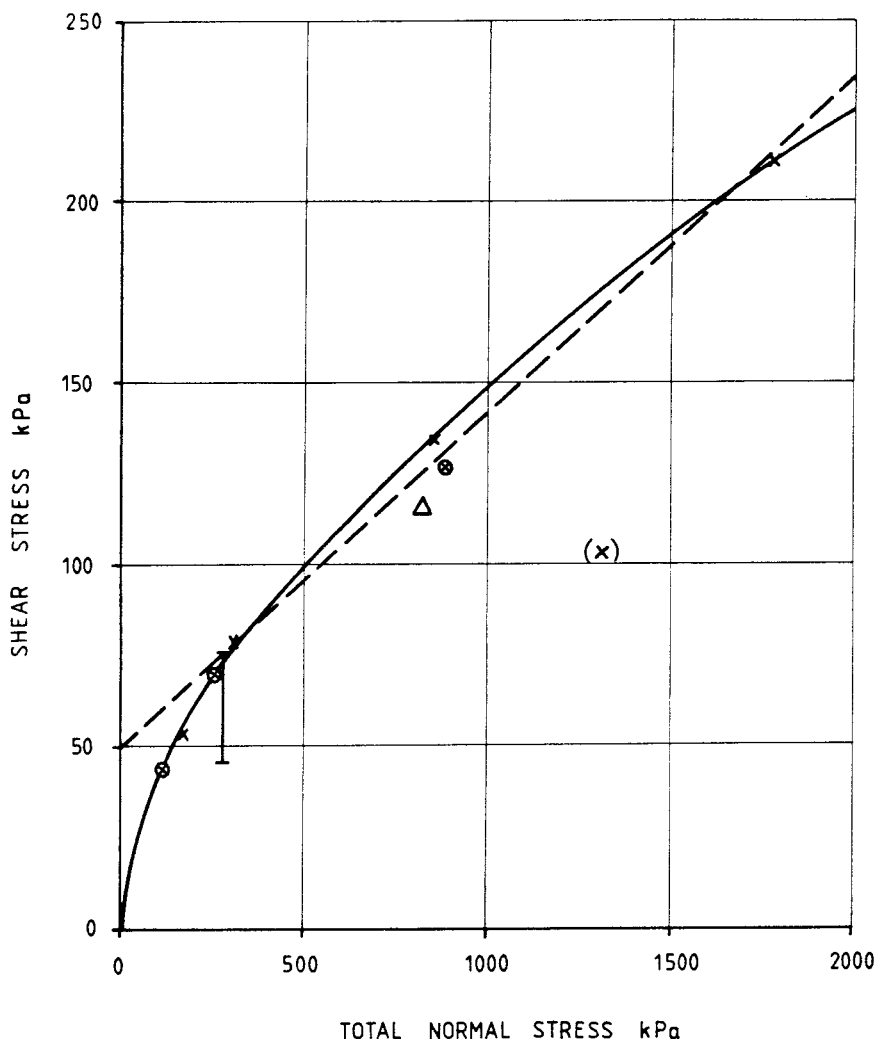


Fig 3.16. Failure stresses from the simple shear tests. Notice the difference in scale of the axis

- x Undrained tests
- ⊗ Drained tests
- △ Natural "undisturbed" clay

line approximation of the failure envelope. This evaluation yielded the two parameters

$$\text{cohesion } c = 50 \text{ kPa}$$

$$\text{angle of friction } \phi = 5.2^\circ$$

which are only valid at stresses exceeding 200 kPa. A similar evaluation at stresses below 200 kPa gave

cohesion $c = 0$
 angle of friction $\phi = 18^\circ$

The Mohr-Coloumb parameters agree very well with those measured at the triaxial tests ($c = 50$ kPa, $\phi = 4.4$ deg if $\sigma_3 > 200$ kPa and $c = 0$ kPa, $\phi = 22^\circ$ if $\sigma_3 < 200$ kPa) from which it is concluded that the difference in testing technique is of minor importance as to the stress-strain-strength behavior of this clay.

The tests were made at a constant room temperature of 22°C. Originally, some tests using higher temperatures were planned but the nice agreement between the triaxial and shear tests did not call for further double-checking.

Test S3 falls outside the pattern of all shear and triaxial tests. S3 was the first test made with the shear apparatus and an error in the normal load measurement was probably made. The result from this test is put in brackets in Fig. 3:16.

3.7.3 *Test on a natural clay*

One of the tests was made on a piece of "undisturbed" clay. The sample was prepared from a block of clay taken in situ, the natural density being 1.85 t/m³. The test is termed S6. This test matches perfectly the pattern of the other tests with respect to the stress-strain-strength properties, which means that the procedures of drying, grinding and recompaction do not effect these properties.

3.7.4 *Strain rate dependence*

The last test, T10, was made at a varying rate of strain in order to investigate the rate dependance as mentioned in Chapter 3.6. The sample was compacted, saturated and mounted in the normal way. It was sheared until 2.5 % shear strain at the very slow rate 0.005 % per hour. The shear rate was then increased by 10 times at every 1.0 % further strain until the rate 500 % per hour.

The stress-strain relation from this test is shown in Fig 3:17. The increased shear resistance at increased strain rate is clearly seen. The increase in strain rate had to be preceded by a short stop which is seen as a small decrease in shear stress between the curves.

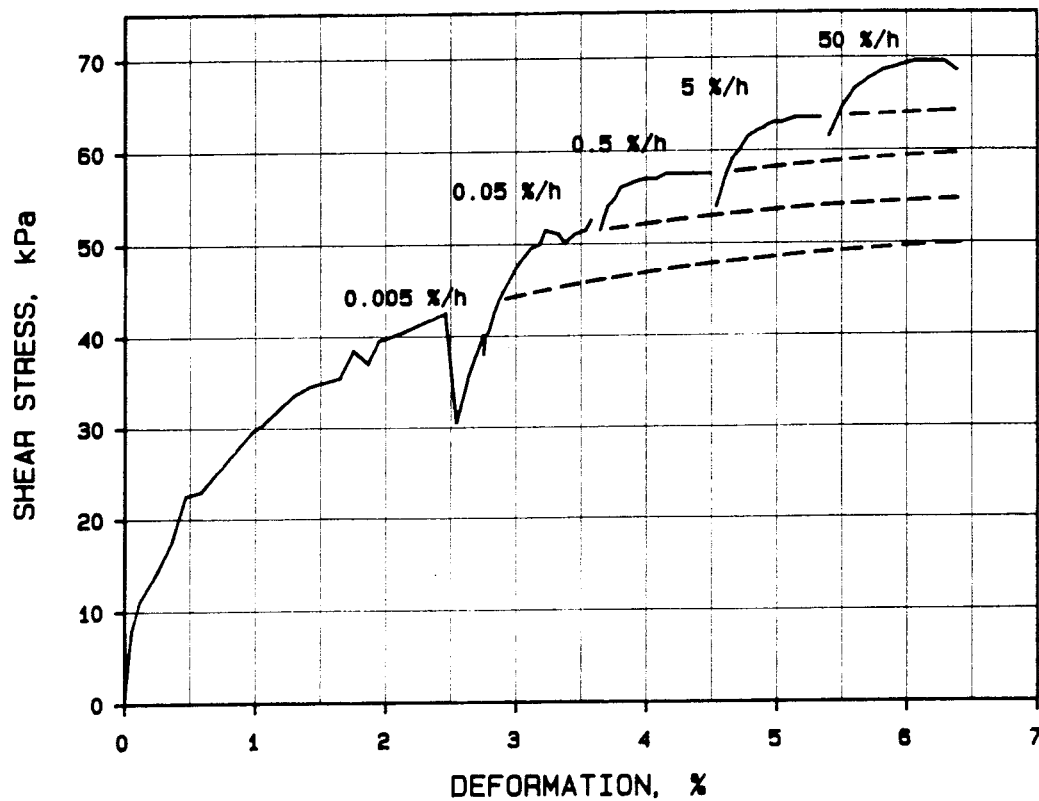


Fig 3.17. Stress/strain relation at the shear test S10 using different rates of strain. The dashed lines are extrapolations

The difference in shear strength can be evaluated from Fig. 3.17 by extrapolating the curves at the different strain-rates according to a general stress strain curve drawn from the other tests. Such a curve is easy to obtain since the stress-strain relation is very similar in the different tests if they are normalized with respect to the maximum shear stress. If this is made and the shear stress at failure is plotted as a function of the rate of strain in a double logarithmic diagram, Fig. 3:18 is obtained.

The dashed line in Fig. 3:18 forms a straight line in the double logarithmic diagram. Such a relation can be expressed by the formula:

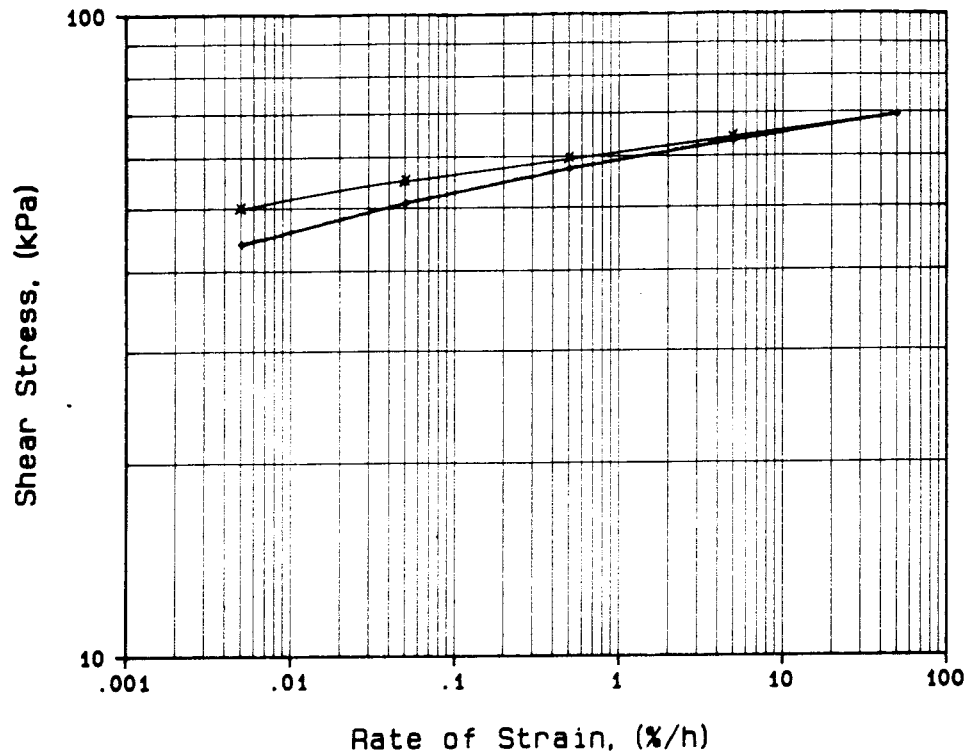


Fig 3.18. The shear stress at the end of each rate step in Fig 3.17 (thick line) and the shear stress at 6 % strain from the extrapolated curves (thin line)

$$\tau_f = m \cdot \left(\frac{\dot{\gamma}}{\dot{\gamma}_0} \right)^n \quad (7)$$

- where
- τ_f = shear strength (Pa)
 - $\dot{\gamma}$ = rate of shear strain (1/s)
 - $\dot{\gamma}_0$ = reference rate of shear strain = 1.0 (1/s)
 - m = shear stress (Pa) at $\dot{\gamma} = \dot{\gamma}_0 = 1.0$
 - n = inclination of the straight line in the double logarithmic diagram

Thus n is a measure of the rate dependence and m a measure of the strength level. For a material with Newtonian behavior $n = 1.0$ and m will be equal to the

ordinary viscosity. If the parameters m and n are evaluated from Fig. 3:18 we get the following data:

$$m = 1.0 \cdot 10^5 \text{ Pa}$$

$$n = 0.036$$

It is interesting to note that Eq. (7) is identical with the relation between the shear resistance and the strain rate derived from viscometer tests on loose bentonite gels with a water content at or exceeding the liquid limit. The parameter n is for those gels $n = 0.07$ which means that the rate dependence of a loose bentonite gel and a compacted sample are of the same low order of magnitude. The value of m is of course much lower for the gels ($m < 10^3 \text{ Pa}$).

The rate dependence of undisturbed sediments of illite has been studied by various investigators. If their results are evaluated with the same technique we arrive at the value $n = 0.05$. Thus the rate dependence of the shear strength of clay seems to be of the same low magnitude irrespective of consistency or type of clay mineral.

The stress-strain relation of all shear tests are similar (except for the erroneous test T3). An initial stiff elastic deformation until about 1% deformation is followed by a strain-hardening plastization resulting in an increased shear resistance until failure occurs at about 12% strain. After failure there is a slow decrease in shear resistance but no residual strength within 15% strain. At strains exceeding 15% the results are not reliable according to normal geotechnical standard.

3.8 Creep tests using the direct shear apparatus (shear box)

3.8.1 *General*

All creep tests except one, which was accounted for in the chapter about the triaxial tests, were made using the direct shear apparatus shown in Fig. 3:19. The principles of direct shear are also shown in the figure. Direct shear has the advantage that the sample is very effectively confined and that tests can be made at high swelling pressures and temperatures. However it has the disadvantage that the sample is not homogeneously sheared as shown in the figure and that the volume involved in the shear process is not known. The measured shear deformation, which is the displacement of the upper half of the shear box, cannot be

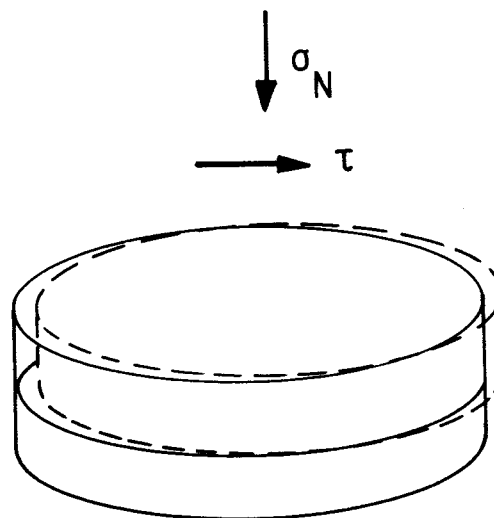
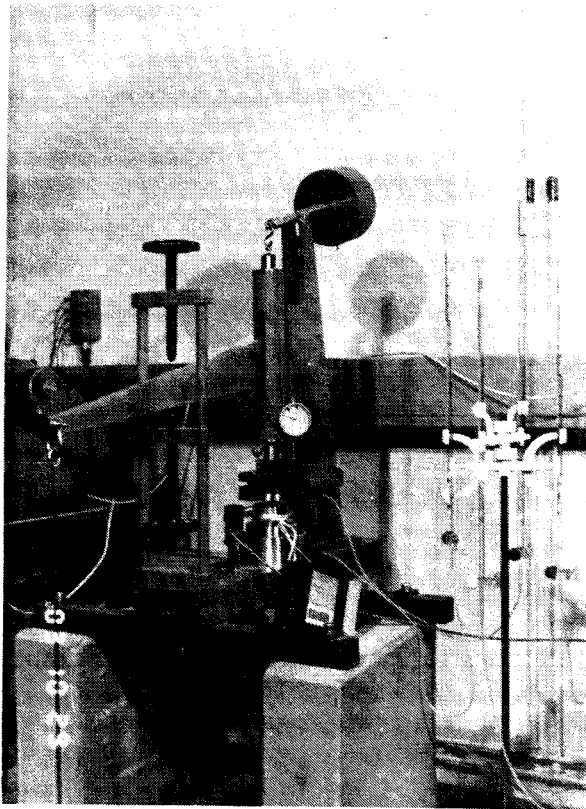


Fig 3.19. Appearance and function of the direct shear apparatus used for the creep tests

directly expressed in terms of shear strain since the height of the involved sample is not fully known. A procedure to arrive at a defined strain is described by Pusch, Børgesson and Hökmark (1987). The strain referred to in this text and in the

strain-time curves in Appendix C is the so called corrected angular strain according to this procedure.

The preparation involves compaction and saturation of air-dry bentonite powder. A normal pressure is applied to balance the swelling pressure which is successively built-up in the course of the saturation process.

After saturation, the shear stress is applied by applying dead loads that create a constant shear force. The stress is applied stepwise and the sample allowed to creep for a few days at every load. The creep deformation is continuously measured and the relation between the corrected angular strain and the time is calculated and plotted.

3.8.2 Performed tests

All results are accounted for in Appendix C. The creep tests are summarized in Table VII.

- * Column 1 shows the test number
- * Column 2 shows the temperature (T)
- * Column 3 shows the density at saturation (ρ)
- * Column 4 shows the applied normal pressure (σ_N)
- * Column 5 shows the number of steps that have been applied until failure is reached (n)
- * Column 6 shows the applied shear stress at step $n-1$ (τ_{n-1})
- * Column 7 shows the applied shear stress when failure is reached at step n (τ)

The real failure stress is not determined by these tests but it must be between τ_{n-1} and τ_n . Fig. 3.20 shows those stresses as a function of the normal stress. If a straight line is drawn to evaluate the cohesion and the angle of friction according to Mohr-Coulomb for the tests at 22°C we arrive at

$$c = 80 \text{ kPa}$$

$$\phi = 6.4^\circ$$

Table VII. Basic data and results from the creep tests

1 Test	2 T °C	3 ρ t/m ³	4 σ_N MPa	5 n	6 τ_{n-1} kPa	7 τ_n kPa
C1	22	1.89	0.80	6	151	181
C2	22	1.98	3.2	4	300	480
C3	22	2.03	9.1	4	850	1090
C4	40	1.87	0.80	6	149	178
C5	40	1.95	3.14	7	417	477
C6	40	2.04	9.1	8	1072	1220
C7	90	1.94	0.8	9	238	274
C8 ¹⁾	22	1.84	0.79	14	194	209
C9	90	2.16	9.1	7	1778	2074
C10 ²⁾	22	2.08	9.0	1		

- 1) Natural clay
- 2) Long time test

Those values are slightly higher than those from the triaxial and simple shear tests probably due to the difference in testing technique: Failure is restricted to take place in one plane.

The creep tests at temperatures 40 and 90°C. as well as one test on a natural clay and one comparative test on Na-bentonite are also plotted in Fig. 3:20. Only the high temperature tests at 90°C. differ considerably from the derived Mohr-Colombian parameters.

One long time test C10 was allowed to creep at one step for 70 days in order to study the validity of the creep models at a long time perspective.

3.8.3 Creep results

Creep of soils can be expressed by use of different constitutive relationships, a general totally empirical law being that suggested by Singh & Mitchell (1968).

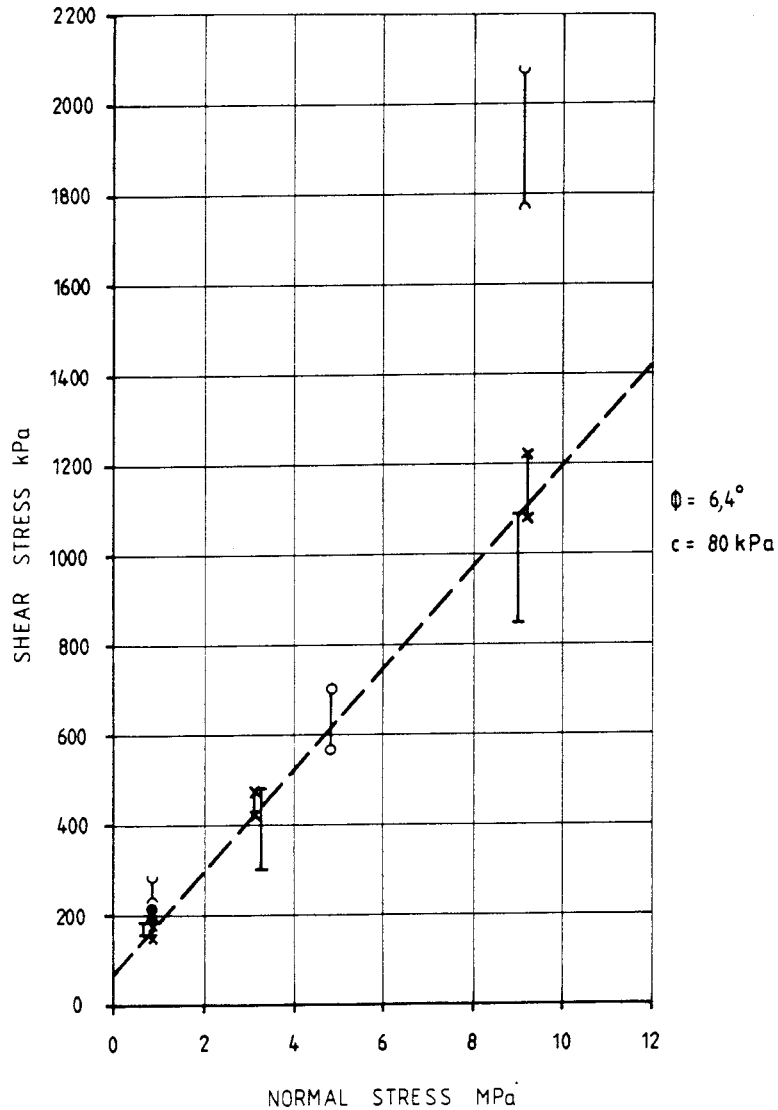


Fig 3.20. Failure stresses at the creep tests

- I 22°C
- I 40°C
- I 90°C
- I Natural clay at 22°C

Other laws have been developed on the basis of theoretical physics, such as the one forwarded by Pusch and Feltham (1981, see also Pusch 1986). Both methods express the rate of creep dy/dt in the form given by Eq. (8):

$$dy/dt = A \cdot f(\tau) \cdot (t+t_0)^n \quad (8)$$

where A and n are constants

$f(\tau)$ = function of the applied shear stress

t = time from applying the shear stress τ
 t_0 = constant

$f(\tau)$ can either be written as

$$f(\tau) = e^{a\tau} \quad (9)$$

where a is a constant according to Mitchell or as

$$f(\tau) = \tau^a \quad (10)$$

which is a common form in various other branches of material research. The term:

$$(t+t_0)^n \quad (11)$$

in Eq. (8) has an exponent n which should be equal to -1 for moderate shear stresses according to Pusch & Feltham while experience shows that n may deviate slightly from this figure, i.e. $-1 < n < 0$. t_0 is usually taken to be zero, while it is considered to be a measure of stress-historical structural effects by Pusch & Feltham. Since the temperature also influences the creep rate, the function $f(\tau)$ can be expressed in terms of a function of both shear stress and temperature $g(\tau, T)$.

Fig. 3:21 shows, as an example, the creep curves evaluated from test C1. Failure occurred after 6 steps of which the 5 first are shown in the figure. These results will be analyzed according to the methods mentioned.

The creep theory by Singh & Mitchell

According to Singh & Mitchell Eqn. (8) can be written as:

$$\frac{d\gamma}{dt} = A e^{a\tau} t^n \quad (12)$$

or

$$\log \dot{\gamma} = \log A + a\tau + n \log t \quad (13)$$

Eqn. 13 means that the relation between $\dot{\gamma}$ and t is a straight line in a double logarithmic diagram with the inclination n .

The creep rate $\dot{\gamma}$ can be evaluated from the strain-time relation exemplified in Fig 3:21. This was made by use of a computer-derived curve fitting method using 8 successive measurements for each rate determination.

The time-dependent creep rates evaluated from test C1 are shown in Fig 3:22. We see that the patterns are not perfectly regular but it is still possible to draw three parallel straight lines along which the results are grouped after more than 5000 sec. The scatter is partly due to the stress loading technique. The shear stress is stepwise increased which means that the strain rate at every step is lower than it would be if the shear stress was applied in only one step.

The exponent n , which is given by the inclination of the curve, is 0.83 for test C1.

The influence of the shear stress can also be evaluated according to eqn. (13) where the relation between $\dot{\gamma}$ and τ is a straight line in a semi-logarithmic diagram. The evaluation is preferably made by referring to a definite reference time. Using $t_r = 10^4$ sec for this purpose and relating the shear stress to the failure shear stress by the quotient τ/τ_f we get the results in Fig 3:23. Since these tests have been performed using stepwise loading not only the shear stress level τ/τ_f will influence the strain rate but also the magnitude of the additional shear stress. Eq. 12 is valid only if the whole shear stress is applied in one step but it is assumed that the strain rate at any shear stress level can be calculated as the sum of the prior strain rates. This summation is also shown in Fig. 3:23. The relation between the shear stress level and the strain rate seems to form a straight line in a semilogarithmic diagram except at low stresses and stresses close to failure.

The relation which seems to be valid in the range $0.1 \tau_f \leq \tau \leq 0.9 \tau_f$ can be written:

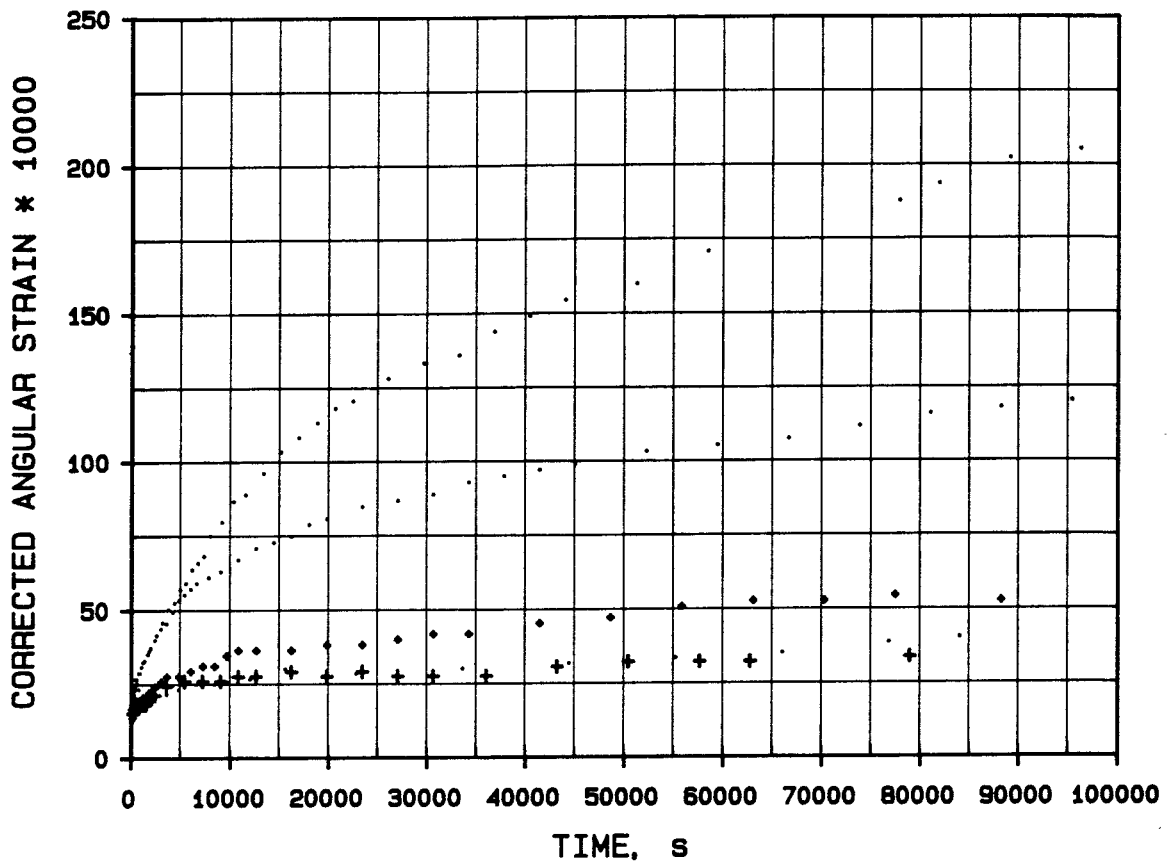


Fig 3.21.

Creep curves from test C1

$$\rho_m = 1.89 \text{ t/m}^3, \sigma_N \sim 800 \text{ kPa}$$

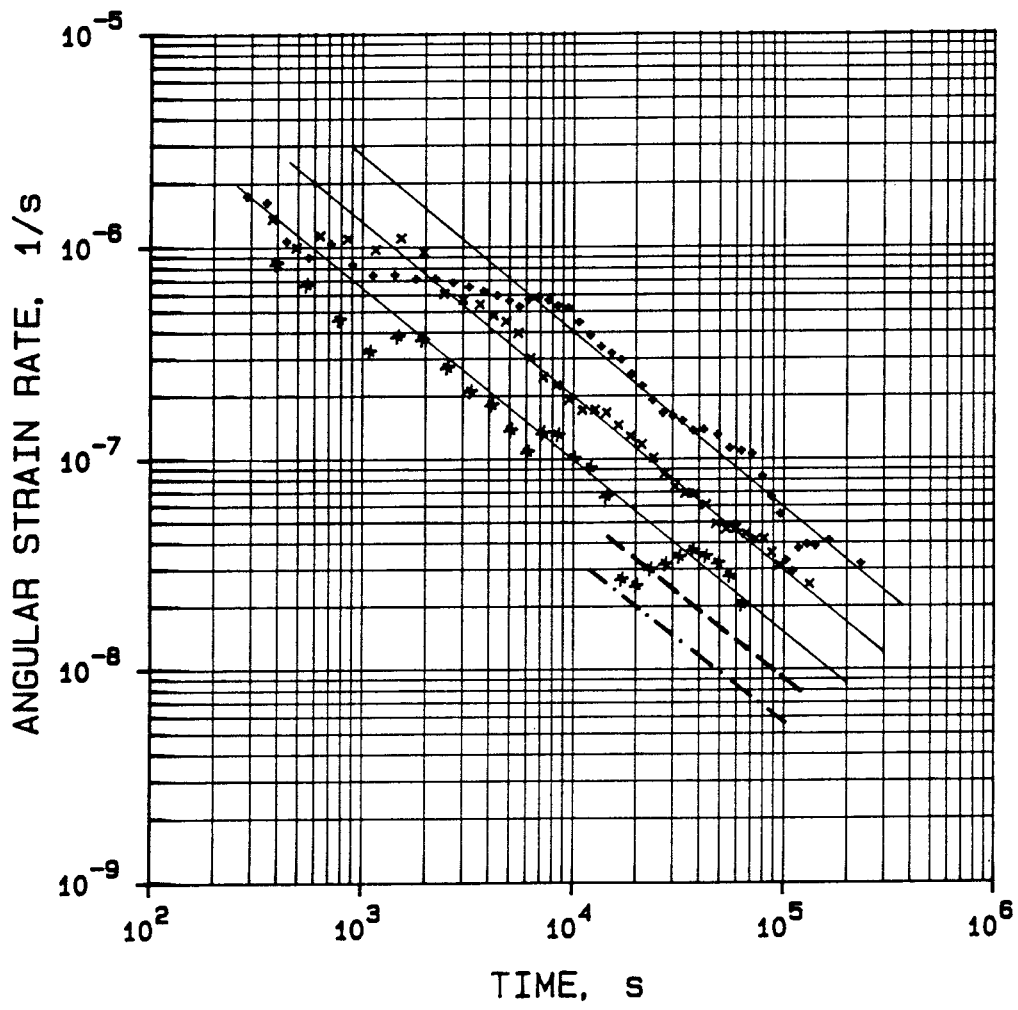


Fig 3.22. Strain rate plotted as a function of time at test C1

+ $\tau = 151$ kPa
 x $\tau = 121$ kPa
 * $\tau = 91$ kPa
 ---- $\tau = 60$ kPa
 $\tau = 30$ kPa

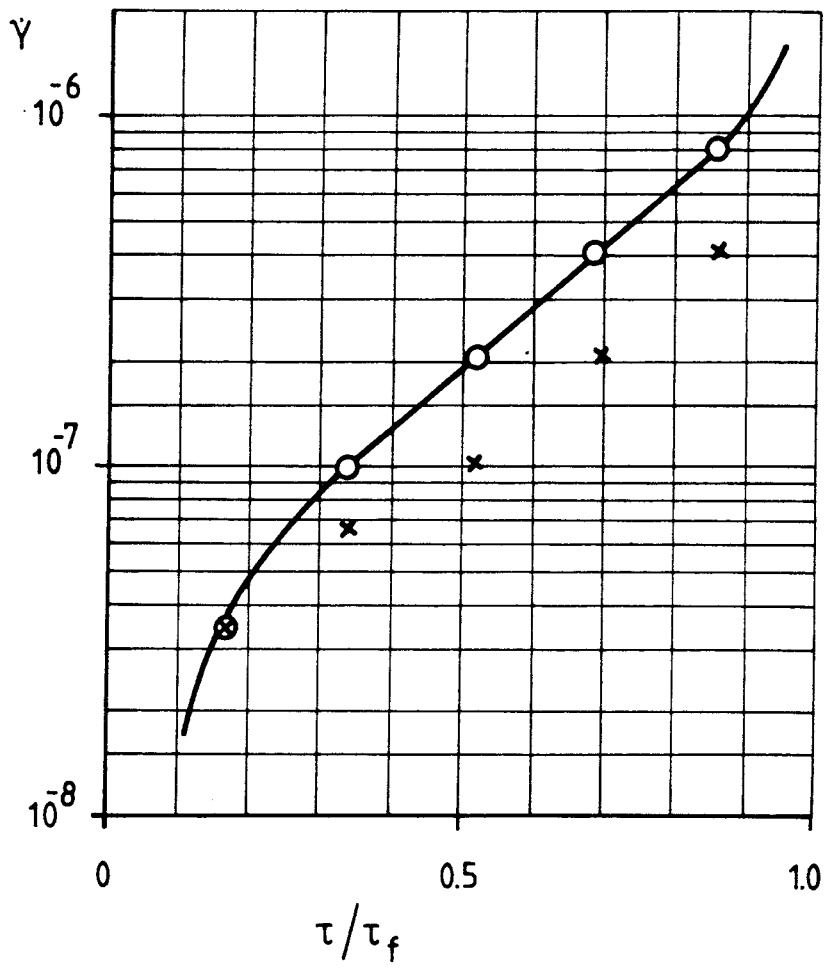


Fig 3.23. Relation between strain rate $\dot{\gamma}$ and the shear stress level τ/τ_f

x $\dot{\gamma}$
o $\Sigma \dot{\gamma}$

$$\log \dot{\gamma} - \log \dot{\gamma}_o = \alpha \left(\frac{\tau}{\tau_f} - \frac{\tau_o}{\tau_f} \right) \tag{14}$$

$$\dot{\gamma} = \dot{\gamma}_o \cdot e^{\alpha \frac{\tau}{\tau_f}} \cdot e^{-\alpha \frac{\tau_o}{\tau_f}} \tag{15}$$

yielding the general expression

$$\dot{\gamma} = \dot{\gamma}_o \cdot e^{a \frac{\tau}{\tau_f}} \cdot e^{-a \frac{\tau_o}{\tau_f}} \cdot \left(\frac{t}{t_r}\right)^n \quad (16)$$

For test C1 the parameters

$$t_r = 10^4 \text{ sec}$$

$$\frac{\tau_o}{\tau_f} = 0.5$$

yield the following values

$$\dot{\gamma}_o = 1.9 \cdot 10^{-7} \text{ s}^{-1}$$

$$a = 3.9$$

and for test C1 the strain rate relation will thus be:

$$\dot{\gamma} = 1.9 \cdot 10^{-7} \cdot e^{1.95 \cdot \frac{\tau}{\tau_f}} \cdot e^{-3.9 \frac{\tau_o}{\tau_f}} \cdot \left(\frac{t}{10^4}\right)^{-0.83} \quad (17)$$

or (since $\tau_f = 175 \text{ kPa}$)

$$\dot{\gamma} = 1.34 \cdot 10^{-6} \cdot e^{0.0223 \cdot \tau} \cdot \left(\frac{t}{10^4}\right)^{-0.83} \quad (18)$$

However, it is more convenient to use the parameters in Eqn. 16 to describe the creep rate.

All creep tests have been evaluated according to this method and the creep rate/time relations are given in Appendix C. As can be seen, Eq. (12) is not valid for the high temperature tests C7 and C9. In these tests the creep rates fluctuate, probably due to microstructural strengthening effects of the heating.

Similarly, the creep rates recorded at the testing of the natural clay do not follow Eq. (12). The creep rates decreased so fast that the n value at the end of the load steps would correspond to a value of $n \approx -2$. Since the shear strength of this sample

was much higher than the shear strength determined in the simple shear apparatus and since the sample was very stiff as compared to the natural clay in the simple shear apparatus, it is concluded that the heterogeneity of the natural clay is the reason for the strange creep behavior. Since the creep tests yield shear in a narrow zone, inclusions of stiffer material will effectively block the strain. This is not the case when using the triaxial and simple shear devices.

All creep tests at the temperatures 22 and 40°C have been evaluated according to Eqn. (16). The relation between $\Sigma\dot{\gamma}$ and τ/τ_f are plotted in Fig 3:24. The evaluated parameters are shown in Table VIII. It should be added here that the evaluation of n is open to discussion but the long time creep tests shown in Chapter 3.8.4 support the evaluation made here.

Table VIII. The parameters in Eqn. (16) determined for the creep tests C1-C6 using $t_0 = 10^4$ sec and $\tau_0/\tau_f = 0.5$

Test	Temp °C	τ_f kPa	$\dot{\gamma}$ s ⁻¹	a	n
C1	22	175	$1.9 \cdot 10^{-7}$	3.9	0.83
C4	40	180	$1.4 \cdot 10^{-7}$	5.1	0.92
C2	22	480	$2.4 \cdot 10^{-7}$	3.6	0.74
C5	40	460	$1.0 \cdot 10^{-7}$	6.5	1.03
C3	22	1100	$5.4 \cdot 10^{-7}$	4.1	0.73
C6	40	1200	$5.2 \cdot 10^{-8}$	7.8	1.00

Table VIII shows that an increase in temperature seems to

- 1 Increase the shear strength
- 2 Decrease the creep rate $\dot{\gamma}_0$
- 3 Cause a faster decrease in creep rate with time (increasing n)

These conclusions are consistent with the observations from the triaxial tests where the increased temperature also created a stronger and stiffer material.

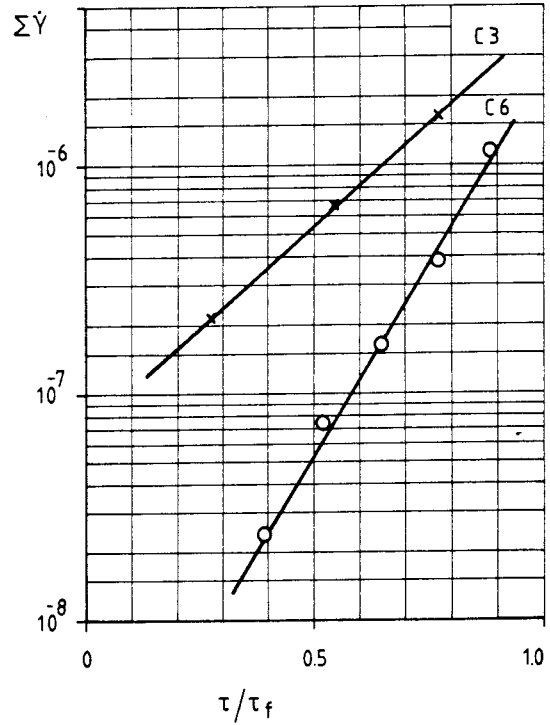
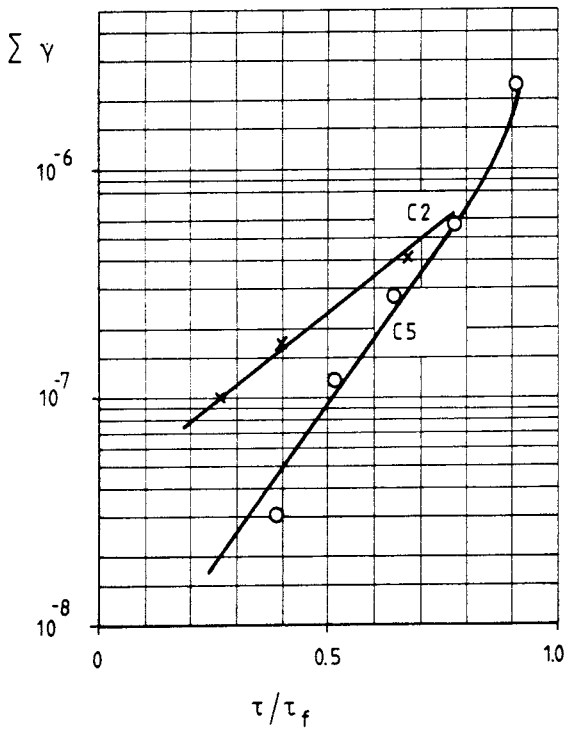
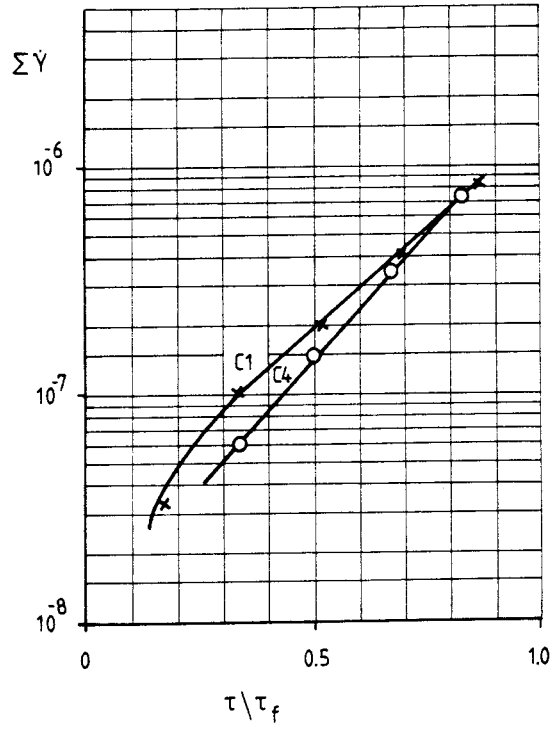


Fig 3.24. $\Sigma \dot{\gamma}$ as a function of τ/τ_f at the three different densities $\rho \approx 1.9$ (C1, C4) $\rho \approx 2.0$ (C2, C5) and $\rho \approx 2.1$ (C3, C6) and the two temperatures 22°C (C1-C3) and 40°C (C4-C6)

The creep theory by Pusch

Approximating the creep curves to be of the $n = -1$ type, Eq. (8) can be written in the following simplified manner:

$$dy/dt = B/(t+t_0) \quad (19)$$

where

$$B = A \cdot g(\tau, T) \quad (20)$$

If dy/dt is integrated we get

$$y = B \cdot \ln(t+t_0) + C \quad (21)$$

where C is the integration constant related to an initial time and t_0 a constant. t_0 is of no significance for longer creep periods but appears to be a determinant of the initial strain rate, which is in turn related to structural effects, such as cementation. B is the stress-related parameter that determines the long time creep properties. By a computer program the parameters B , C and t_0 can be determined and the corresponding strain-time curve can be plotted in the same diagram as the measured values. This is made in Fig. 3:25 where the solid lines originate from Eq. 21 with the parameters according to Table IX:

Table IX. Parameters from test C1

τ	B	C	t_0
30	$3.23 \cdot 10^{-4}$	$-3.74 \cdot 10^{-4}$	207
60	$6.43 \cdot 10^{-4}$	$-35.5 \cdot 10^{-4}$	3732
91	$9.67 \cdot 10^{-4}$	$-56.9 \cdot 10^{-4}$	1614
121	$25.7 \cdot 10^{-4}$	$-175 \cdot 10^{-4}$	1861
151	$60.9 \cdot 10^{-4}$	$-503 \cdot 10^{-4}$	5334

If we consider the important parameter B we can clearly see the dependence of the shear stress. ΣB seems to form a straight line as a function of τ/τ_f in a semi-logarithmic diagram in the same way as $\Sigma \dot{\gamma}$ in the previous evaluation. Fig. 3:26

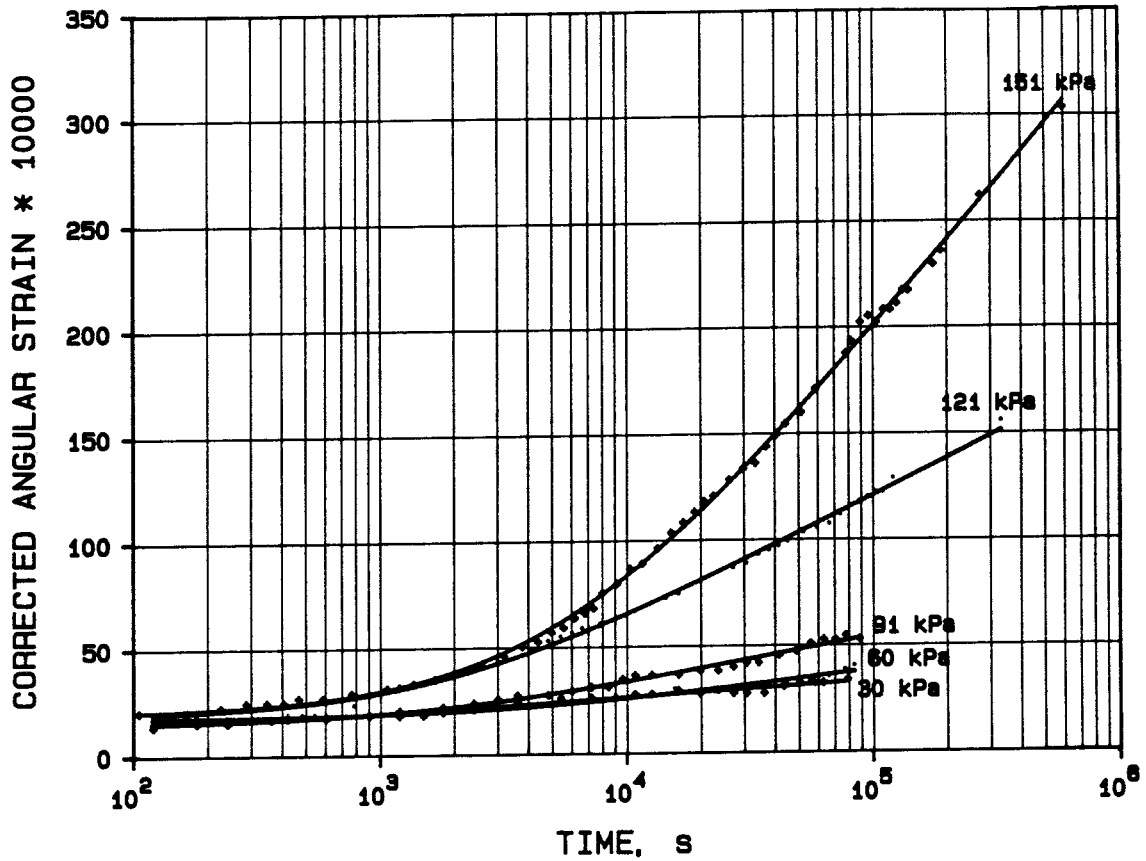


Fig 3.25. Creep curves from test C1 plotted in a logarithmic diagram. The strain-time curves evaluated according to Pusch are drawn as solid lines

shows these relations for tests C1-C6 and NC. The straight line can be described by the following function if B is taken from tests with only one loading:

$$\log B - \log B_o = \alpha \left(\frac{\tau}{\tau_f} - \frac{\tau_o}{\tau_f} \right) \quad (22)$$

which yields

$$B = B_o e^{-\alpha \tau_o / \tau_f} \cdot e^{\alpha \tau / \tau_f} \quad (23)$$

or

$$\dot{\gamma} = B_0 e^{-\alpha \tau_0 / \tau_f} \cdot e^{\alpha \tau / \tau_f} \frac{1}{t + t_0} \quad (24)$$

If B_0 is taken from $\tau_0 / \tau_f = 0.5$ we arrive at Eq. (25) for test C1 provided that

$$B_0 = 2.1 \cdot 10^{-3}, \alpha = 4.6, \tau_f = 175$$

$$\dot{\gamma} = 2.0 \cdot 10^{-4} \cdot e^{0.0263 \tau} \frac{1}{t + t_0} \quad (25)$$

It is, however, better to use Eqn. (24). The parameters from the tests C1-C6 and NC are shown in Table X.

Table X. The parameters in Eqn. (24) evaluated from the creep tests

Test	T °C	B_0	α	τ_f
C1	22	$2.0 \cdot 10^{-3}$	4.6	175
C4	40	$1.7 \cdot 10^{-3}$	4.5	180
C2	22	$4.0 \cdot 10^{-3}$	3.2	450
C5	40	$7.0 \cdot 10^{-3}$	7.9	460
C3	22	$1.5 \cdot 10^{-2}$	2.8	1100
C6	40	$4.3 \cdot 10^{-4}$	9.3	1200
NC	22	$4.0 \cdot 10^{-4}$	6.8	200

3.8.4 Long time creep tests

While the creep rates evaluated from tests C1-C3 at room temperature indicate that the value of n deviates from -1, it was not clear if this would hold also for longer creep periods. Therefore, a long time creep test in the shear box was performed. To compare the results from the shear box tests with a different testing

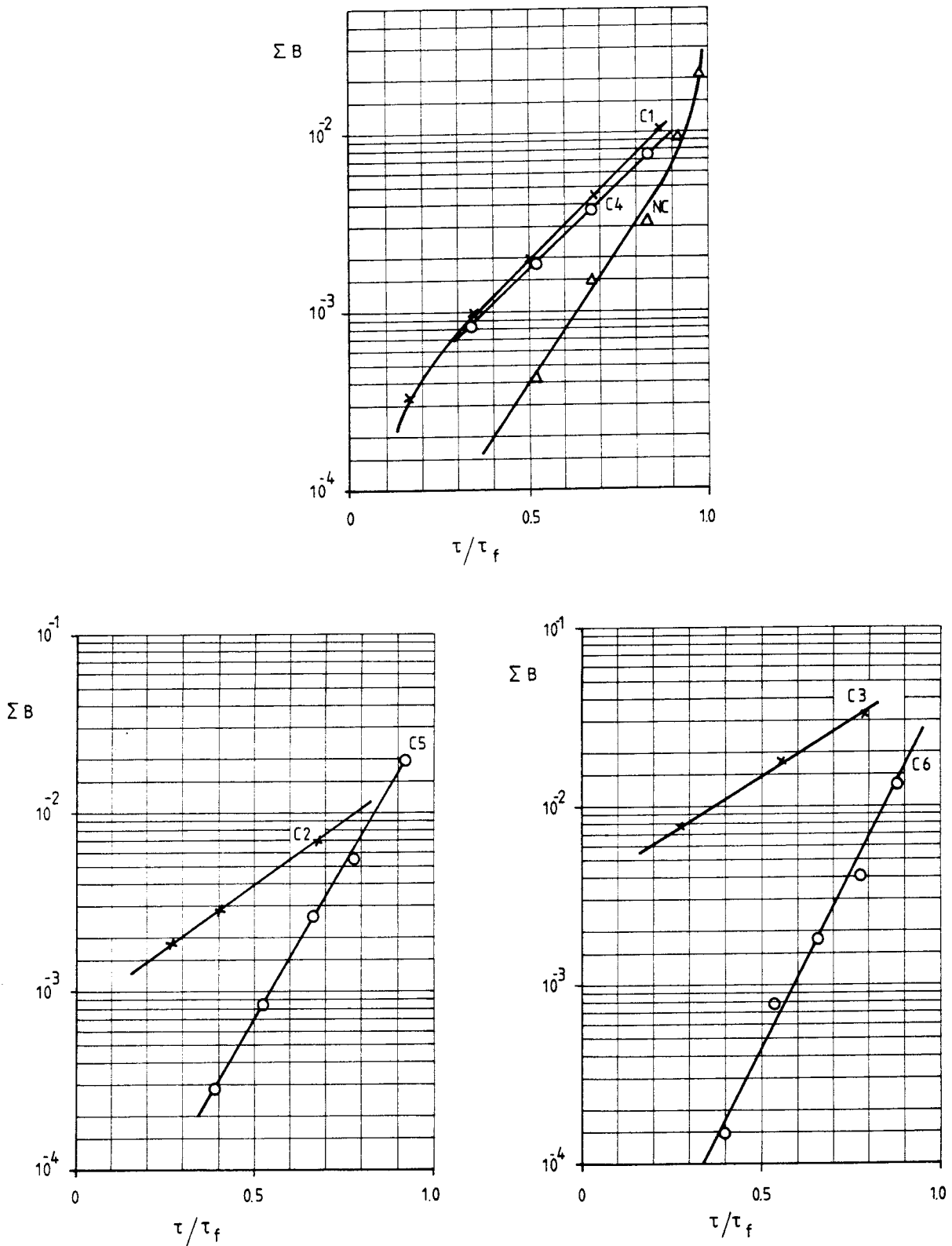


Fig 3.26. ΣB as a function of τ/τ_f at the three different densities $\rho \approx 1.1$ (C1, C4), $\rho \approx 2.0$ (C2, C5) and $\rho \approx 2.1$ (C3, C6) and the two temperatures 22°C (C1-C3) and 40°C (C4-C6). The results from the test on the natural clay (NC) is also plotted

technique a long time creep test using a triaxial cell was also performed. Data from the tests are given in Table XI.

Table XI. Data from the long time creep tests

Test	ρ t/m ³	σ kPa	Load kPa	τ/τ_f
Shear box	2.08	$9.0 \cdot 10^3$	$\tau = 316$	0.29
Triaxial	1.64	25.6	$\sigma_1 - \sigma_2 = 27$	0.72

The strain and strain rate as a function of time for the two tests are plotted in Fig 3:27 and Fig 3:28. The inclination of the strain rate in the double logarithmic diagram is $n = -0.75$ at the triaxial creep and $n = -0.84$ at the shear box creep. These values support the conclusion from tests C1-C3 and show that $n \approx -0.8$ at room temperature. However at 40°C, as shown by tests C4-C6, $n \approx -1.0$ although the scatter is wide.

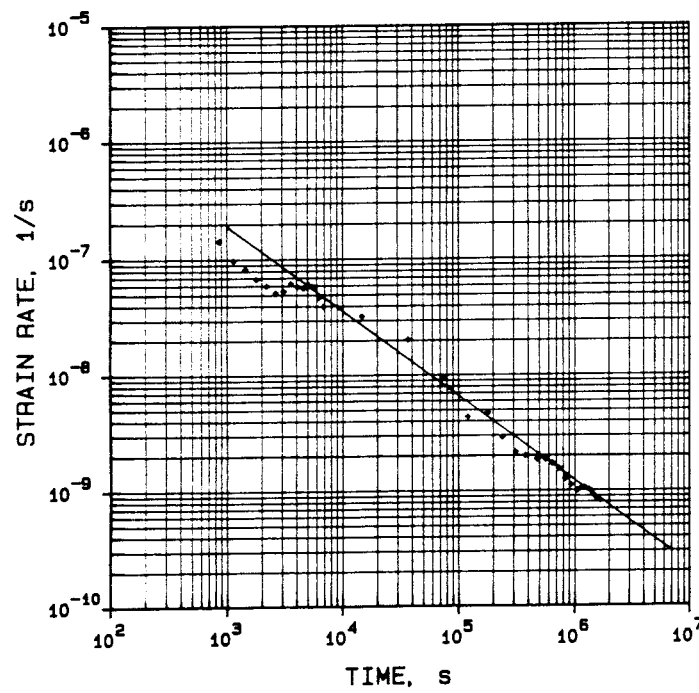
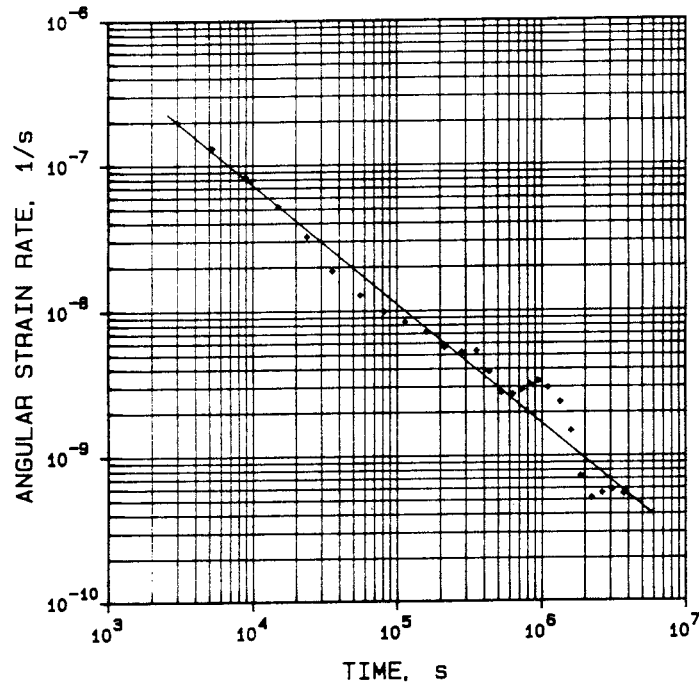


Fig 3.27.

Strain rate as a function of time at the long time creep tests using the shear box (above) and the triaxial cell (below)

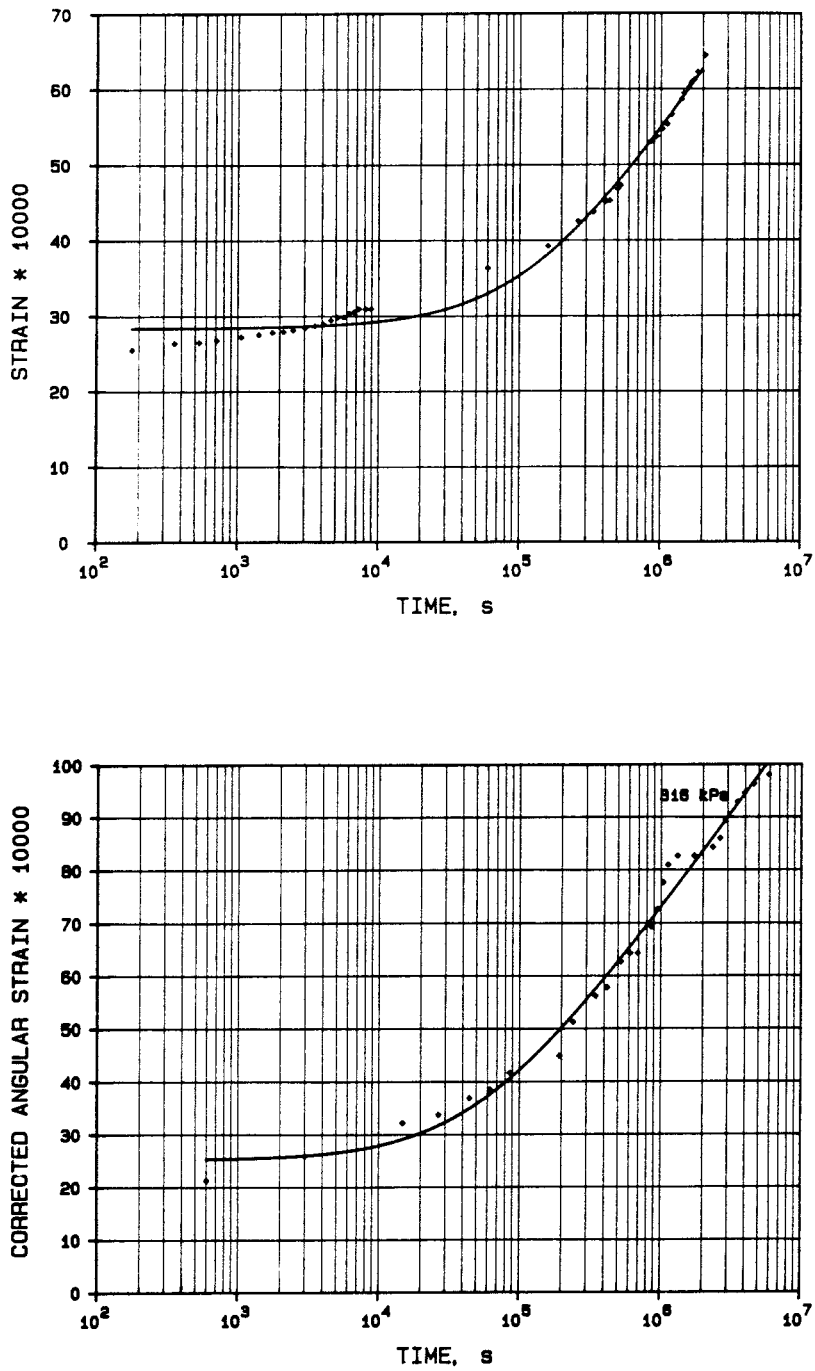


Fig 3.28. Strain as a function of time at the long time creep test using the shear box (above) and the triaxial cell (below). The adaption according to Eq. 21 is also drawn

4 CONCLUSIONS AND REMARKS

4.1 General

The rheological and physical properties of the investigated clay are very similar to the properties of natural and sodium-processed calcium bentonite at densities exceeding $\rho_m = 2.0 \text{ t/m}^3$. At lower densities the swelling pressure, the hydraulic conductivity and especially the swelling potential differ quite a lot. The reason for this is probably that the microstructural difference between a Na- and a Ca-smectite is very small at densities $\rho_m > 2.0 \text{ t/m}^3$. The high density means that there will be space enough for only one or two water molecule layers and the amount of free water and thus the difference in structure will be small.

4.2 Permeability

The permeability of the investigated clay is very low. It varies between $k = 2.8 \cdot 10^{-12}$ and $k = 1.2 \cdot 10^{-14}$ for the density range $\rho_m = 1.7\text{-}2.1 \text{ t/m}^3$ which is in the same order of magnitude as for Na-bentonite.

4.3 Non-saturated flow

The rate of water uptake of a confined unsaturated sample can be modelled in an identical way as the Na-bentonite Mx-80. Under low hydraulic gradient ($i < 1000$) the flow of water can be calculated according to the equation of diffusion (Eq. 3) using a coefficient of diffusion $D = 2 \cdot 10^{-10} \text{ m}^2/\text{s}$.

4.4 Swelling potential

The swelling potential of the investigated clay corresponds to the swelling potential of a mixture of 30% Mx-80 and 70% ballast material. At the density $\rho_m = 2.1 \text{ t/m}^3$ the swelling potential is exceeding 50%.

4.5 Swelling pressure

The swelling pressure is a function of the density. It can be calculated from the following relation:

$$\sigma_s = 3.7 \cdot e^{\frac{\rho_m - 2.0}{0.081}} \quad (4)$$

The swelling pressure is between 50 and 100% of the swelling pressure of MX-80 at densities between 1.65 t/m³ and 2.1 t/m³.

4.6 Stress-strain properties

The stress/strain properties measured by the triaxial tests and shear tests can be described by the following three states:

- 1 Between 0 and 0.5% strain the clay behaves in a stiff elastic way up to about 50% of the shear strength
- 2 Between 0.5 and 5% strain the clay is plasticizing under strain hardening
- 3 After 5% strain the material is ideally plastic

At room temperature there is no brittle behavior except for at very low densities ($\rho_m < 1.7$ t/m³).

At 60°C. there is an increased shear strength by 10 - 30 % yielding also brittle conditions. The residual strength is equal to the strength at room temperature.

The difference in stress-strain behavior at drained and undrained conditions is insignificant especially at high densities.

4.7 Strength properties

The shear strength is a function of the swelling pressure. The relation can be approximated by Mohr-Coloumb's parameters in the following way:

σ_s kPa	c kPa	ϕ deg
<200	0	20
>200	50	5

The influence of heating the samples is as mentioned in Chapter 4.6 an increased strength by 10 - 30 % at a temperature of 60°C compared to 20°C.

4.8 Influence of strain-rate on the strength

An increased strain rate increases the shear strength according to Eq. (7):

$$\tau_f = m \cdot \left(\frac{\dot{\gamma}}{\dot{\gamma}_0} \right)^n \quad (7)$$

The values of m and n where determined on a sample with the density $\rho_m = 1.84$ t/m³ giving

$$m = 100 \text{ kPa}$$

$$n = 0.036$$

at the reference rate $\dot{\gamma}_0 = 1.0$ 1/s

The rate dependance is thus quite low and in the same order of magnitude as of many other clays.

4.9 Creep tests

The creep of this clay can be modelled by Eq. (16) at $0.1 < \tau/\tau_f < 0.9$:

$$\dot{\gamma} = \dot{\gamma}_0 \cdot e^{\alpha \frac{\tau}{\tau_f}} \cdot e^{-\alpha \frac{\tau_0}{\tau_f}} \cdot \left(\frac{t}{t_r} \right)^n \quad (16)$$

This equation describes the influence of time after start (t) and the applied shear stress (τ). Also the influence of the temperature is indirectly accounted for by the values of the parameters α , γ_0 and τ_f .

The parameter n regulating the change in creep rate was found to be $n \approx -0.8$ at room temperature while at 40°C . it seems to be close to -1.0 .

The parameters $\dot{\gamma}_0$ and α are varying a little with temperature and density, the average values being

$$\dot{\gamma}_0 = 2.1 \cdot 10^{-7} \text{ 1/s}$$

$$\alpha = 5.2$$

putting

$$t_0 = 10^4 \text{ s}$$

$$\tau_0 = 0.5 \cdot \tau_f$$

The creep can also be modelled by Eq. (24):

$$\dot{\gamma} = B_0 e^{-\alpha \tau_0 / \tau_f} \cdot e^{\alpha \tau / \tau_f} \frac{1}{t + t_0} \quad (24)$$

Eq. (24) is similar to Eq. (16) but requires that $n = 1$ after a long time. The tests made in this investigation implies that this is only the case at temperatures around 40°C .

The parameters B_0 and α vary with the applied shear stress and temperature in a similar way as $\dot{\gamma}_0$ and α in Eq. (16.) The average values are

$$B_0 = 5.0 \cdot 10^{-3}$$

$$\alpha = 5.4$$

putting

$$\tau_0 = 0.5 \cdot \tau_f$$

The influence on the parameters in Eqs. (16) and (24) when applying the load in one step in stead of applying it stepwise is not yet fully cleared. Ongoing research work is investigating this matter.

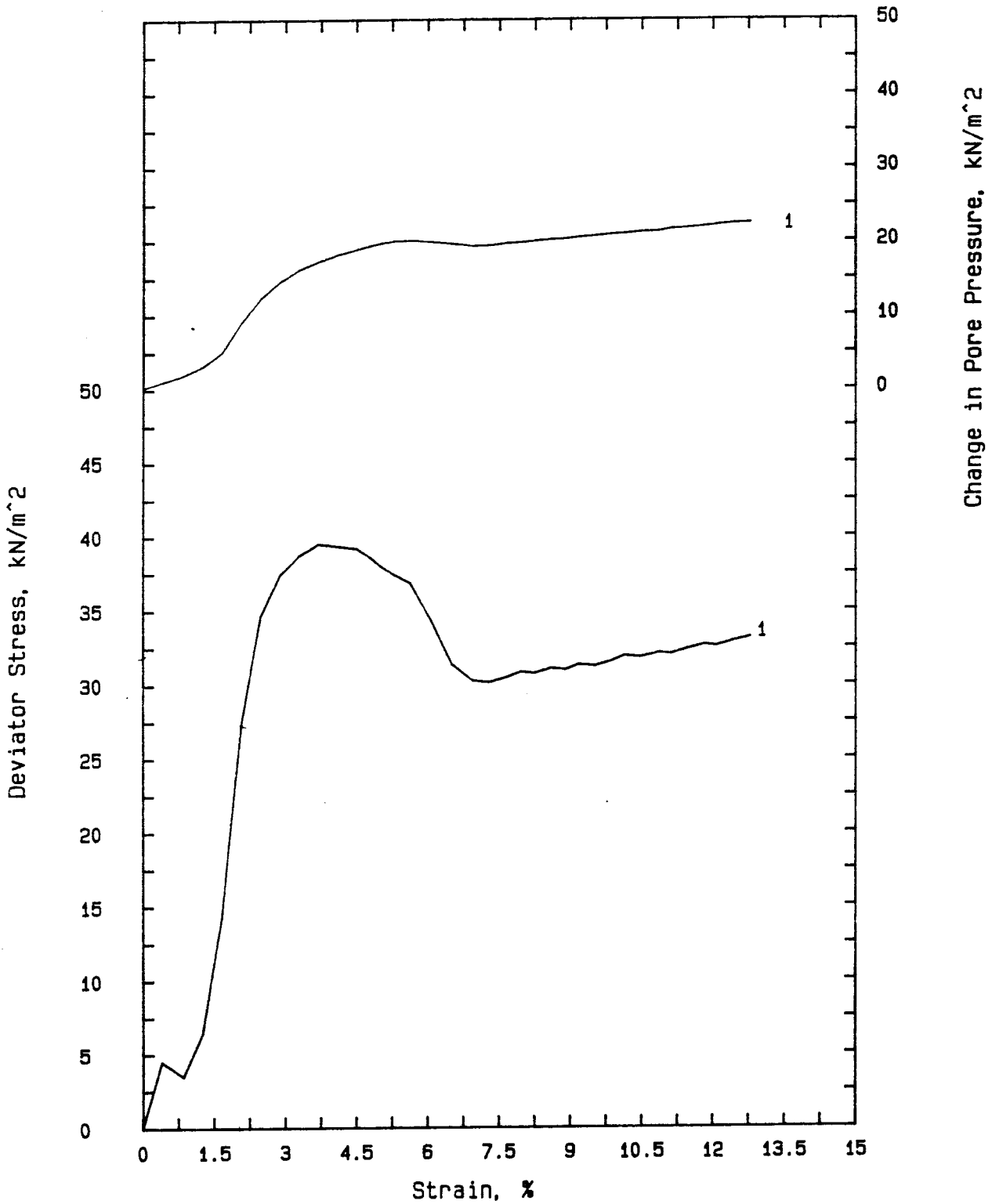
5 REFERENCES

- 1 Börgesson, L. 1985. Water flow and swelling pressure in non-saturated bentonite-based clay barriers. *Eng. Geol.*, 21:229-237
- 2 Börgesson, L. & Stenman, U. 1985. Laboratory determined properties of sand/bentonite mixtures for WP-cave. Internal report SGAB IRAP 85511
- 3 Börgesson, L. 1986. Model shear tests of canisters with smectite clay envelopes in deposition holes. SKB Technical Report 86-26
- 4 Lambe, T.W. & Whitman, R.V. 1969. *Soil Mechanics*. John Wiley & Sons, Inc.
- 5 Larsson, R. 1977. Basic behaviour of Scandinavian soft clays. SGI Report No 4
- 6 Pusch, R. 1980. Swelling pressure of highly compacted bentonite. SKBF/KBS Technical Report 80-13
- 7 Pusch, R. 1983. Use of clays as buffers in radioactive repositories. SKBF/KBS Technical Report 83-46
- 8 Pusch, R. 1986. Settlement of canisters with smectite clay envelope in deposition holes. SKB Technical Report 86-23
- 9 Pusch, R., Börgesson, L. & Erlström, M. 1987. Alteration of isolation properties of dense smectite clay in repository environment as exemplified by seven pre-quatarnary clays. SKB Technical Report 87-29
- 10 Singh, A. & Mitchell, J.K. 1968. General stress-strain-time function for soils. *American Society of Civil Engineers, Proceedings*, Vol. 94, No SM1

APPENDIX A

Results from the triaxial tests T1 - T12

CONSOLIDATED UNDRAINED TRIAXIAL COMPRESSION TEST

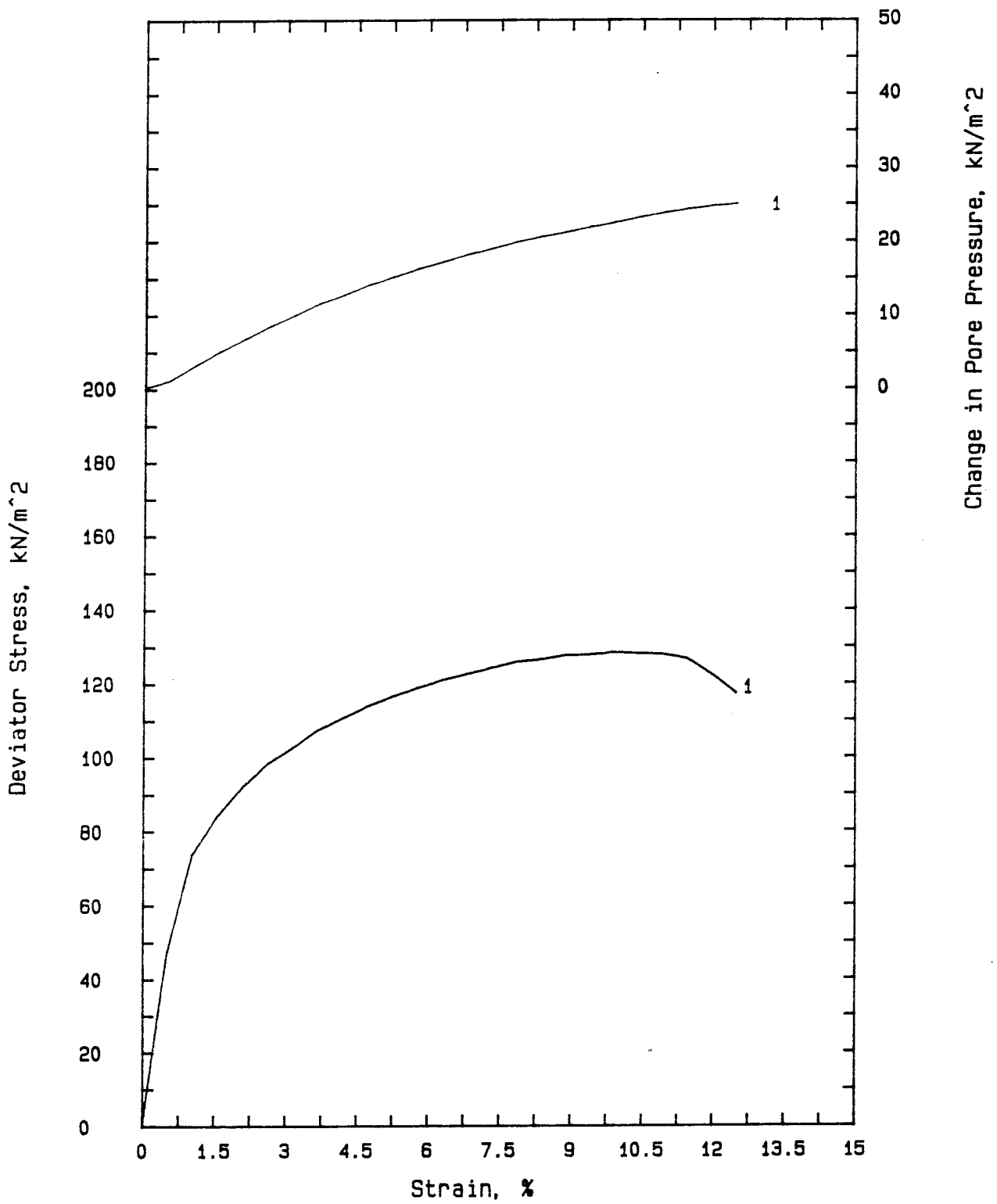


Report: FRENCH CLAY
Density: 1.65 g/cm³

Sample: T1
Rate: 0.6 %/h

SGAB SWEDISH GEOLOGICAL

CONSOLIDATED UNDRAINED TRIAXIAL COMPRESSION TEST

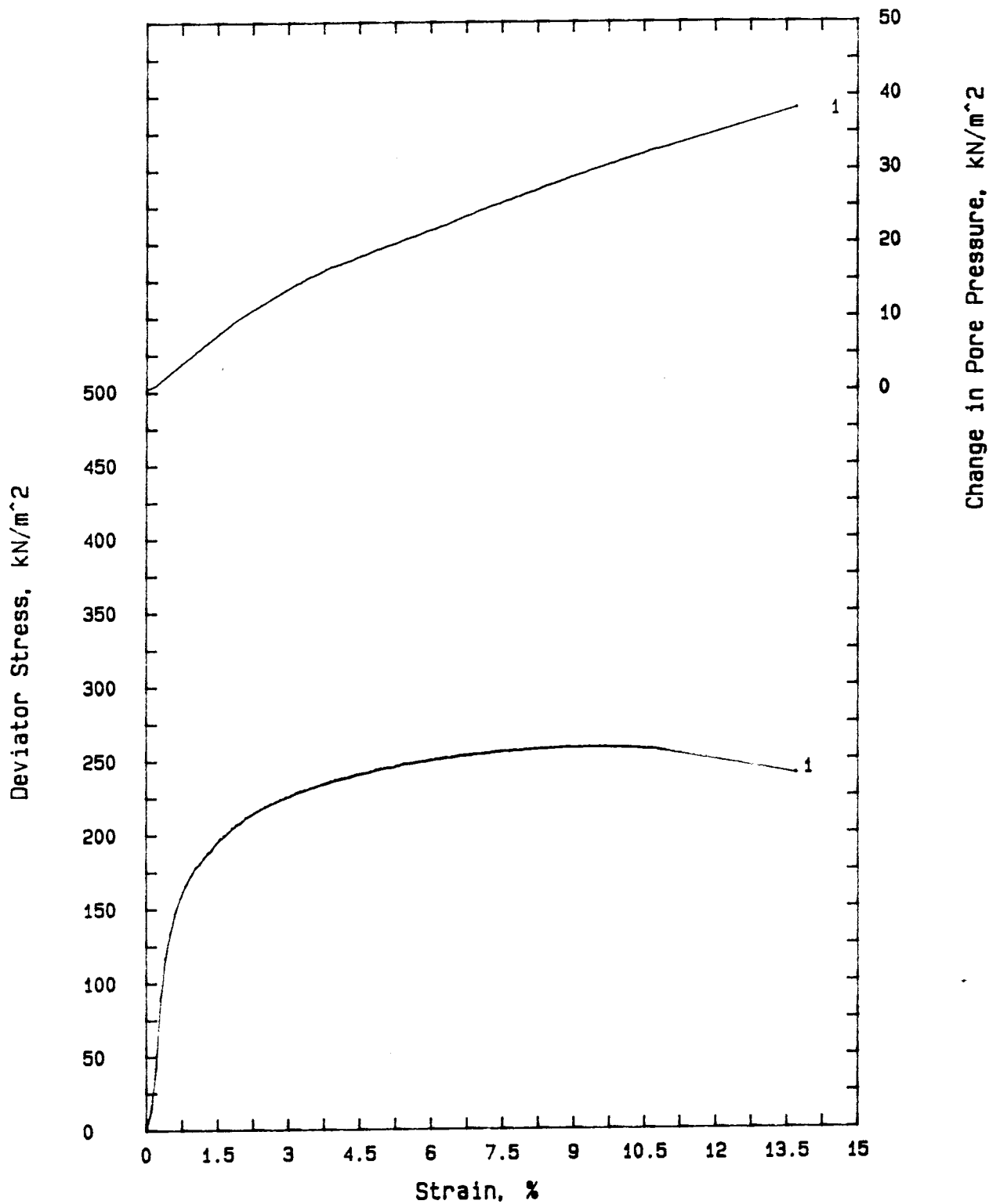


Report: FRENCH CLAY
Density: 1.79 g/cm³

Sample: T2
Rate: 0.6 %/h

SGAB SWEDISH GEOLOGICAL

CONSOLIDATED UNDRAINED TRIAXIAL COMPRESSION TEST

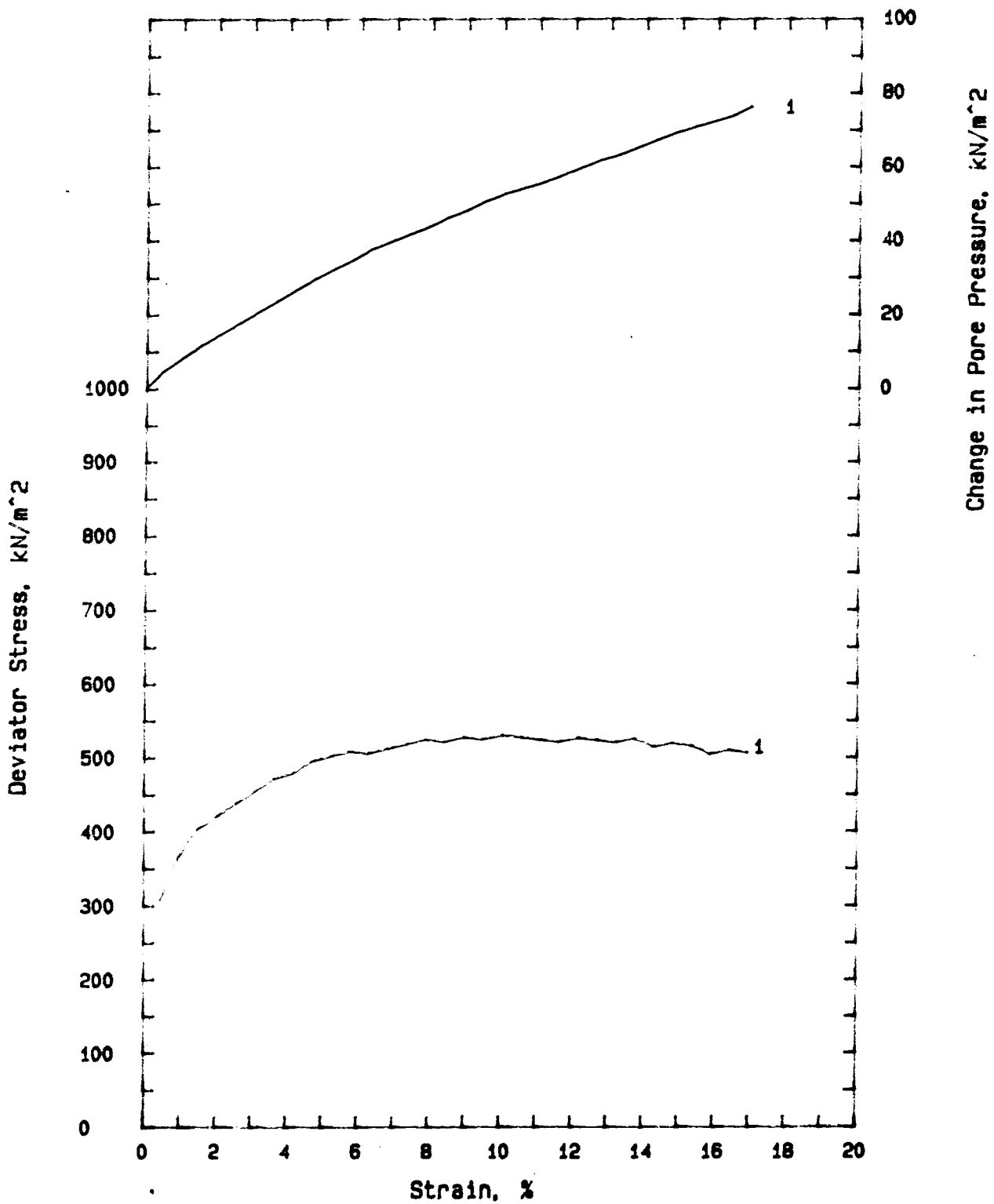


Report number: FRENCH CLAY

Sample number: T3

SGAB SWEDISH GEOLOGICAL

CONSOLIDATED UNDRAINED TRIAXIAL COMPRESSION TEST

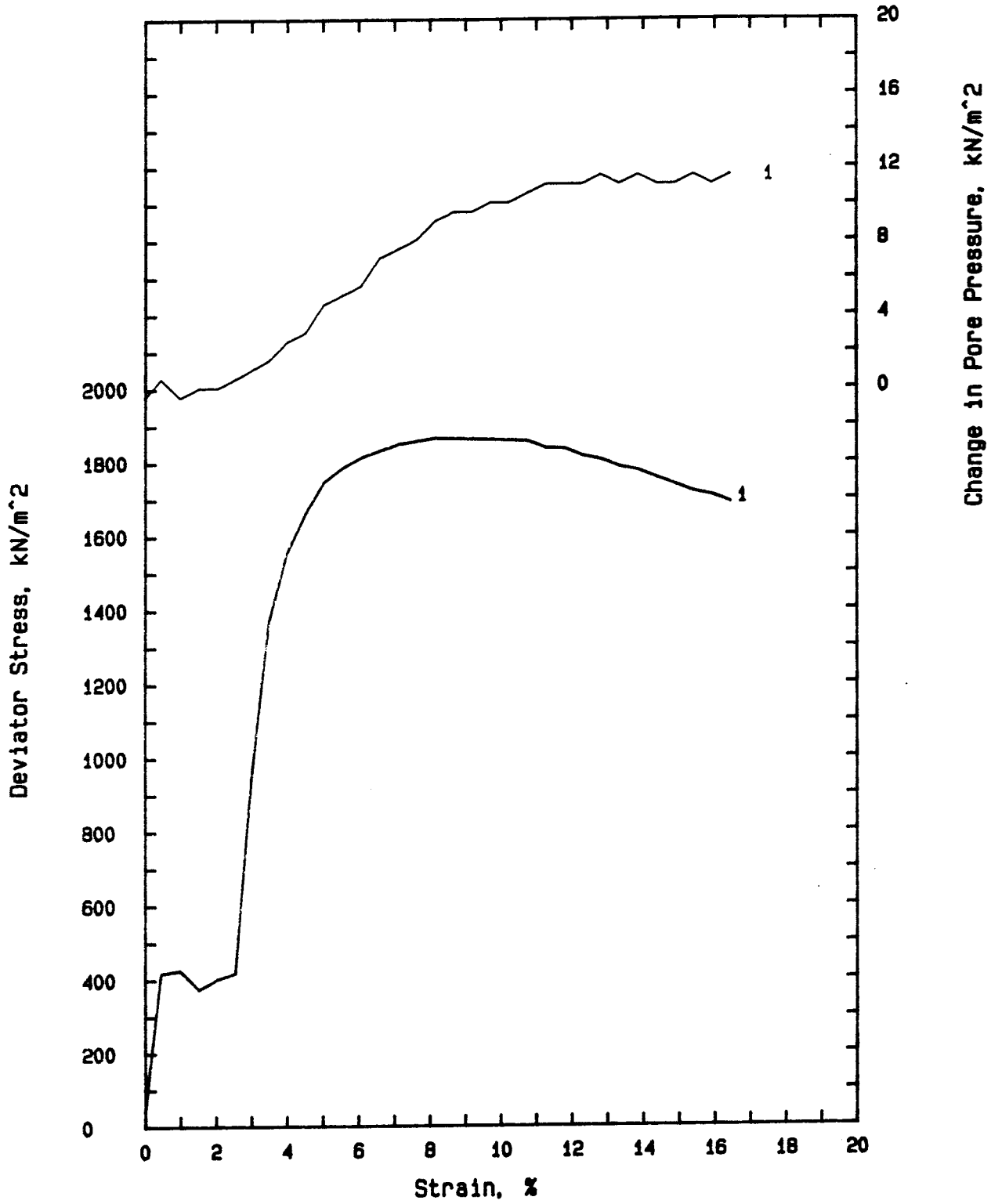


Report number: FRENCH CLAY
DENS=1.98

Sample number: T4

Swedish Geological, SGAB

CONSOLIDATED UNDRAINED TRIAXIAL COMPRESSION TEST

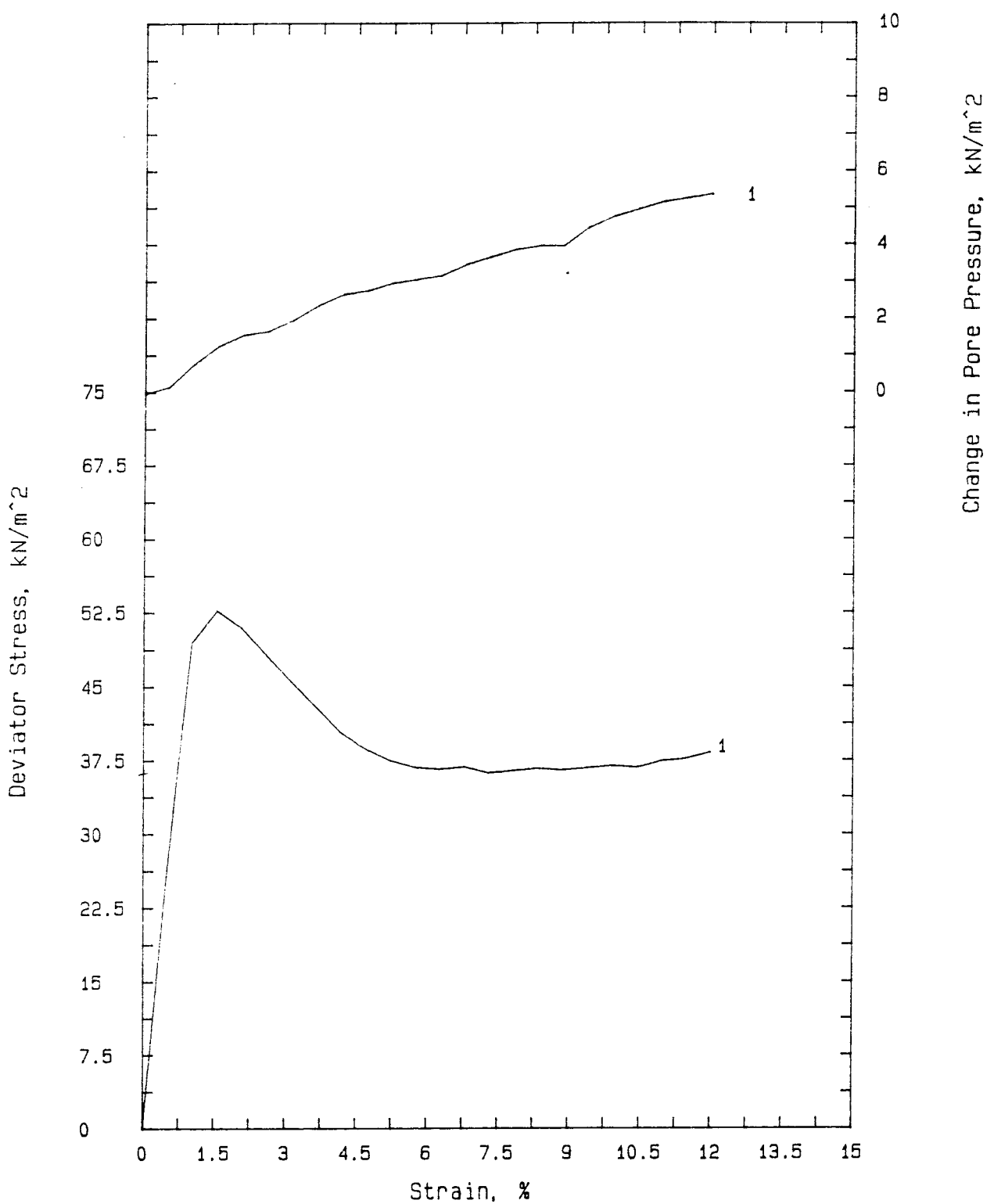


Report number: FRENCH CLAY
DENS=2.06

Sample number: T5

Swedish Geological, SGAB

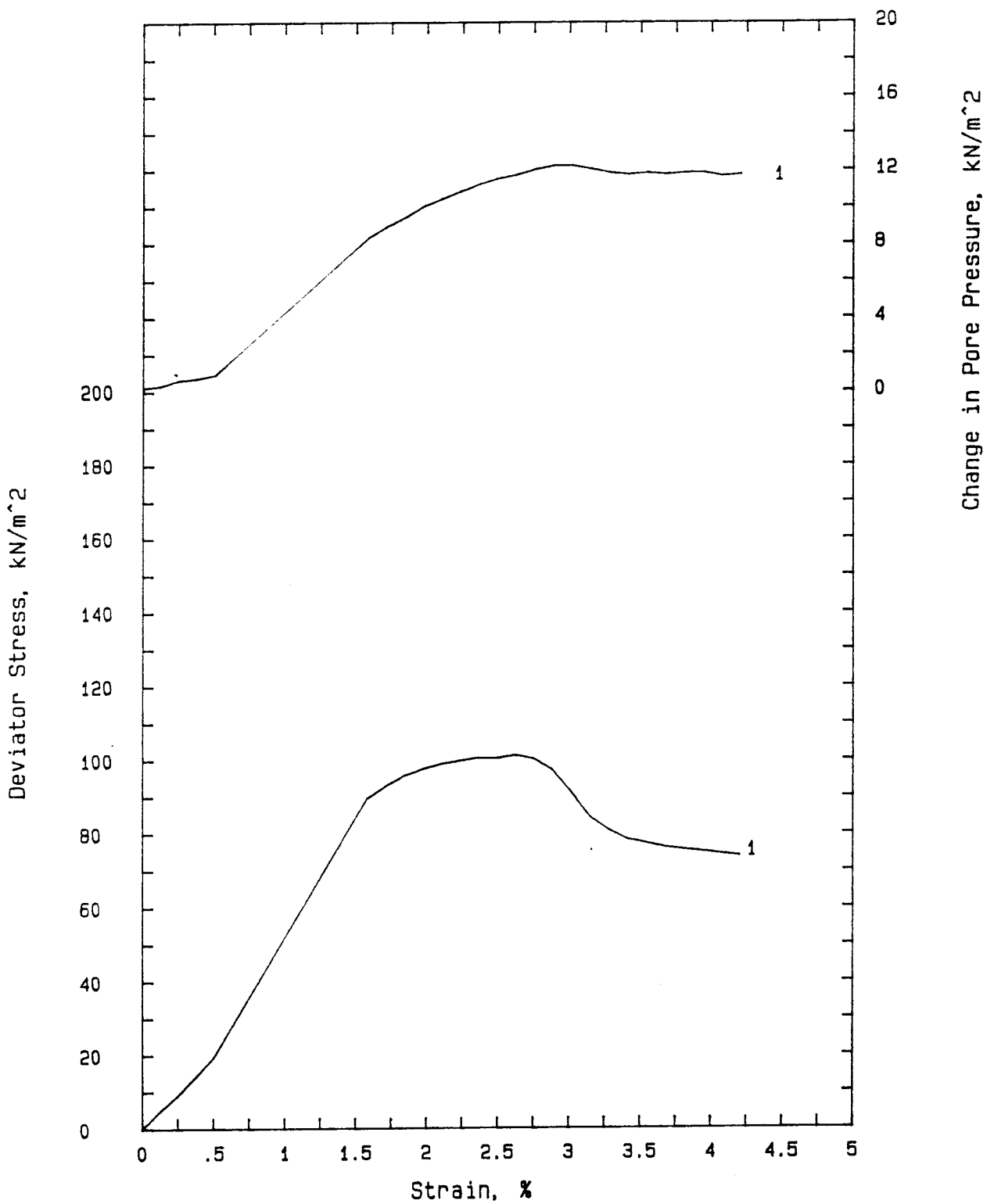
CONSOLIDATED UNDRAINED TRIAXIAL COMPRESSION TEST



Report : FRENCH CLAY T6
Density : 1.64 g/cm^3

Temperature: 60 DEGR C
Rate: 0.6 %/h

CONSOLIDATED UNDRAINED TRIAXIAL COMPRESSION TEST

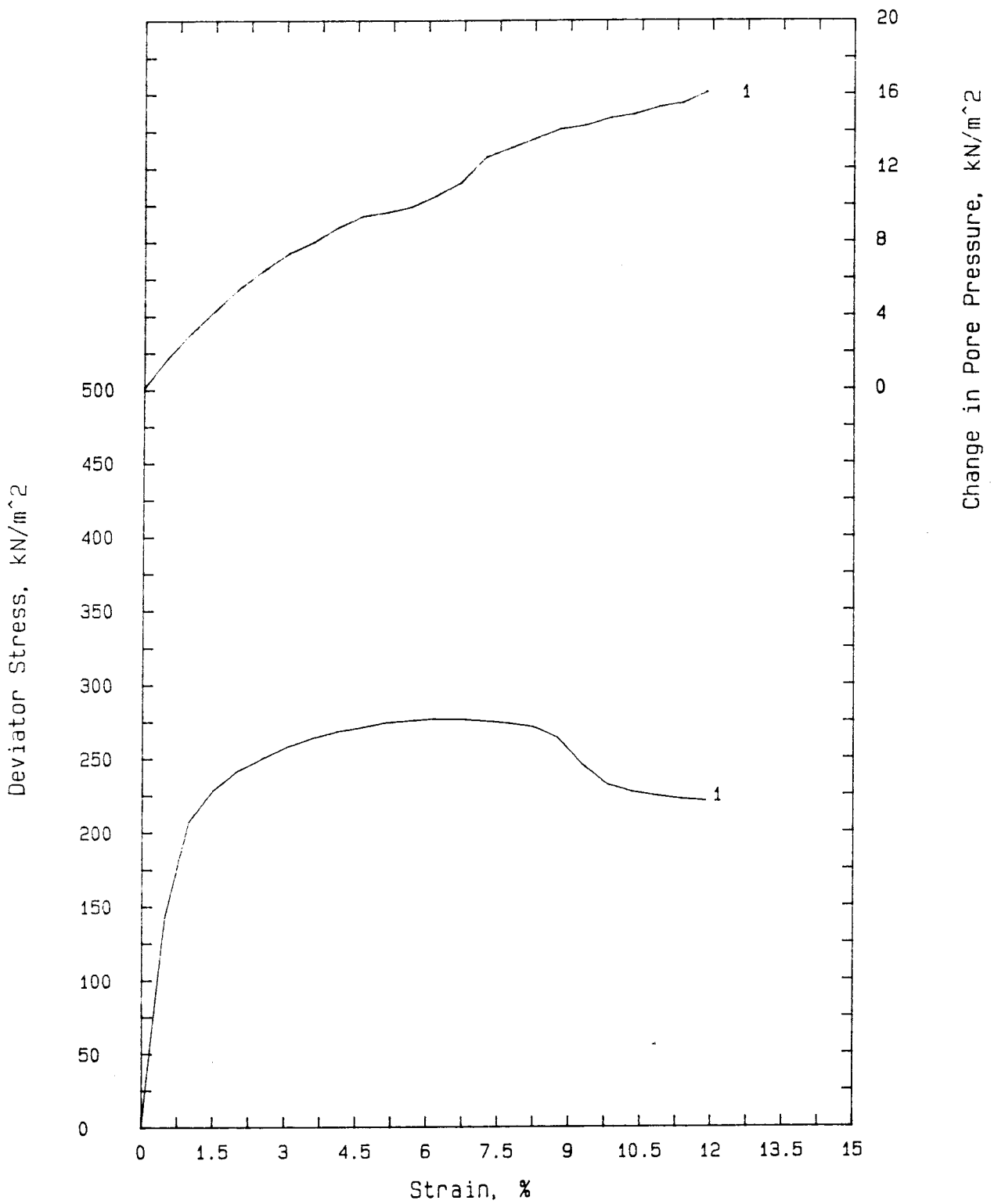


Report : FRENCH CLAY T7
Temperature: 60 DEGR C

Density: 1.77 g/cm^3
Rate: 0.6 %/h

SGAB SWEDISH GEOLOGICAL

CONSOLIDATED UNDRAINED TRIAXIAL COMPRESSION TEST

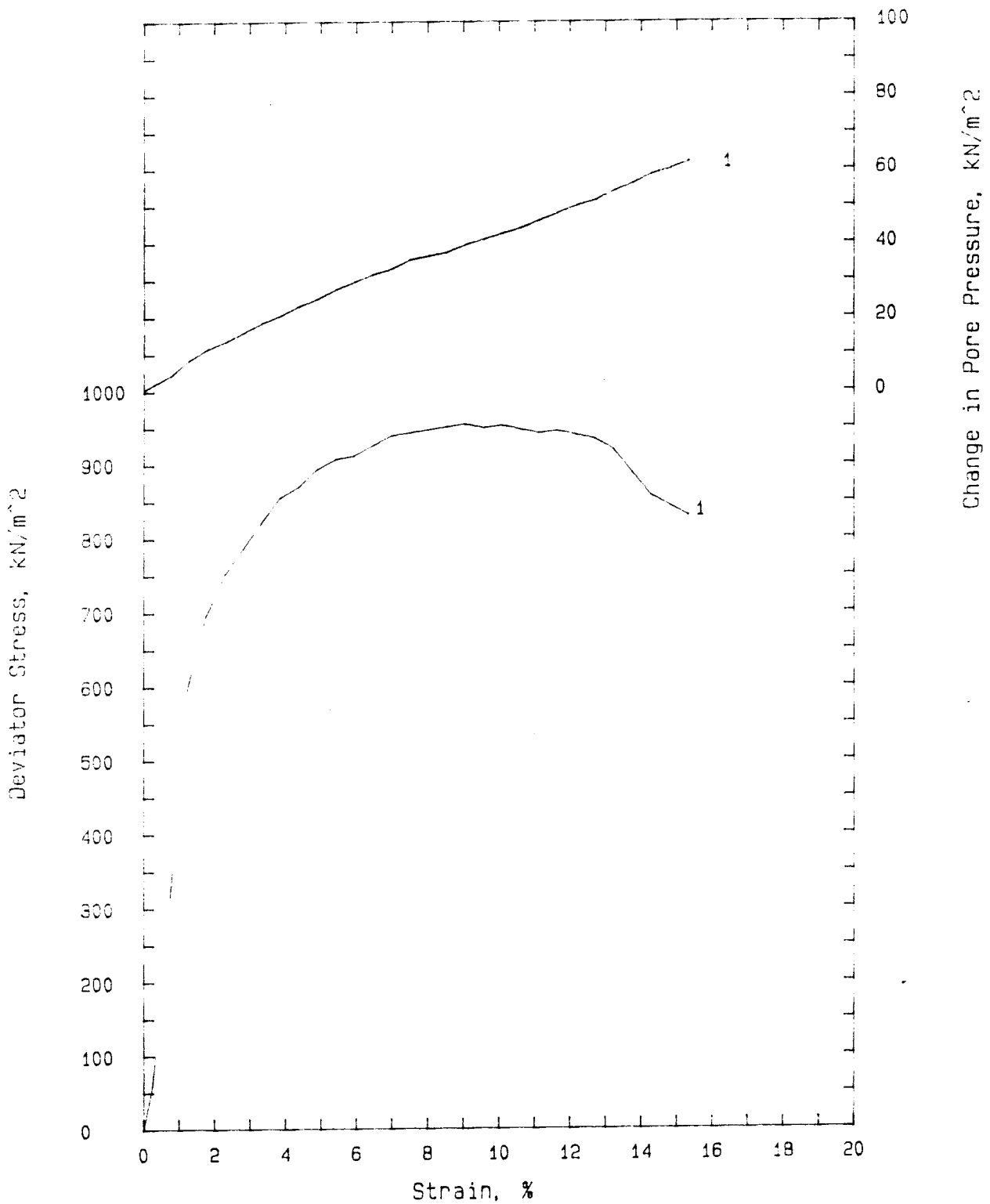


Report : FRENCH CLAY T8
Temperature : 60 DEGR C

Density: 1.89 g/cm³
Rate: .6 %/h

SGAB SWEDISH GEOLOGICAL

CONSOLIDATED UNDRAINED TRIAXIAL COMPRESSION TEST

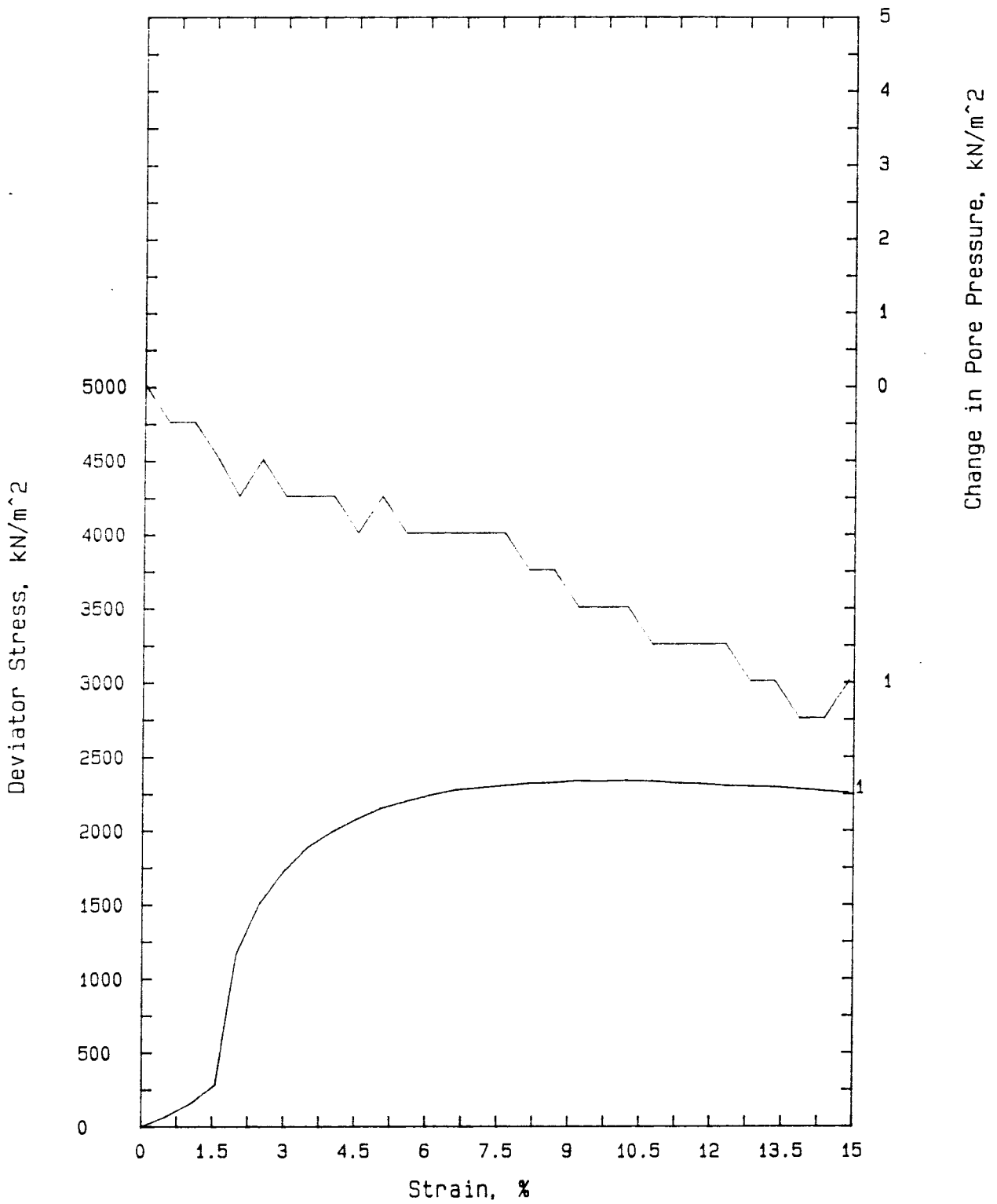


SAMPLE : FRENCH CLAY T9
CELL P : 4830 kPa

DENSITY : 2.00 g/cm³
RATE - TEMP : 0.6 %/h - 60 DEGR C

SGAB SWEDISH GEOLOGICAL

CONSOLIDATED UNDRAINED TRIAXIAL COMPRESSION TEST

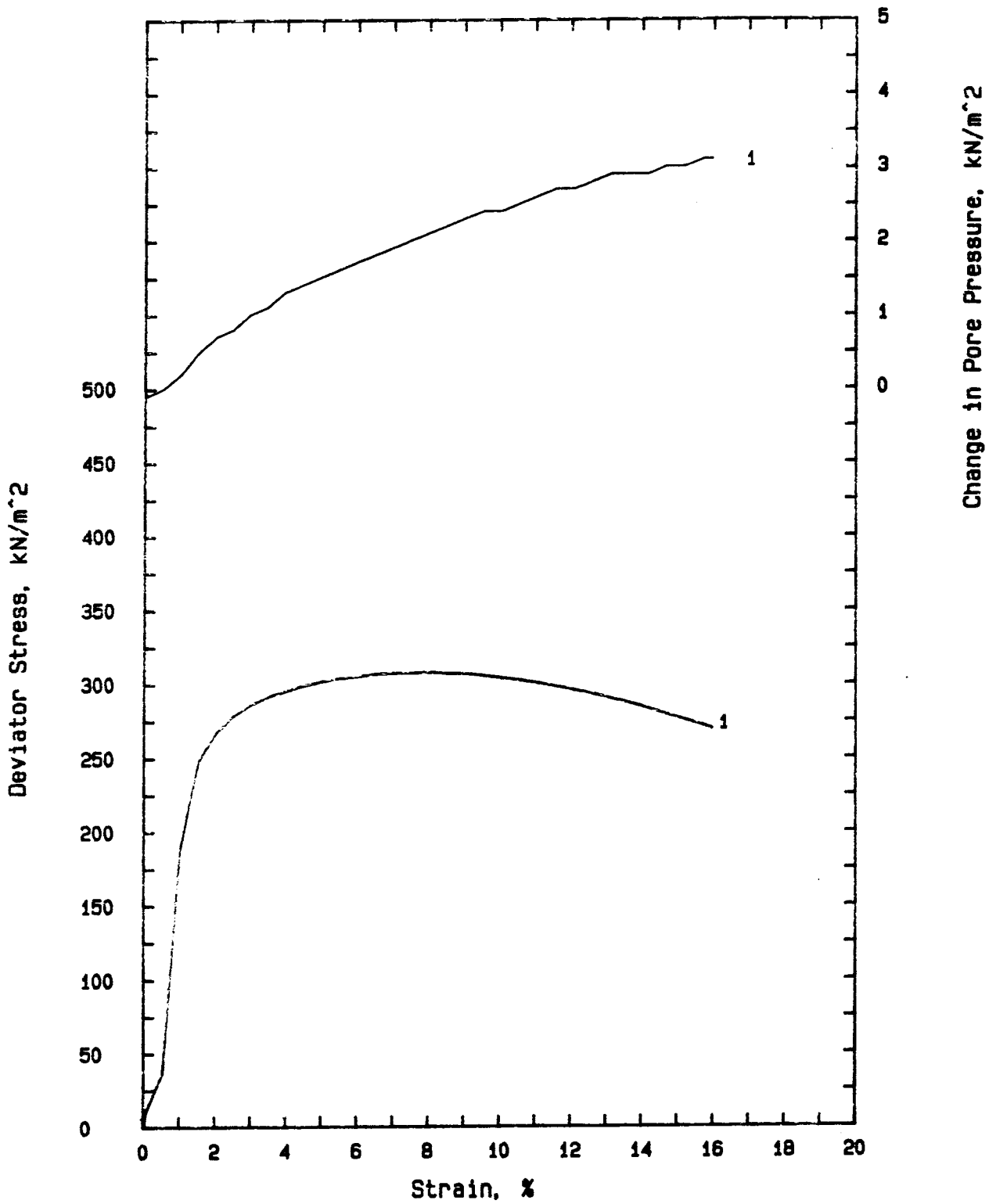


Report : FRENCH CLAY
Density : 2.14 g/cm^3

Sample number: T 10 A
Rate: .6 %/h

SGAB SWEDISH GEOLOGICAL

CONSOLIDATED UNDRAINED TRIAXIAL COMPRESSION TEST

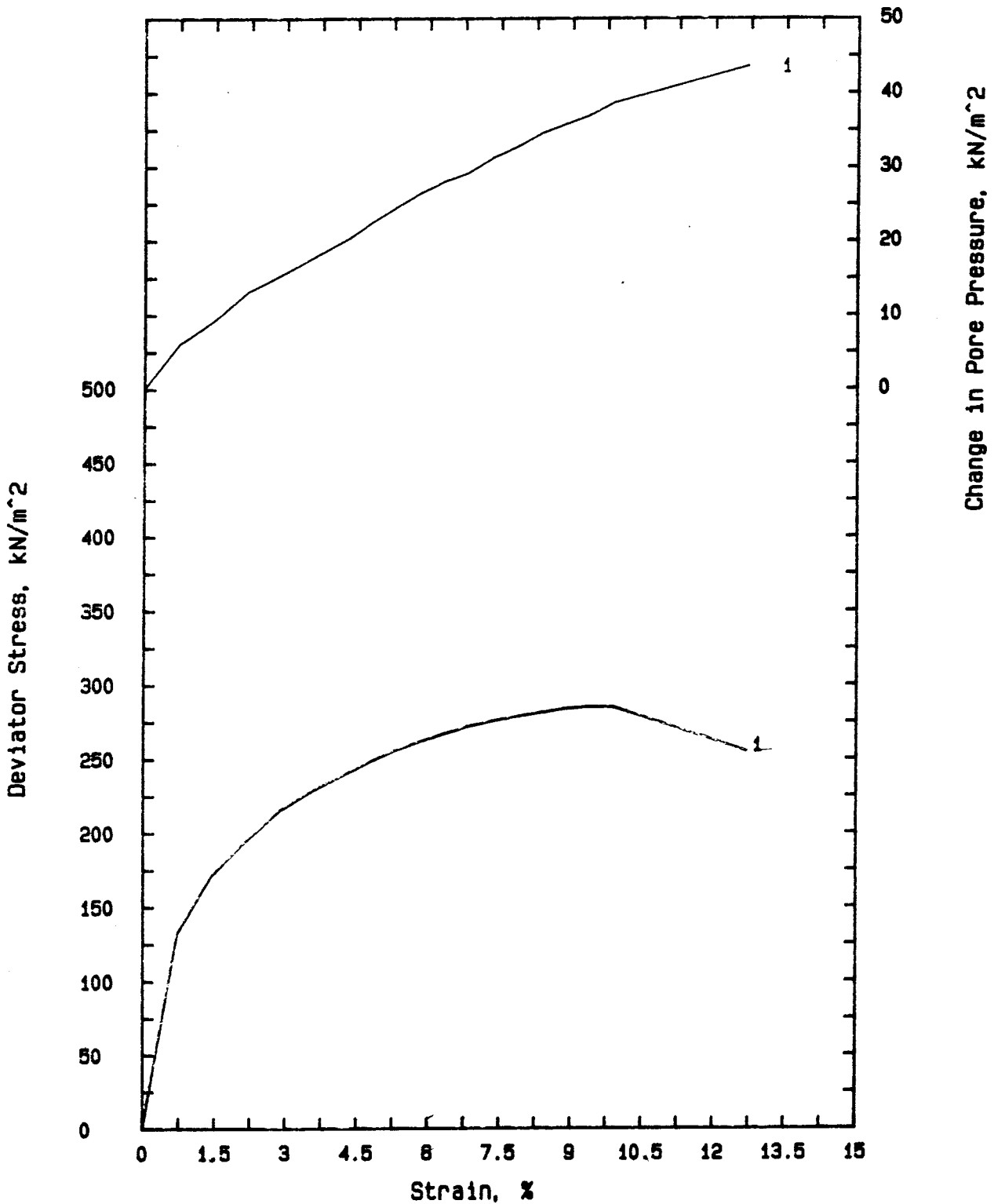


Report : FRENCH CLAY
Density : 1.90 g/cm³

Sample number: T11
Rate: 60 %/h

SGAB SWEDISH GEOLOGICAL

CONSOLIDATED UNDRAINED TRIAXIAL COMPRESSION TEST



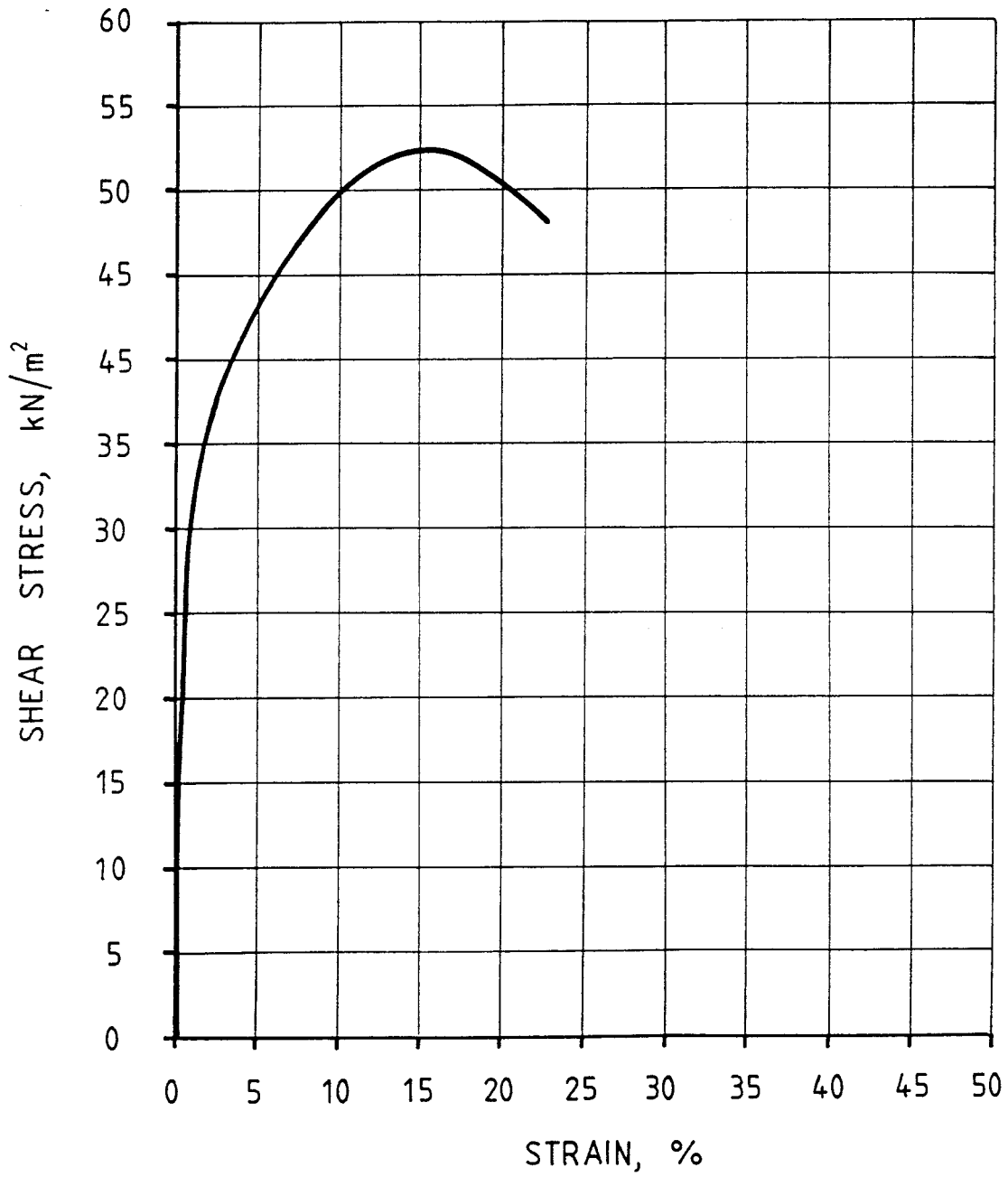
Report number: FRENCH CLAY
Density: 1.85 g/cm³

Sample number: T12
Rate: 0.06 %/h

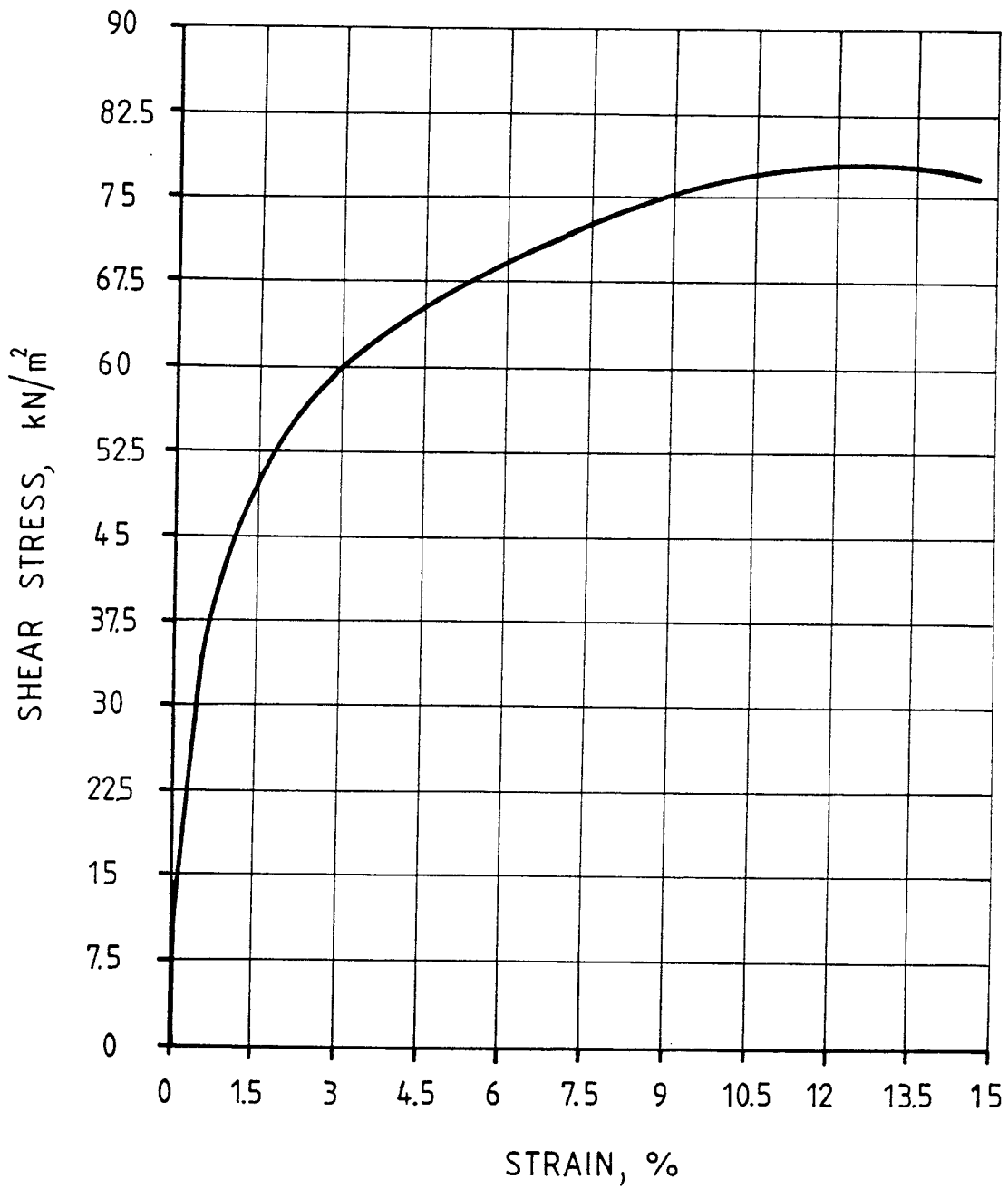
Swedish Geological, SGAB

APPENDIX B

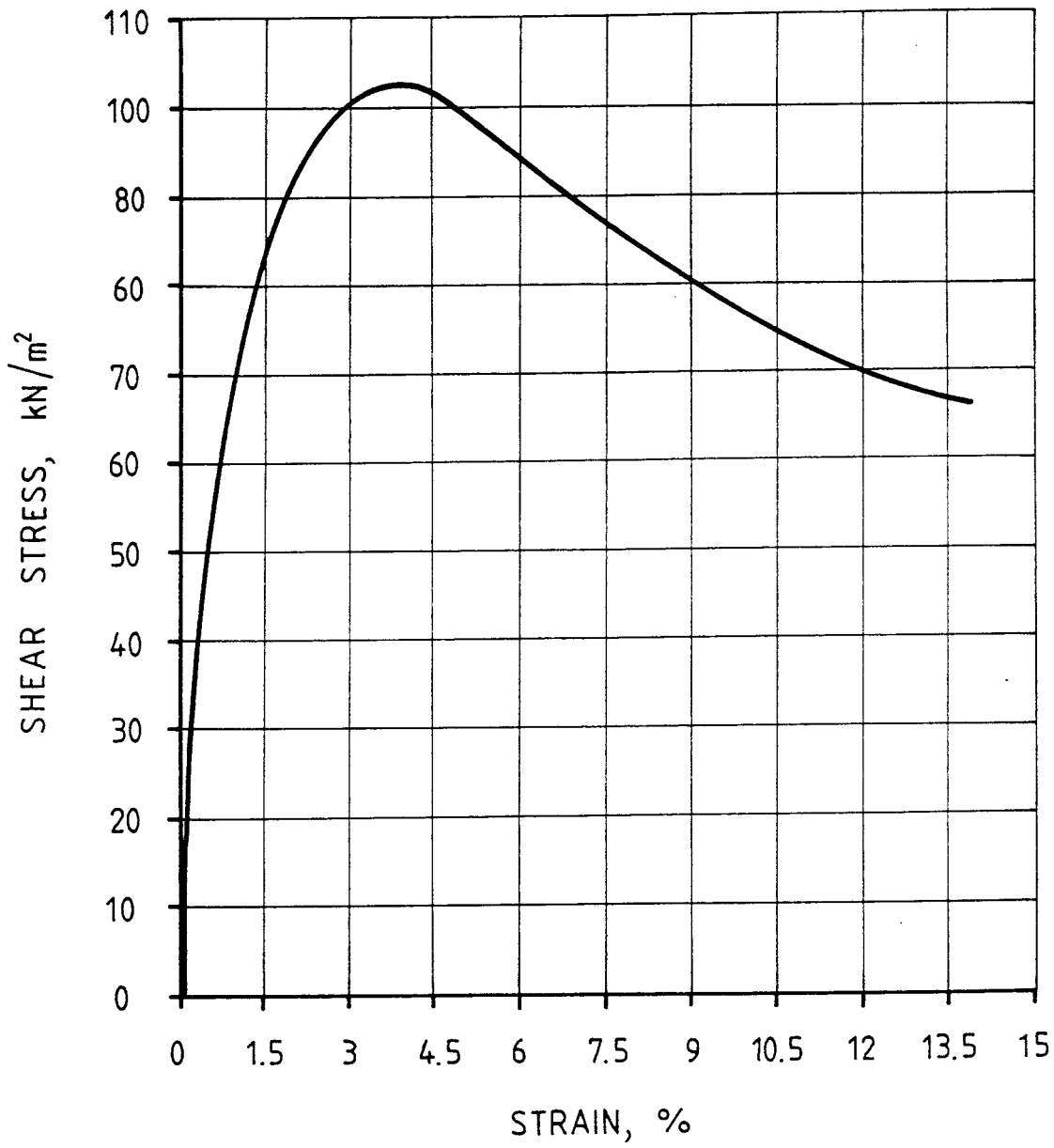
Results from the shear tests S1 - S 10



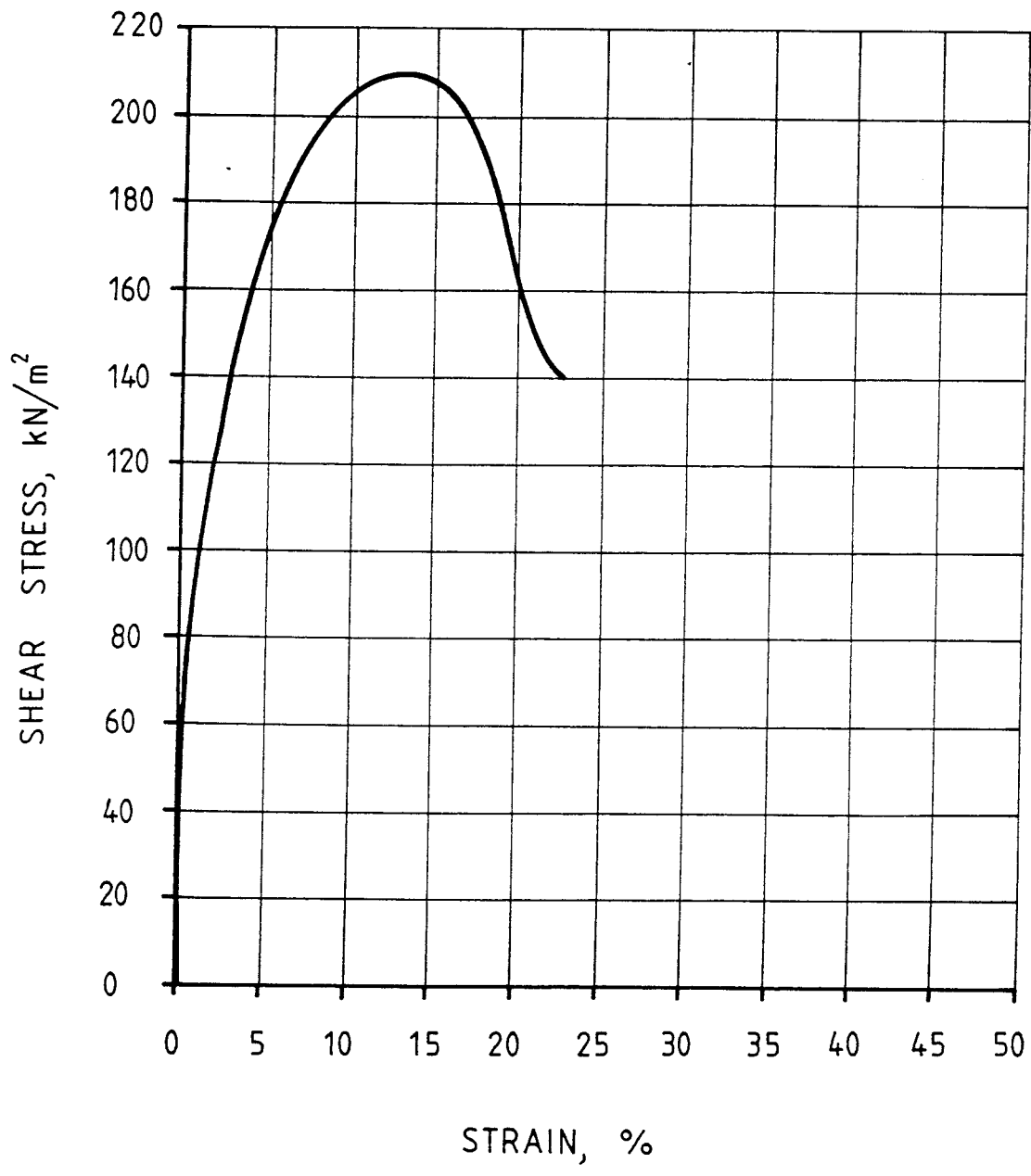
TEST S1



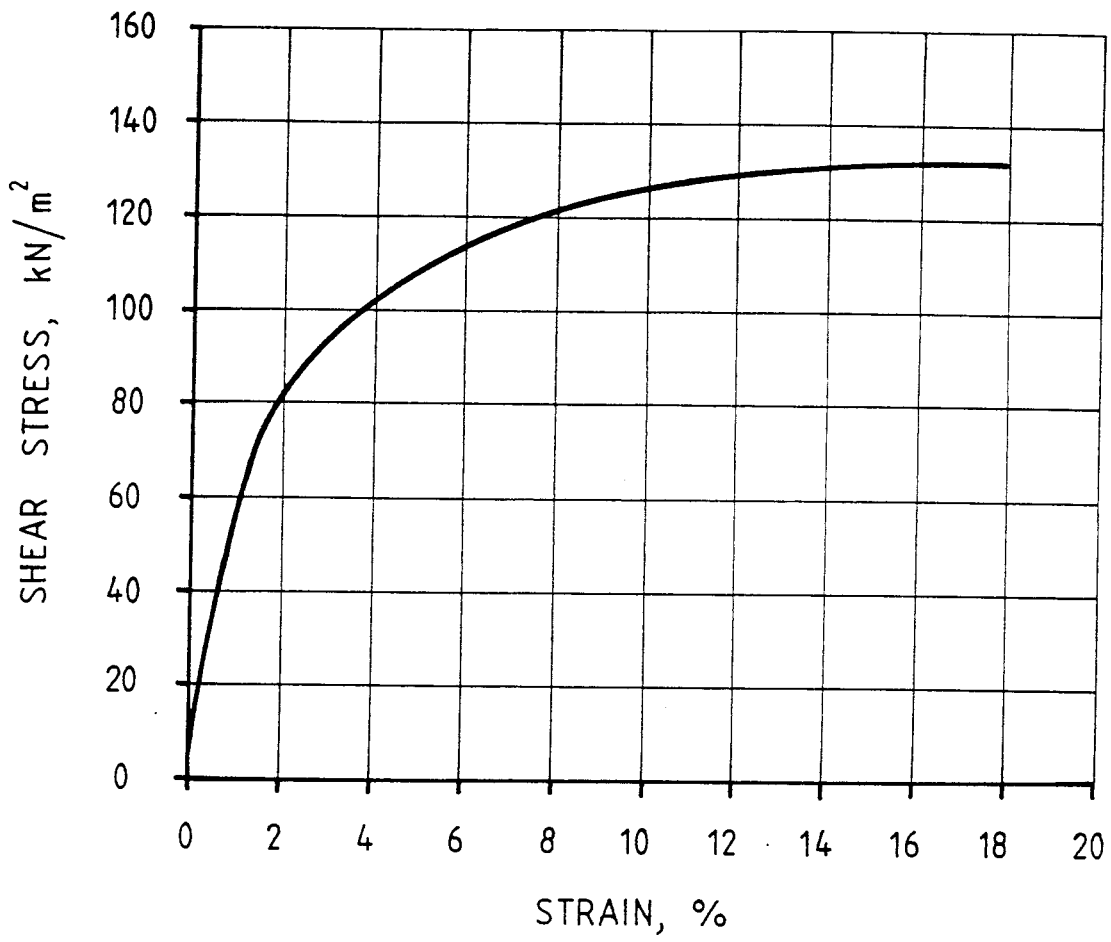
TEST S2



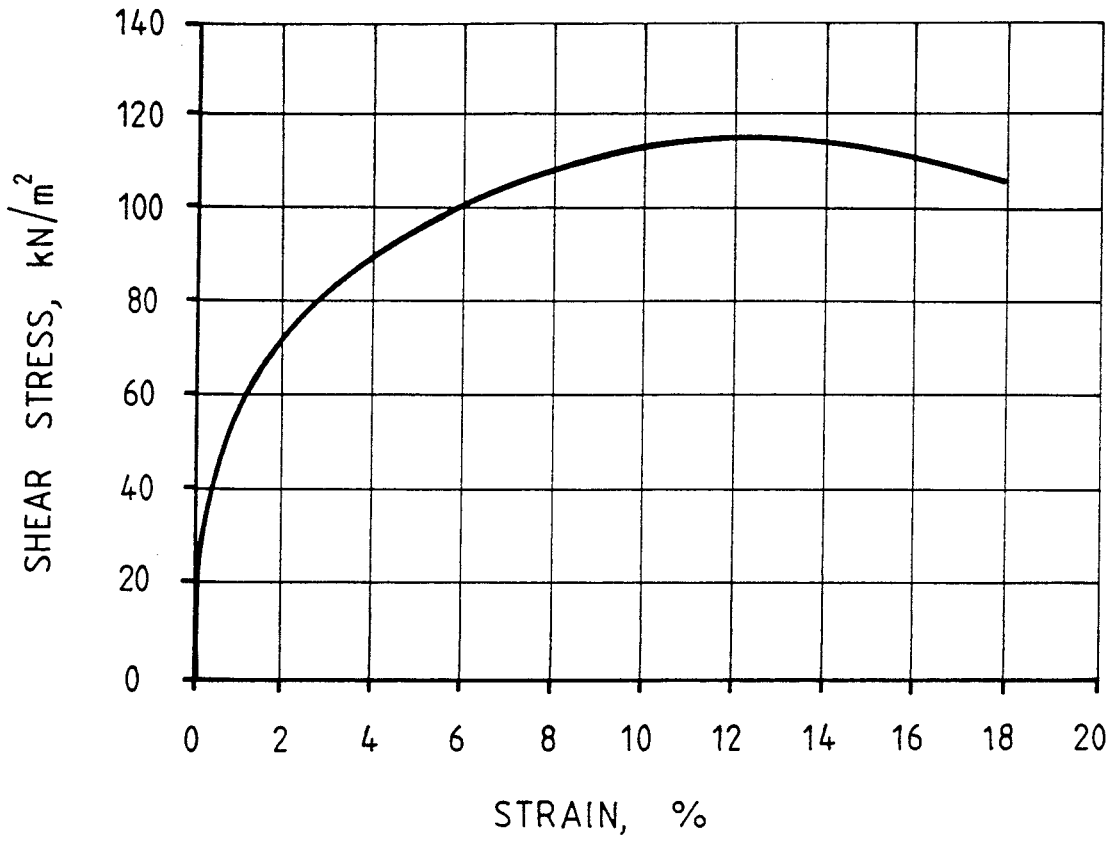
TEST S3



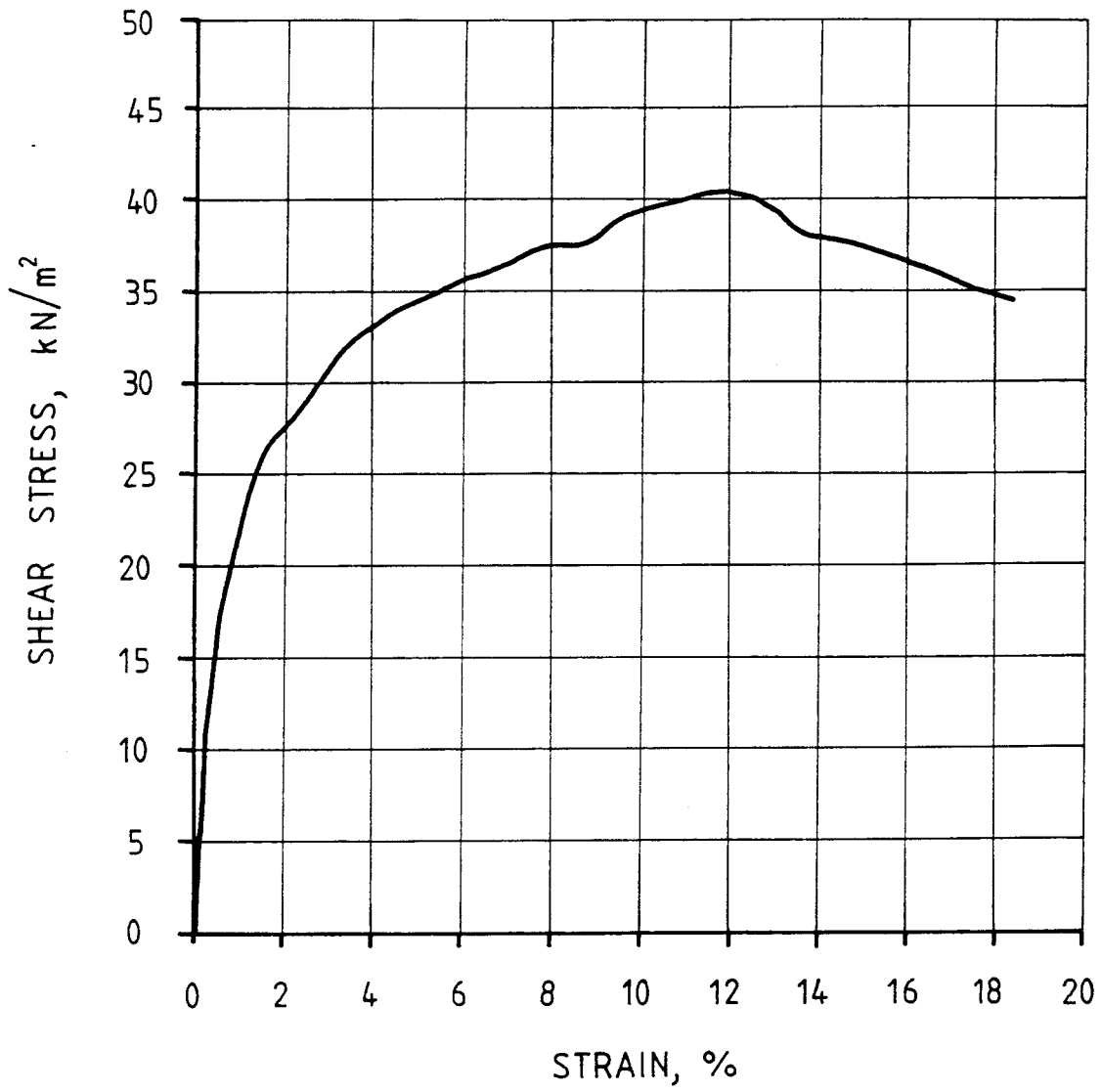
TEST S4



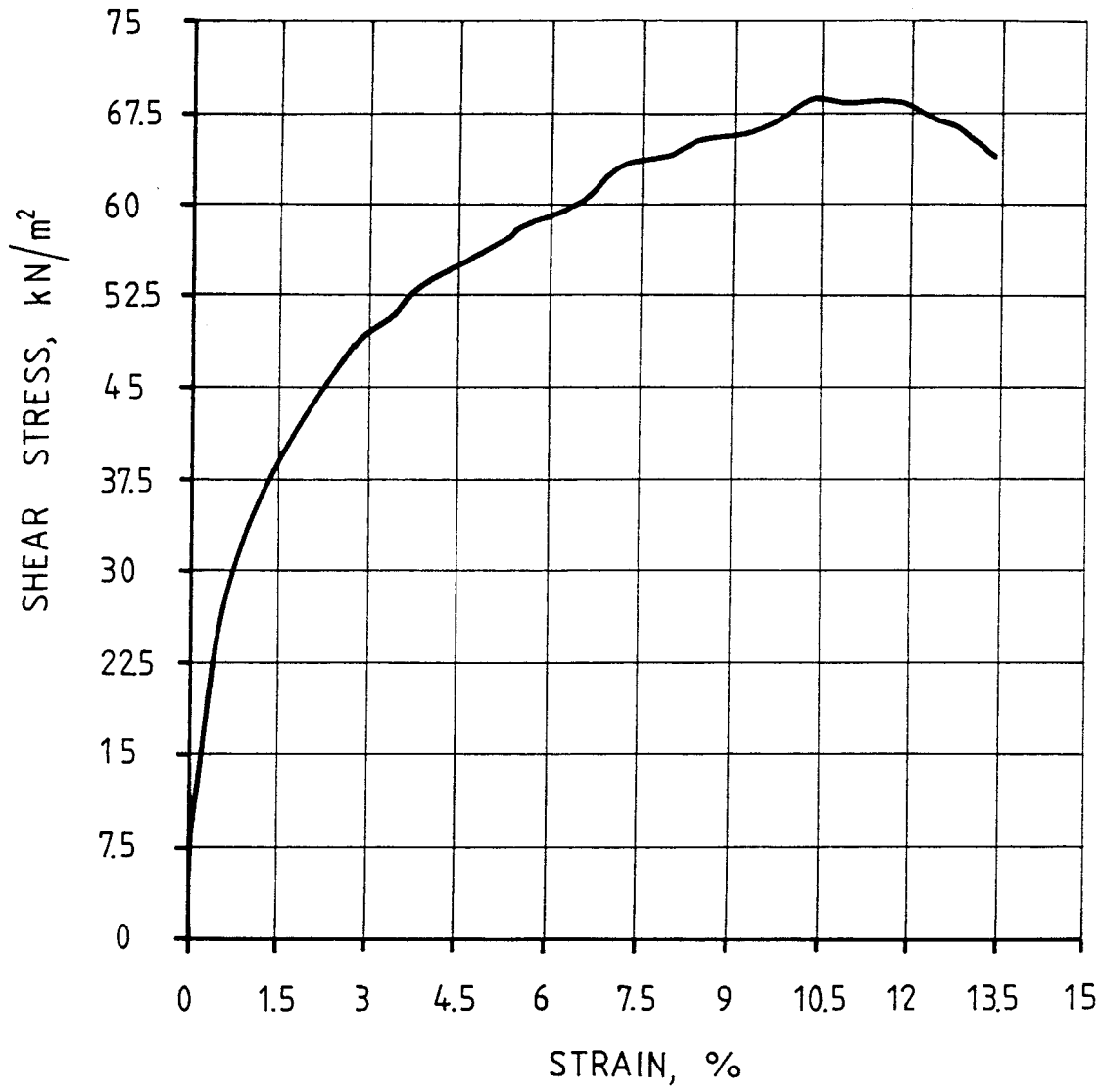
TEST S5



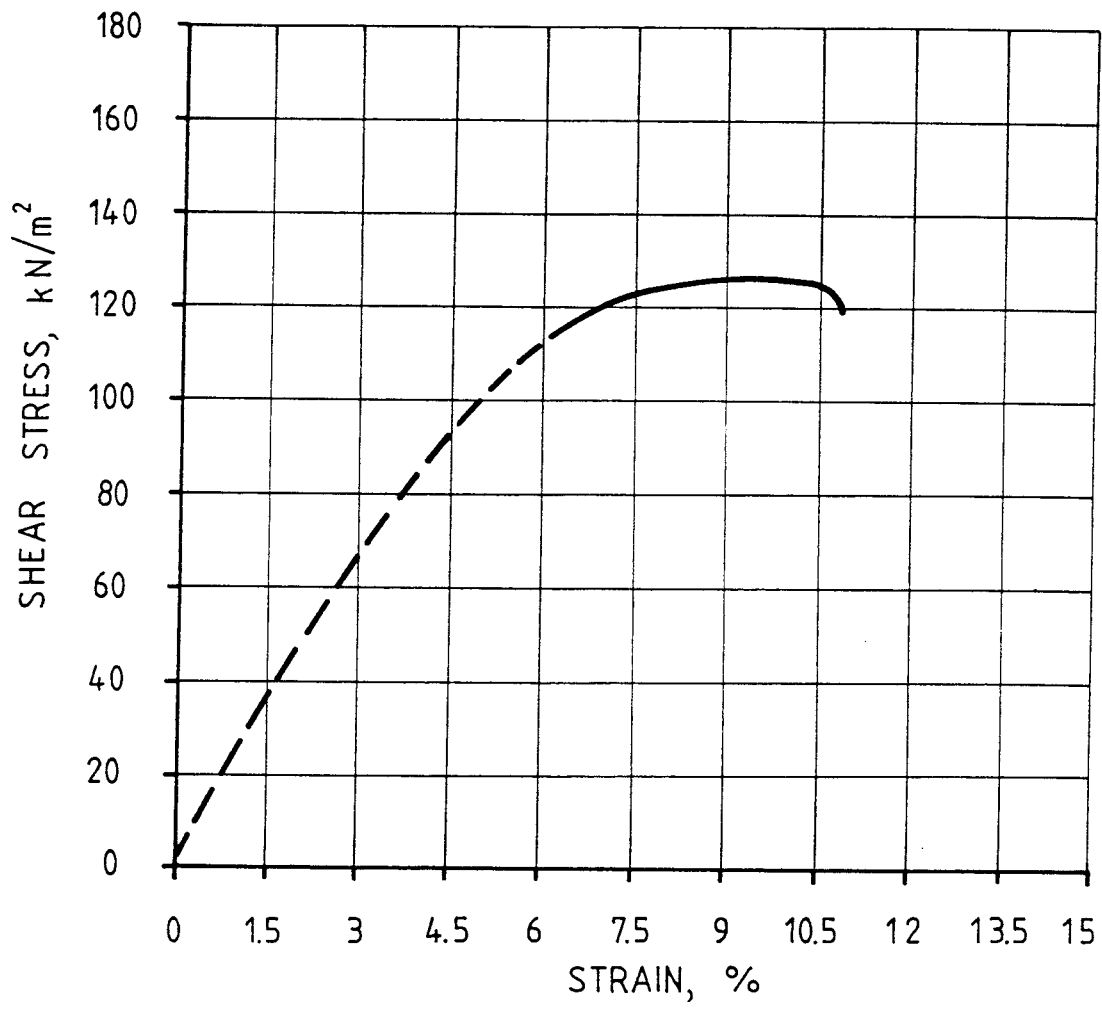
TEST S6



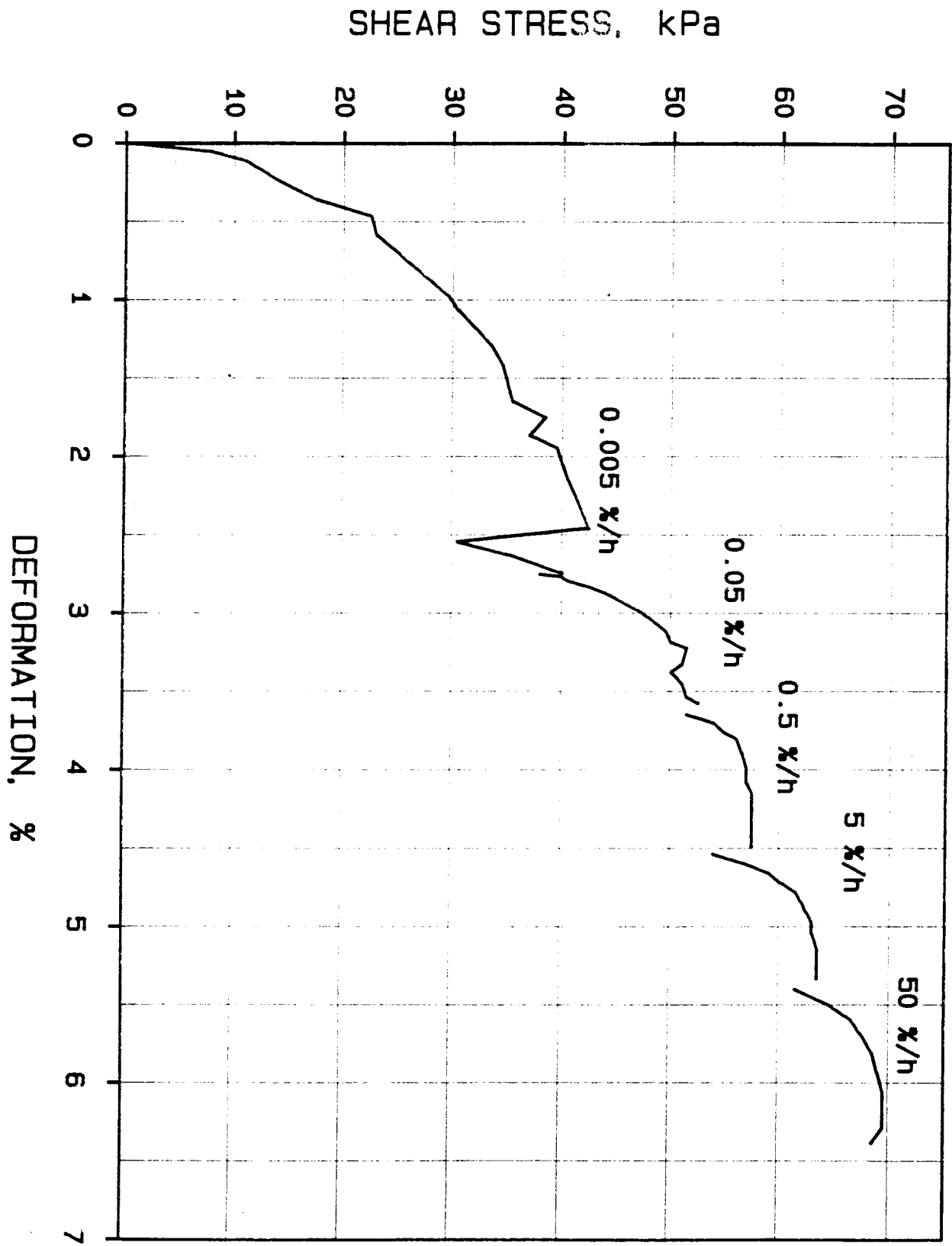
TEST S7



TEST S8



TEST S9

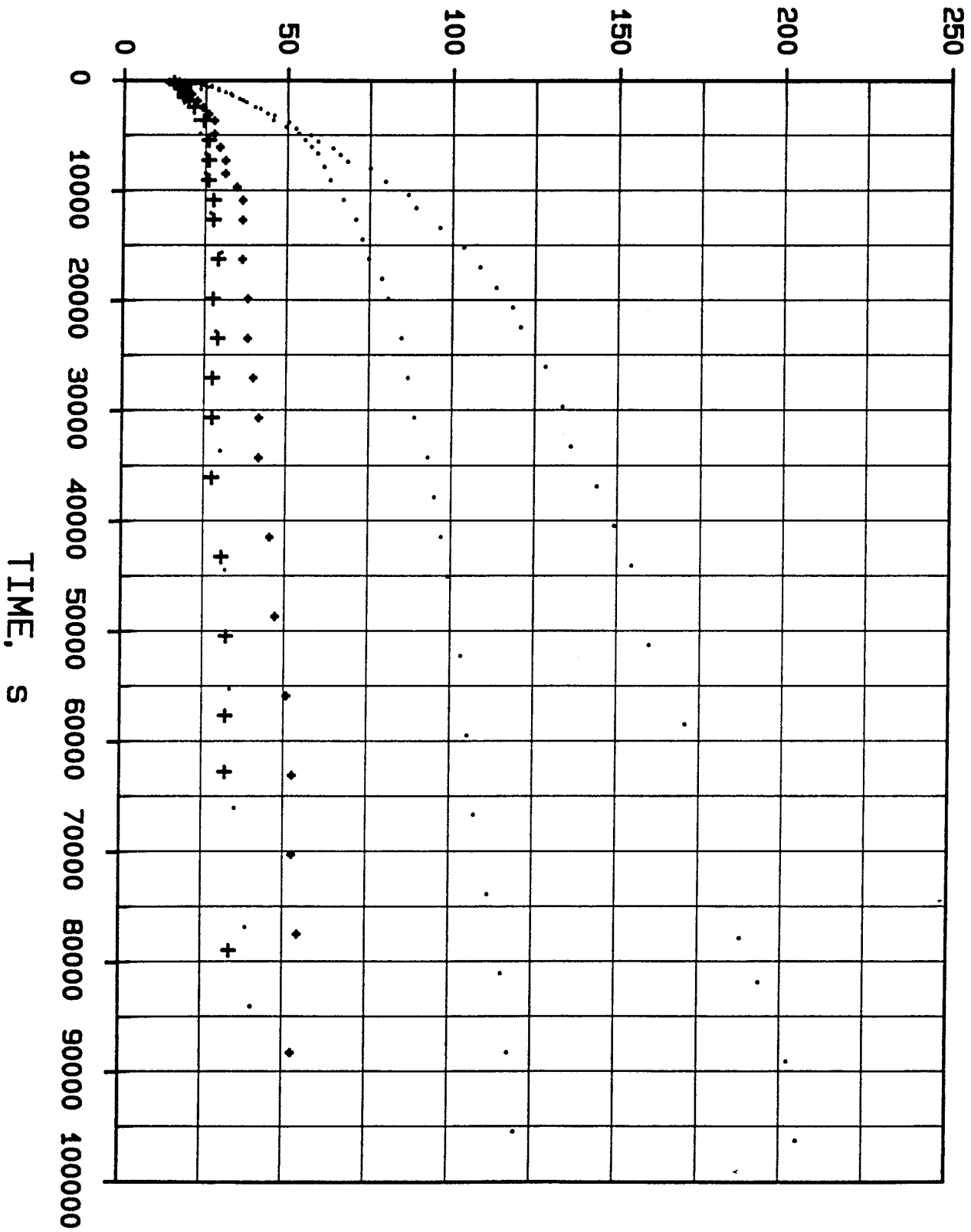


TEST S10

APPENDIX C

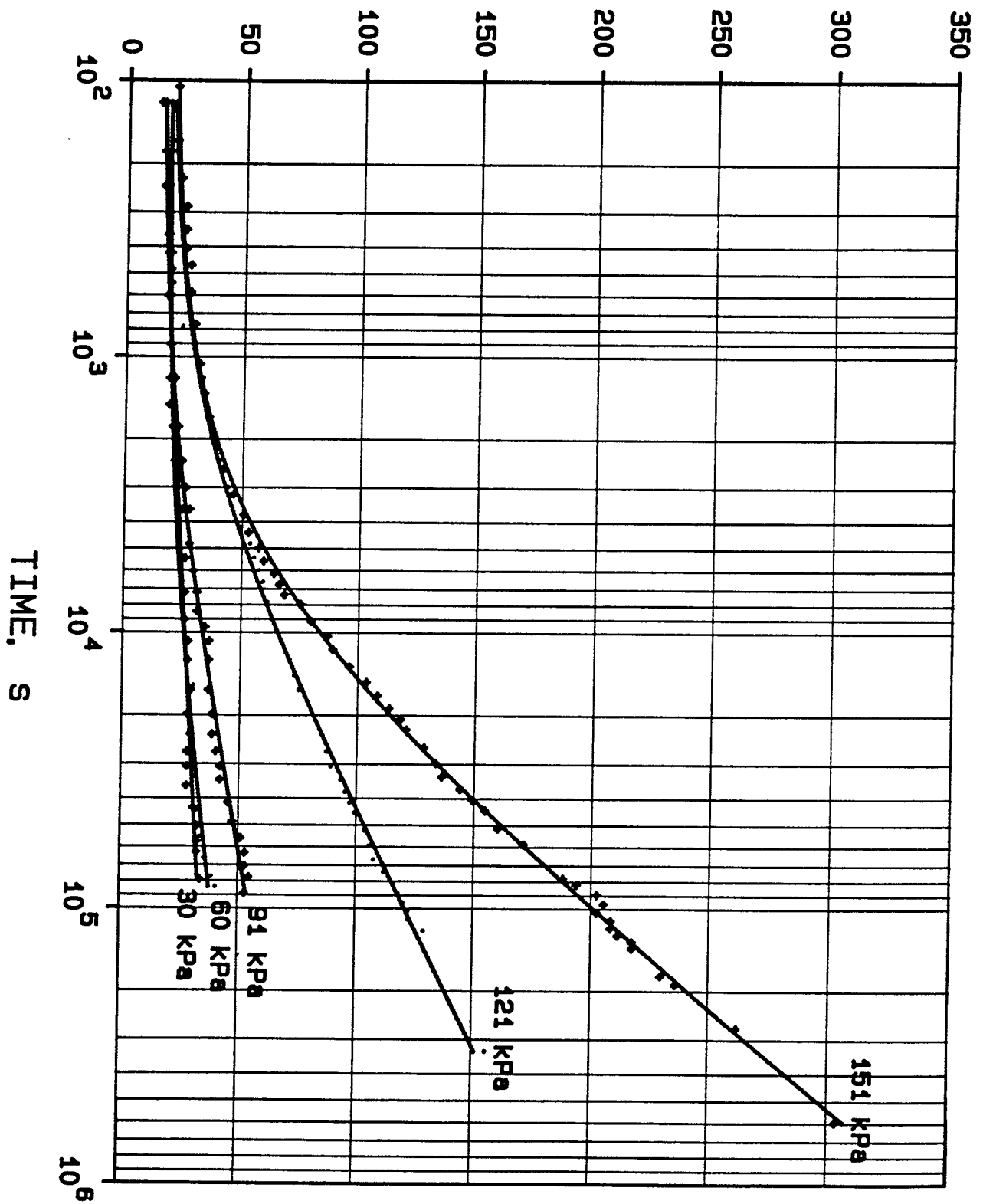
Results from the creep tests C1-C10

CORRECTED ANGULAR STRAIN * 10000



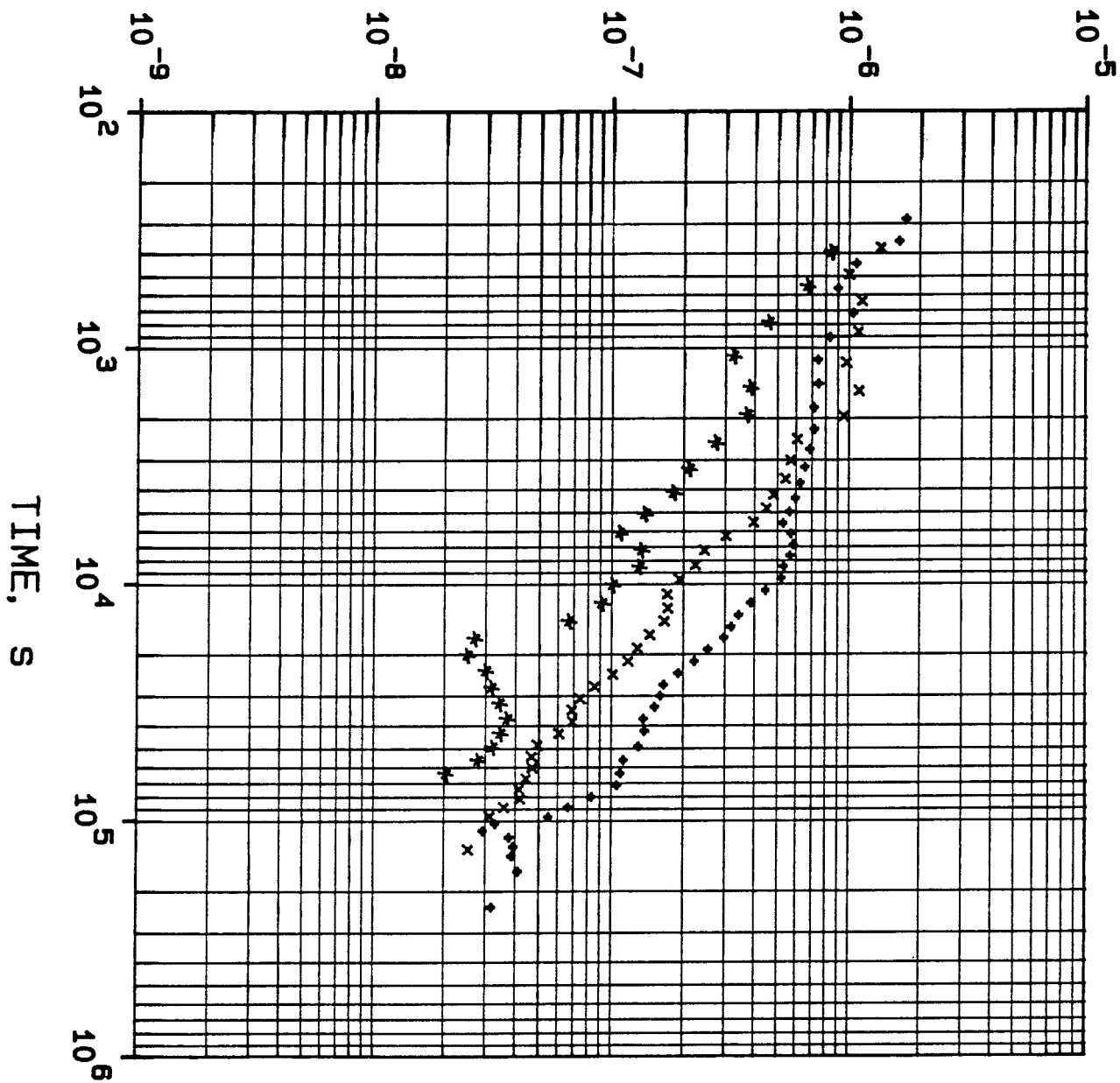
TEST C1

CORRECTED ANGULAR STRAIN * 10000



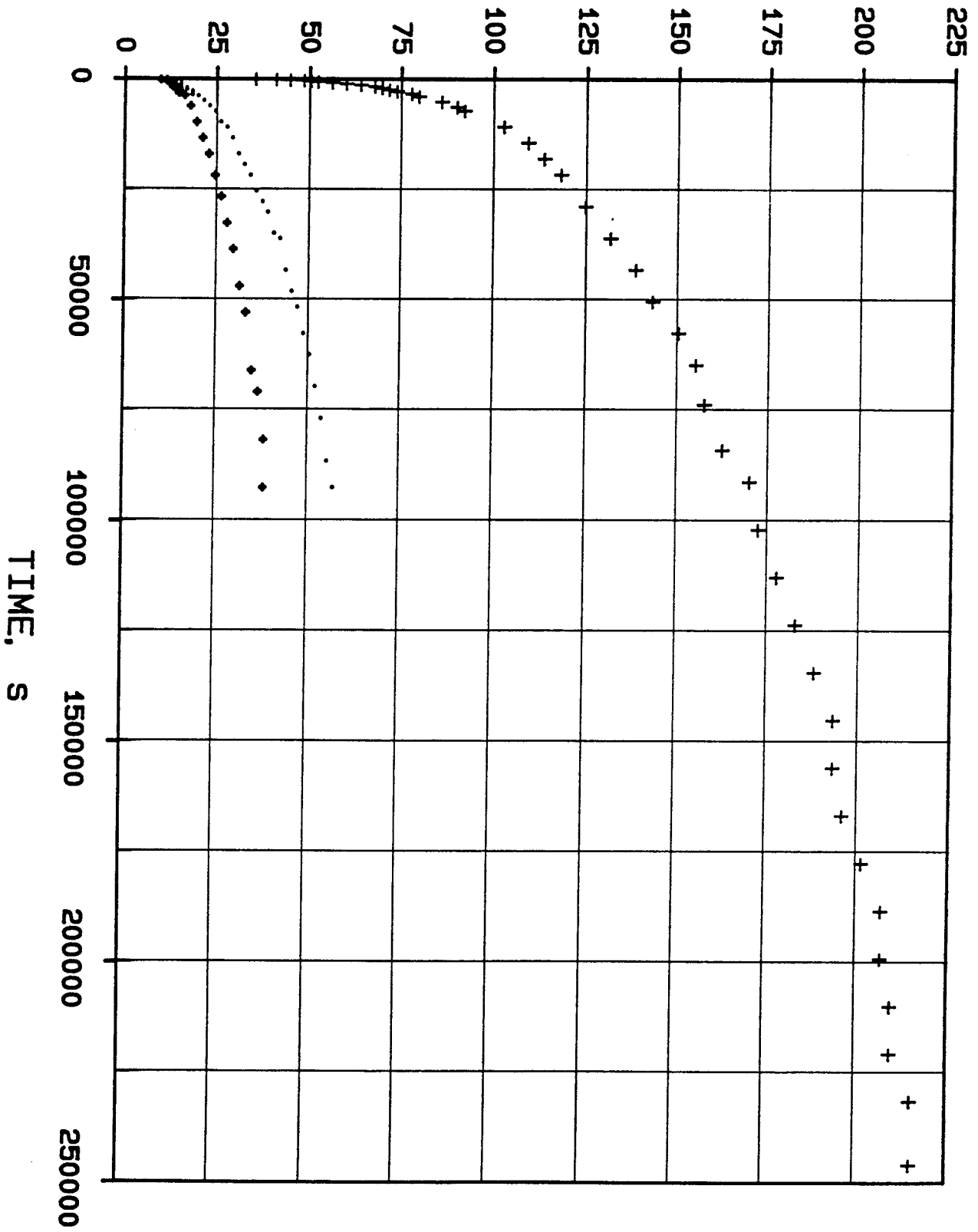
TEST C1

ANGULAR STRAIN RATE, 1/s



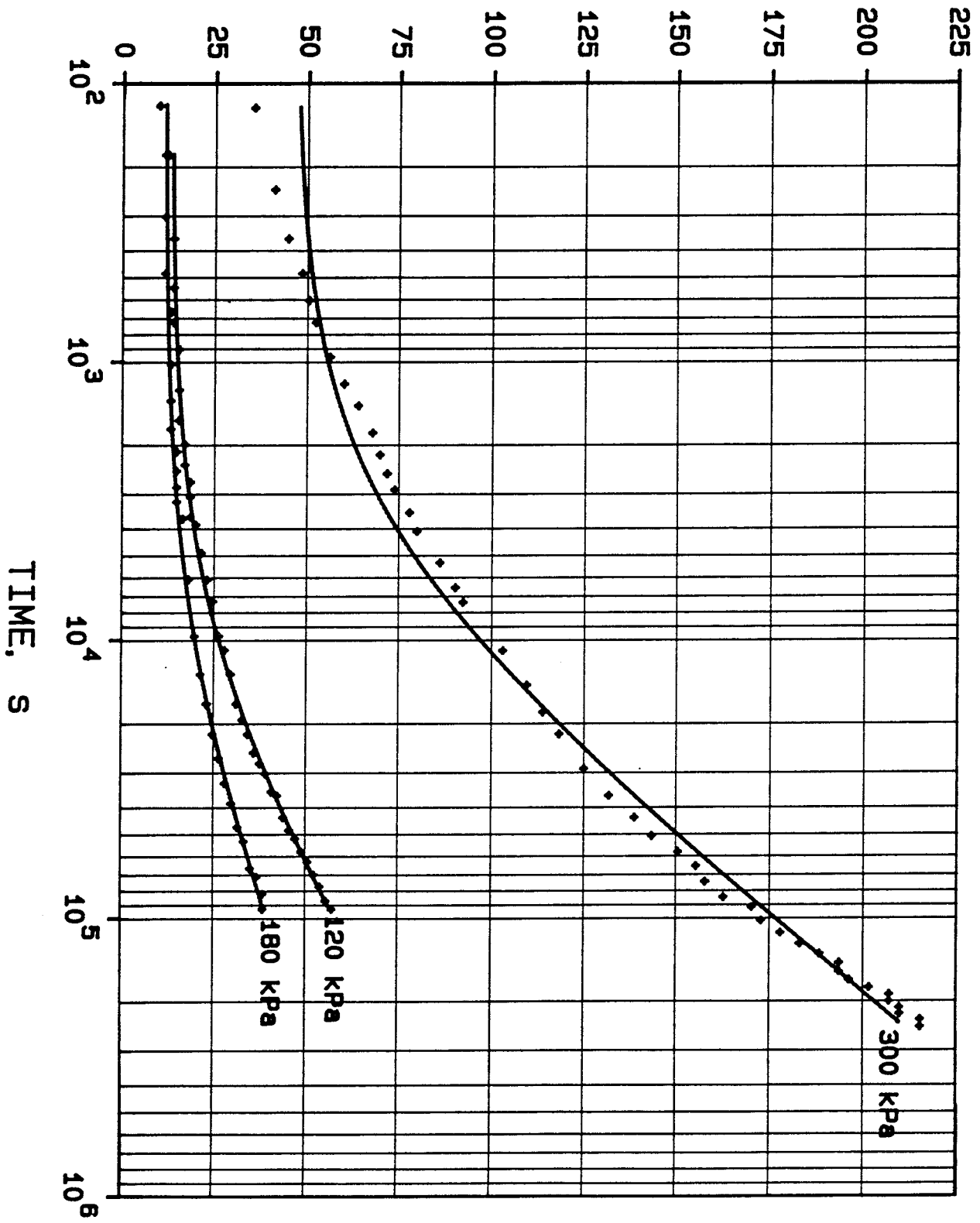
TEST C1

CORRECTED ANGULAR STRAIN * 10000

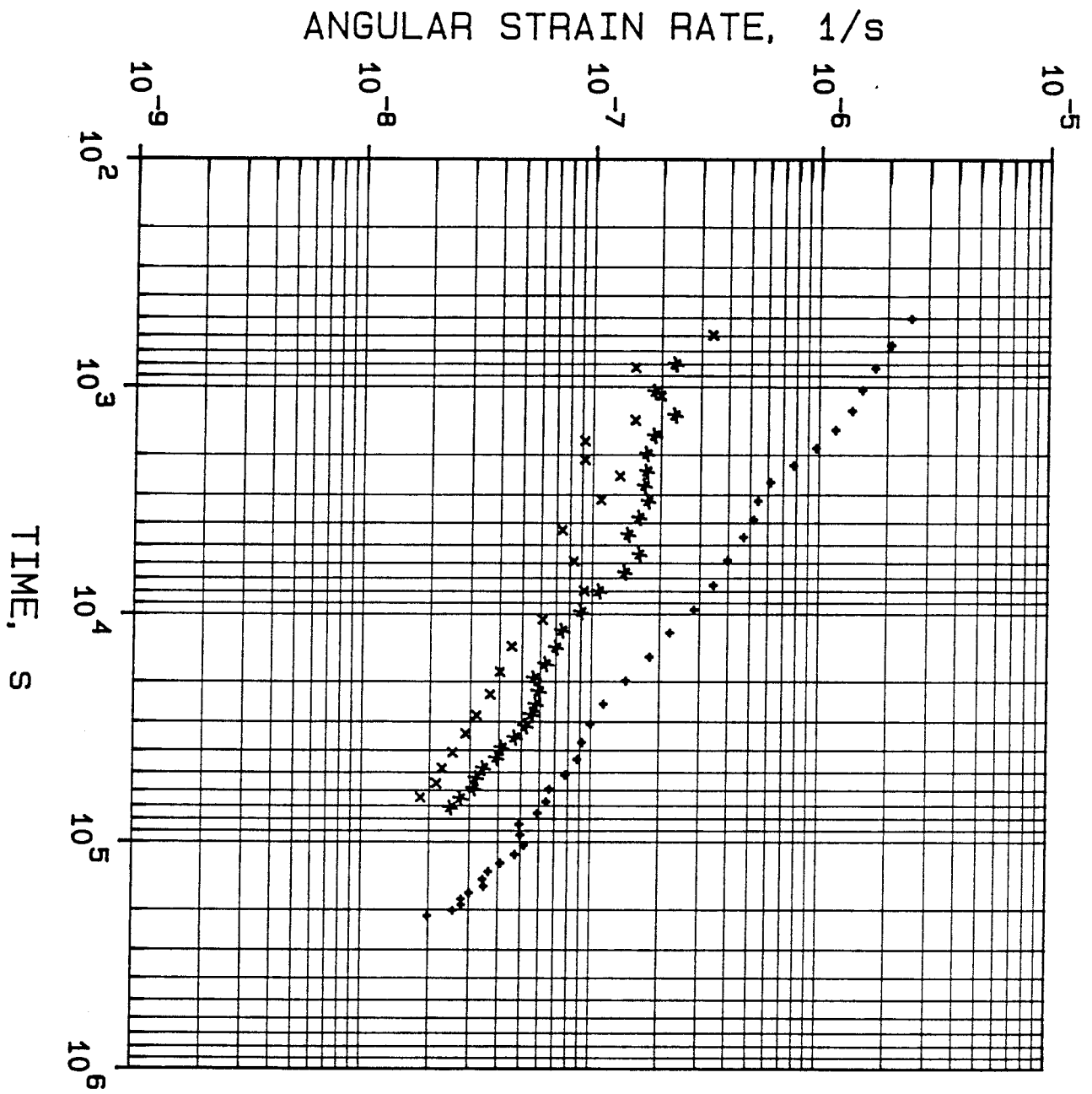


TEST C2

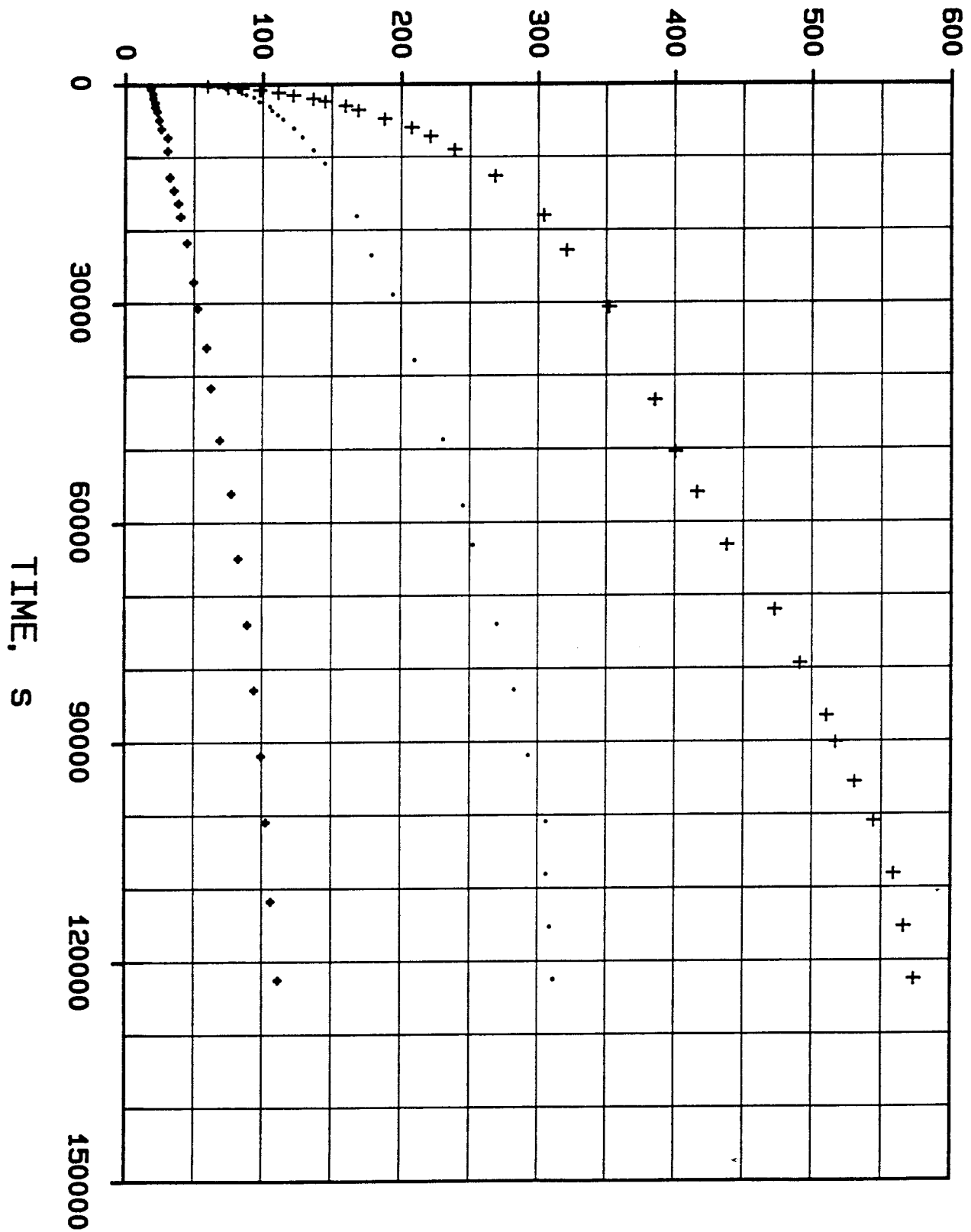
CORRECTED ANGULAR STRAIN * 10000



TEST C2

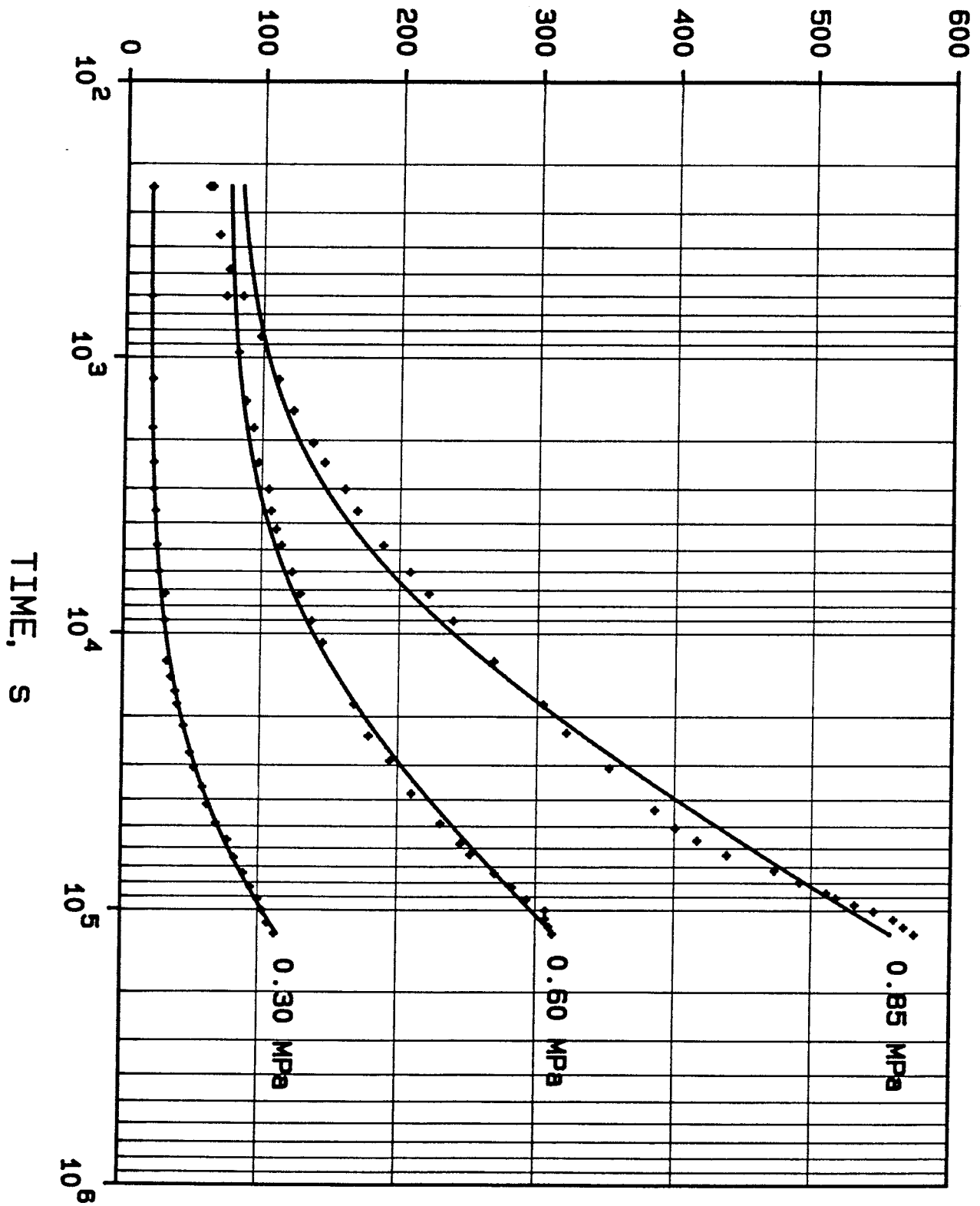


CORRECTED ANGULAR STRAIN * 10000

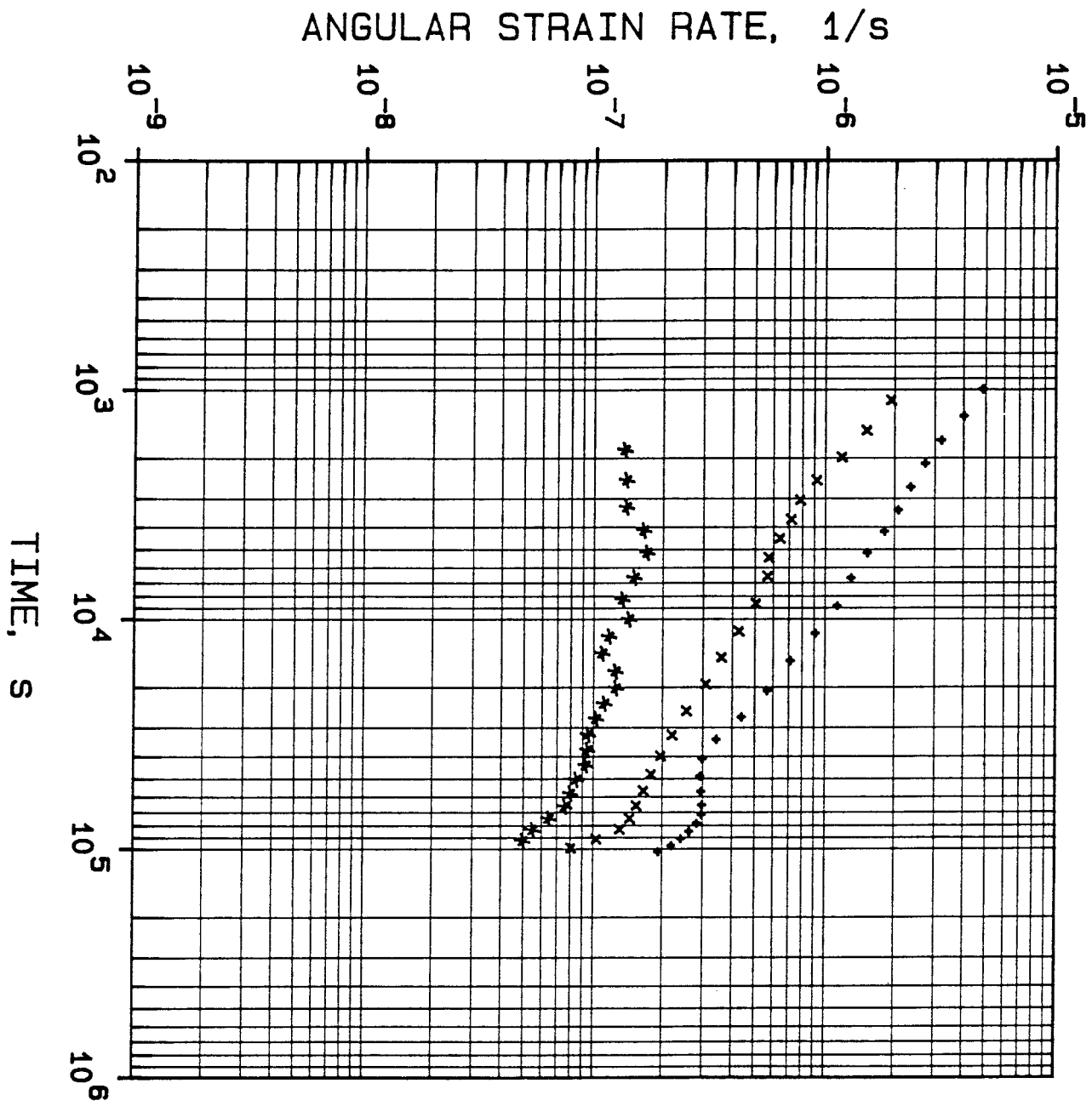


TEST C3

CORRECTED ANGULAR STRAIN * 10000

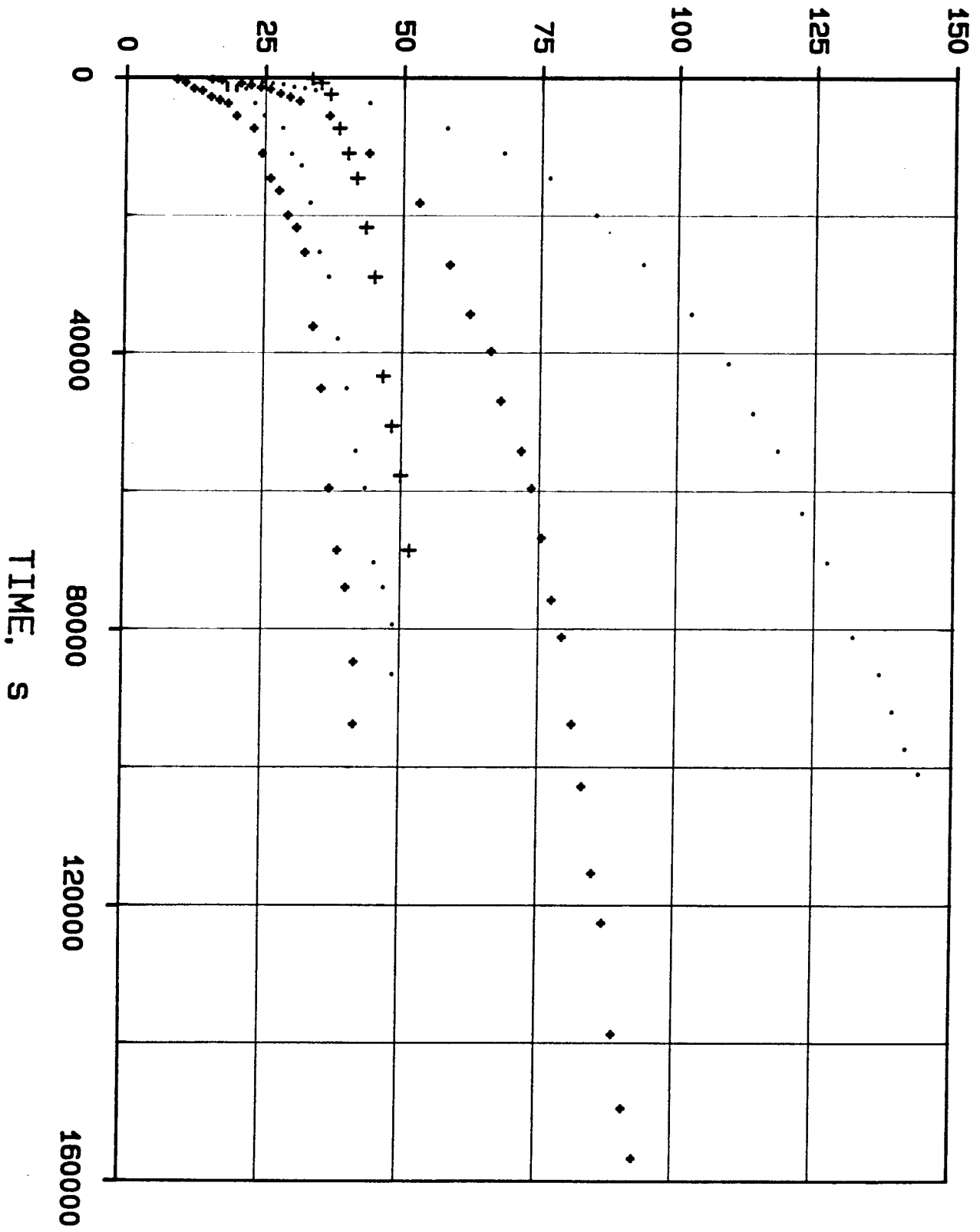


TEST C3



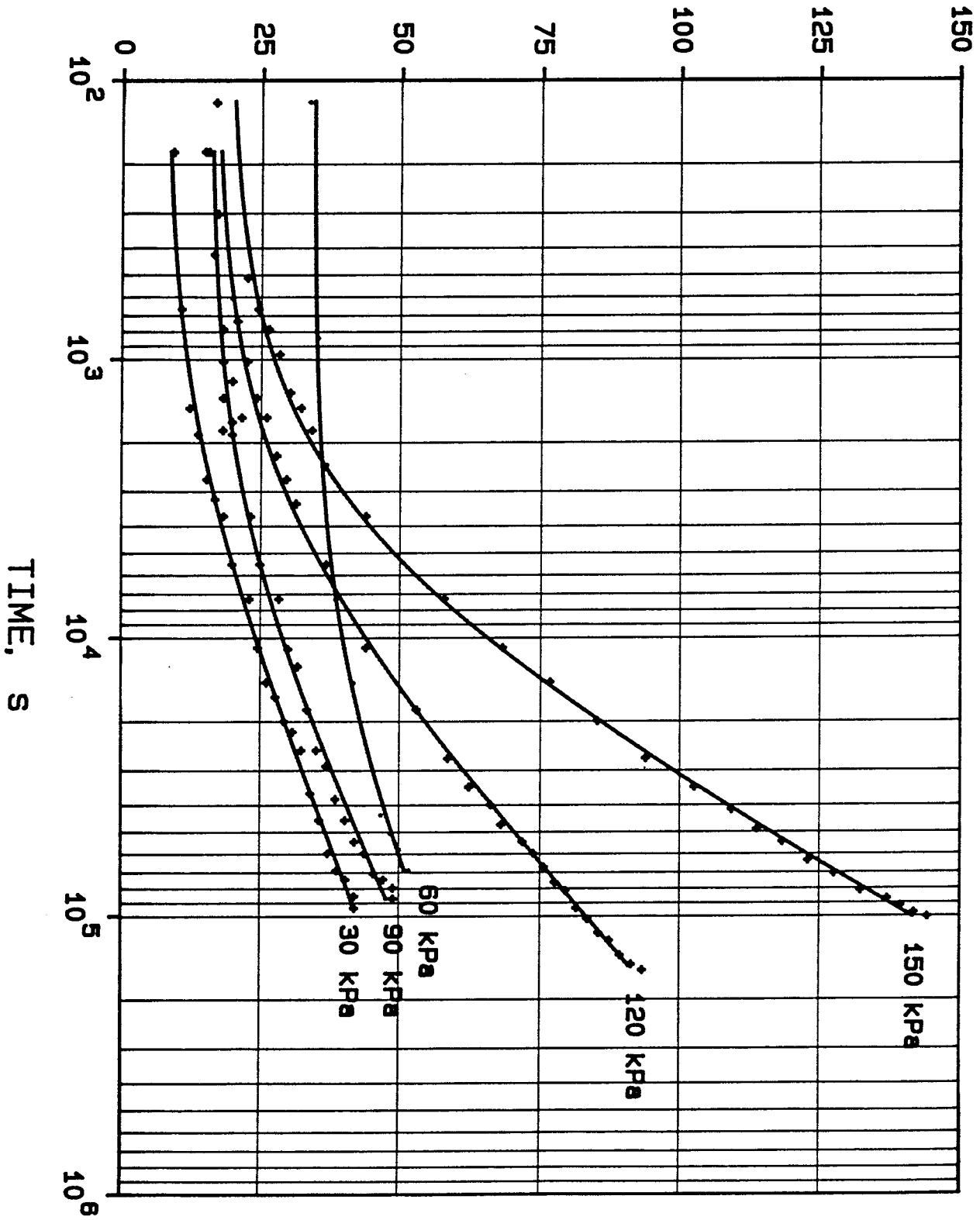
TEST C3

CORRECTED ANGULAR STRAIN * 10000

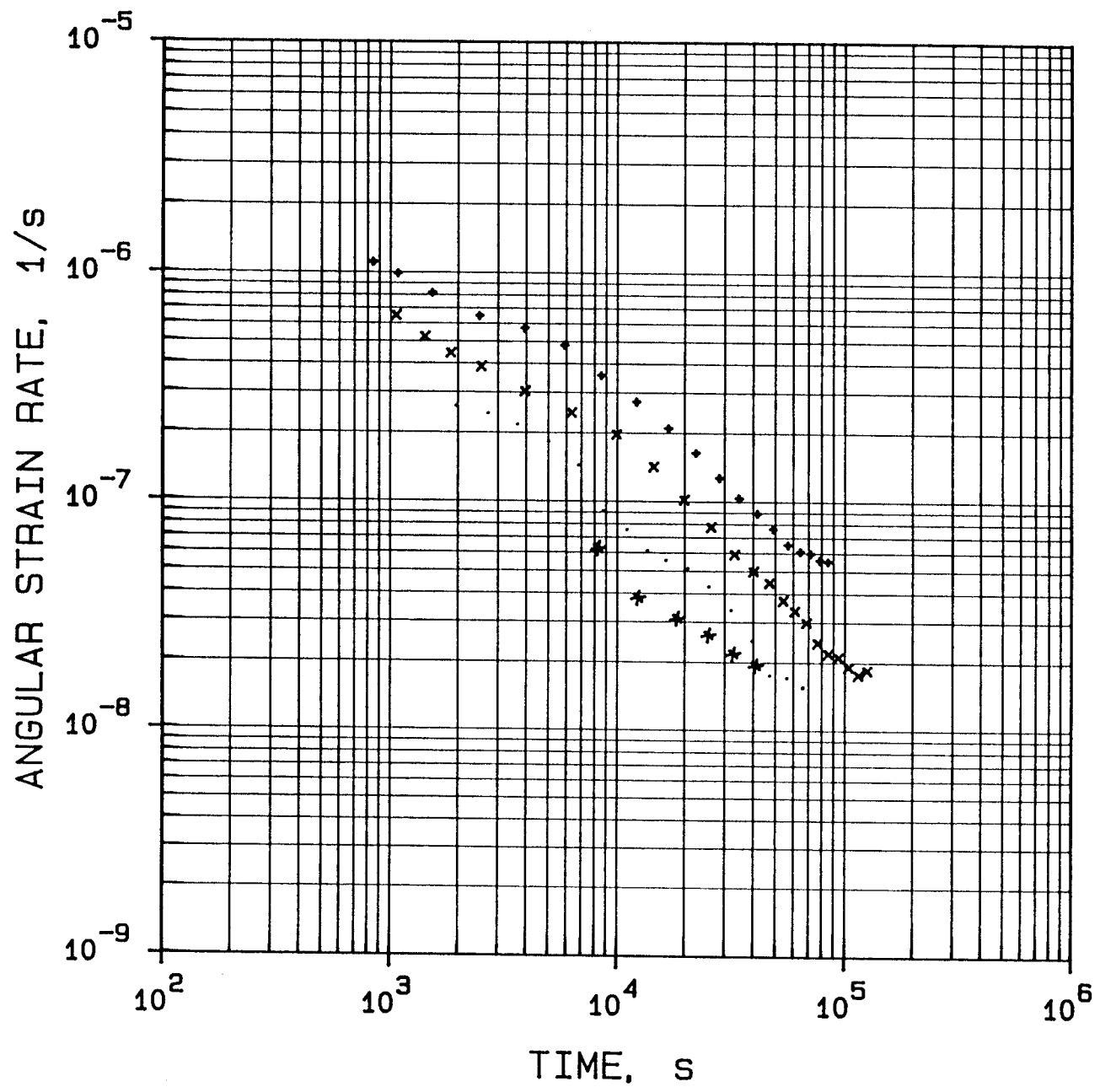


TEST C4

CORRECTED ANGULAR STRAIN * 10000

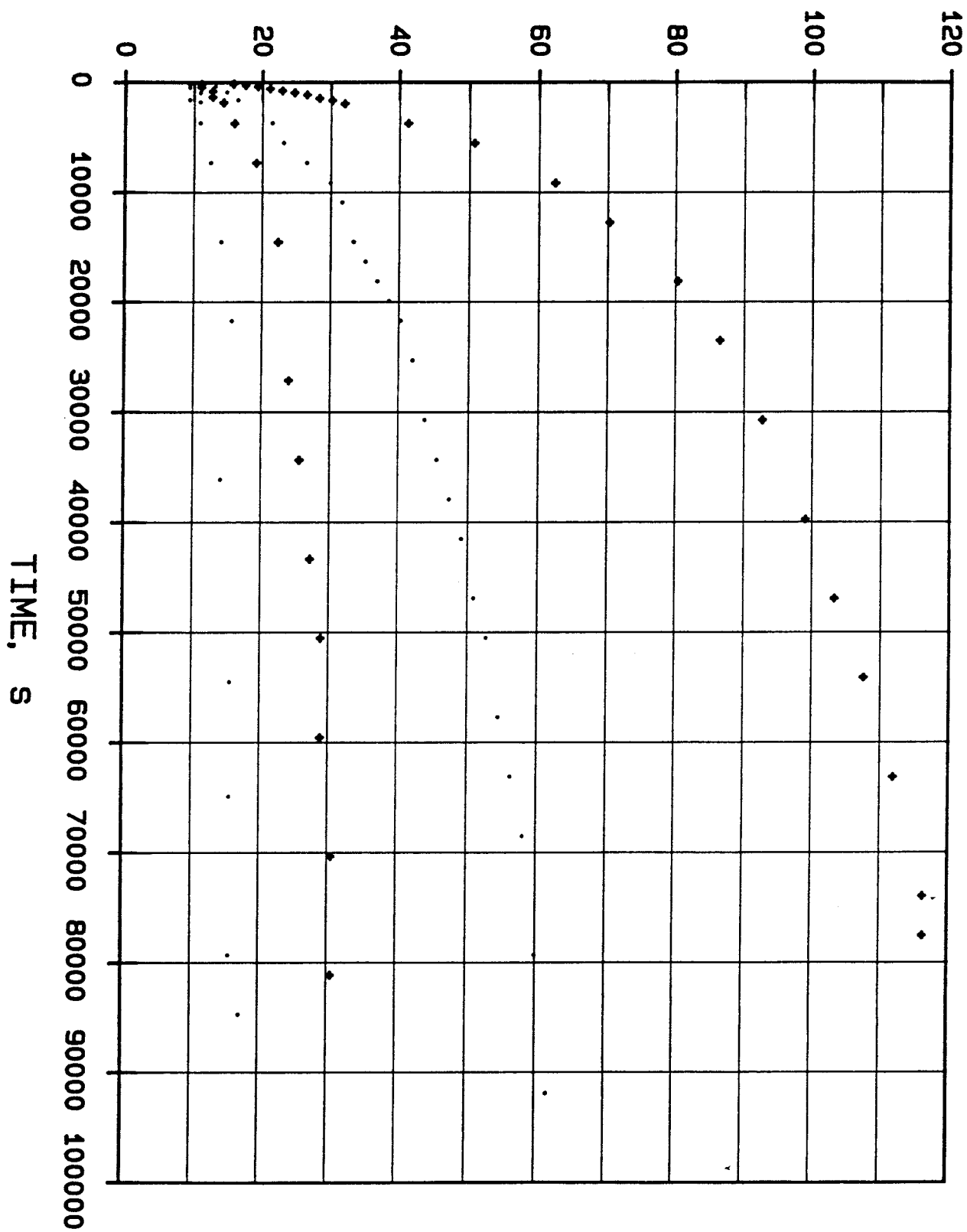


TEST C4

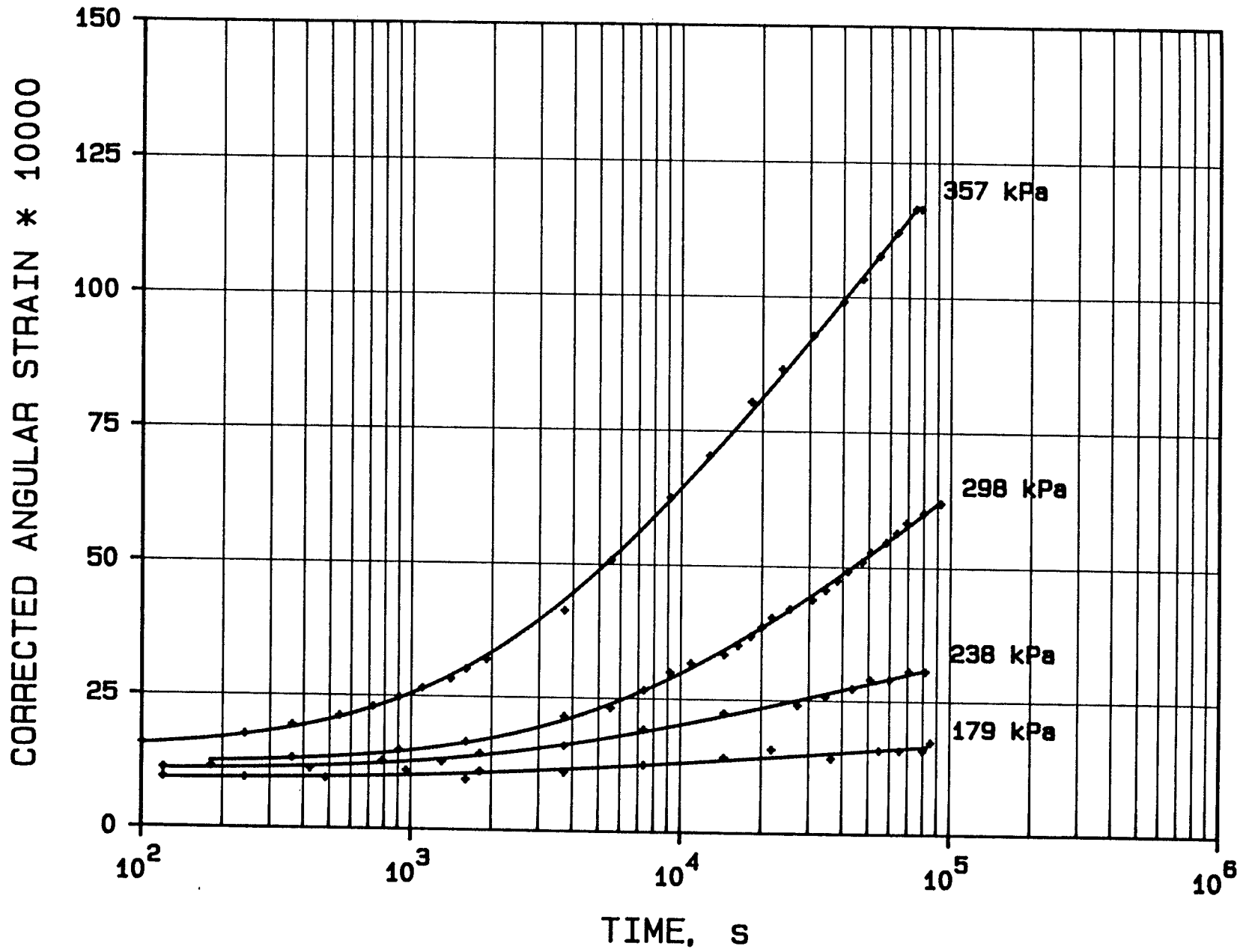


TEST C4

CORRECTED ANGULAR STRAIN * 10000

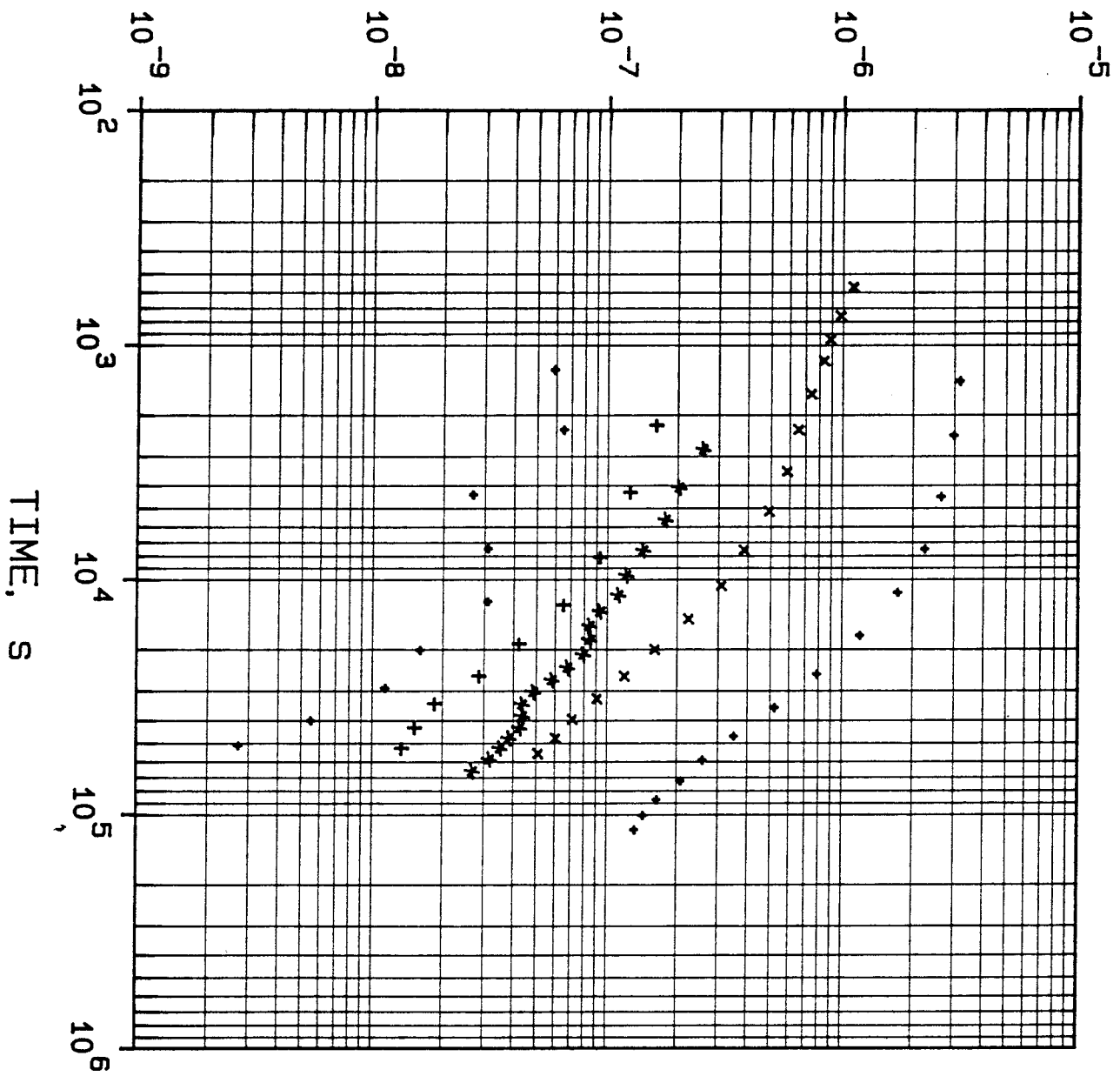


TEST C5



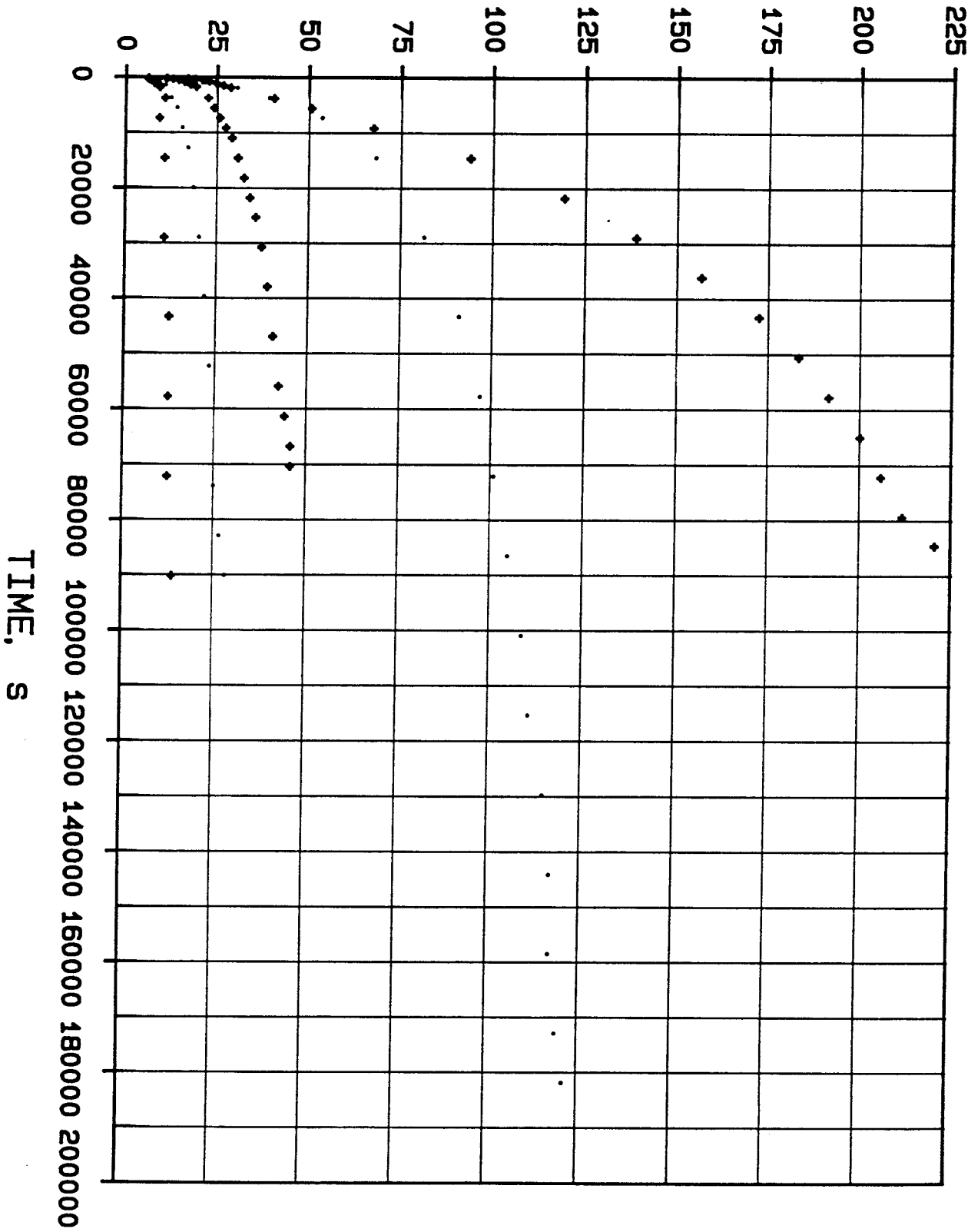
TEST C5

ANGULAR STRAIN RATE, 1/s



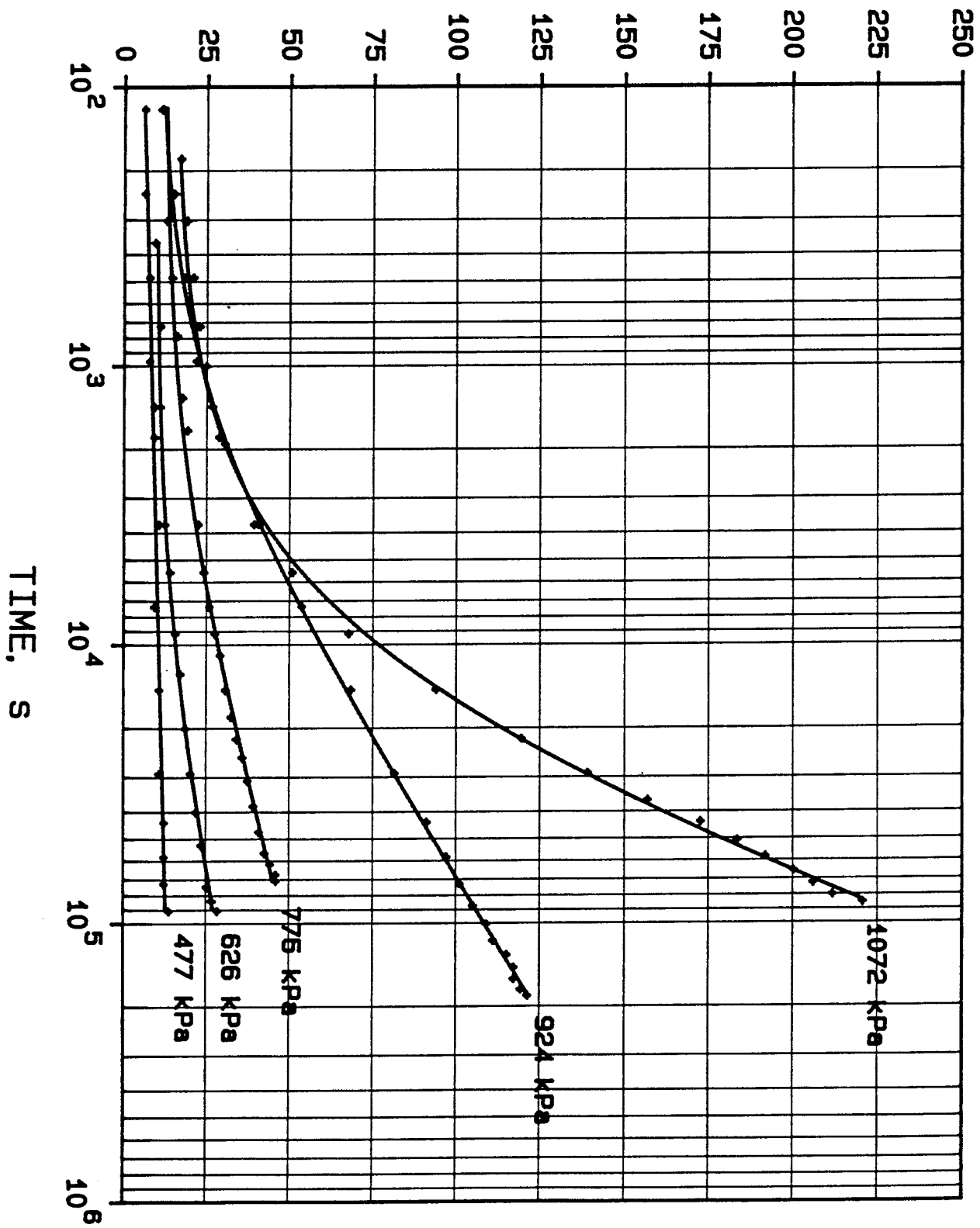
TEST C5

CORRECTED ANGULAR STRAIN * 10000

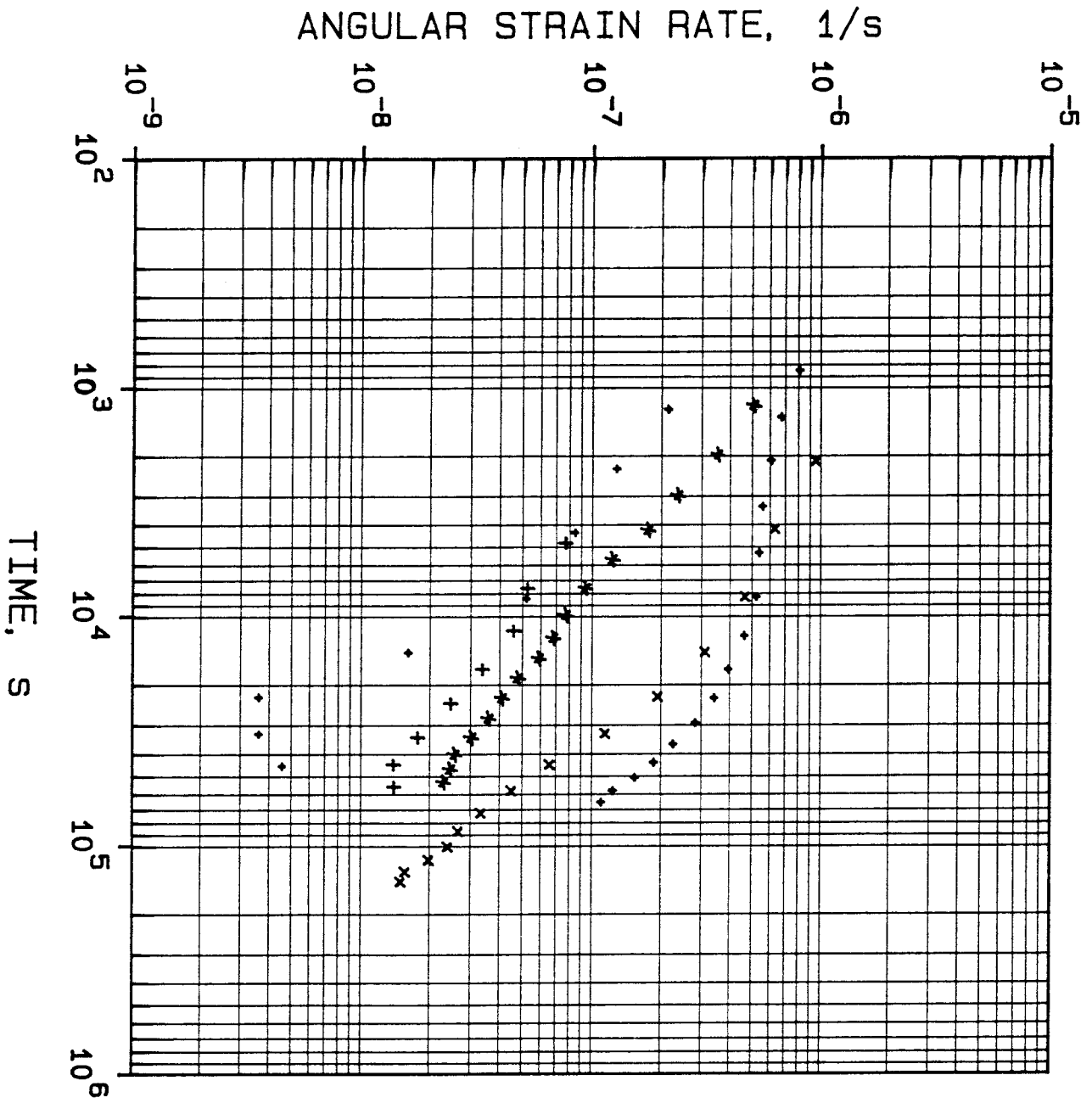


TEST C6

CORRECTED ANGULAR STRAIN * 10000

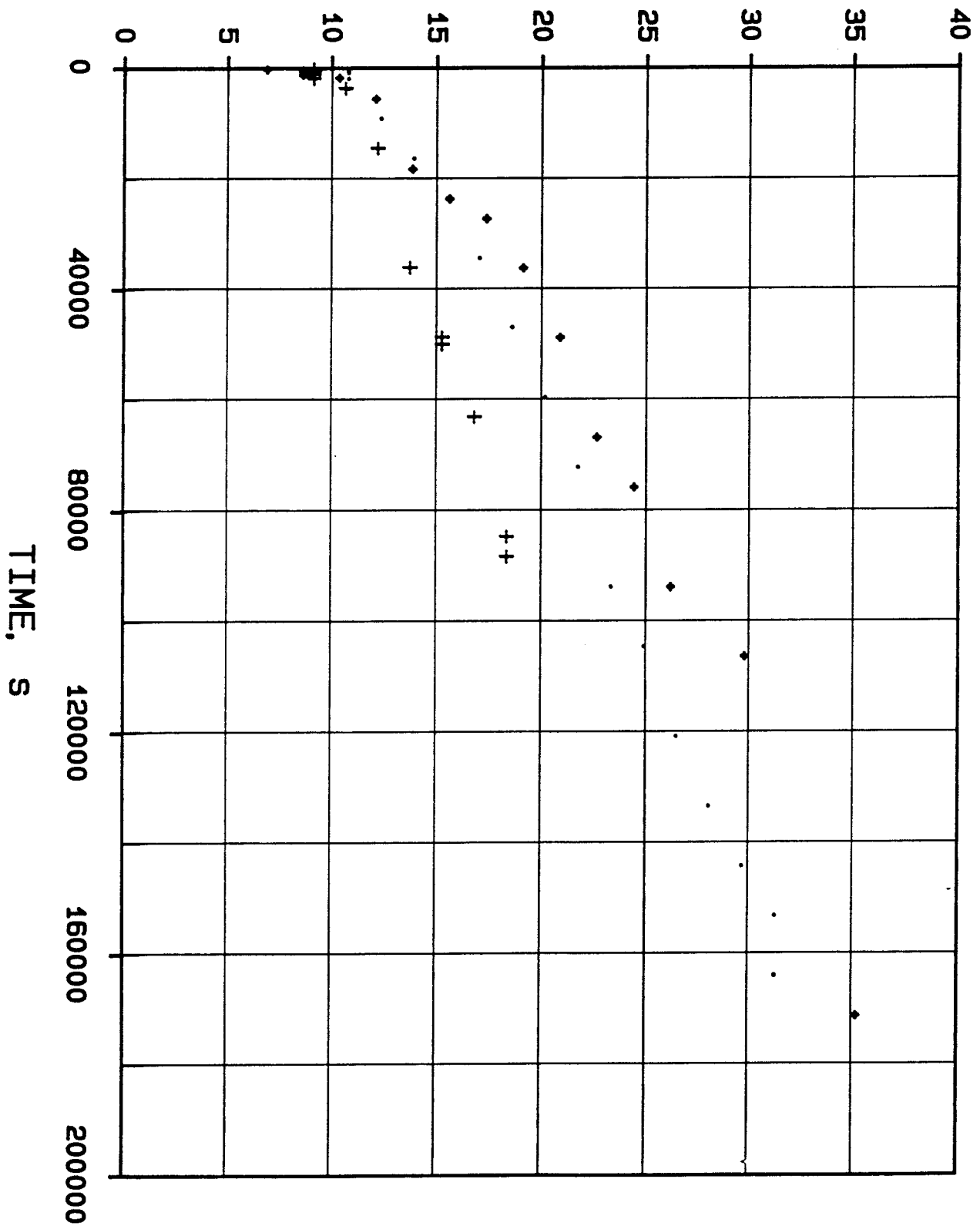


TEST C6



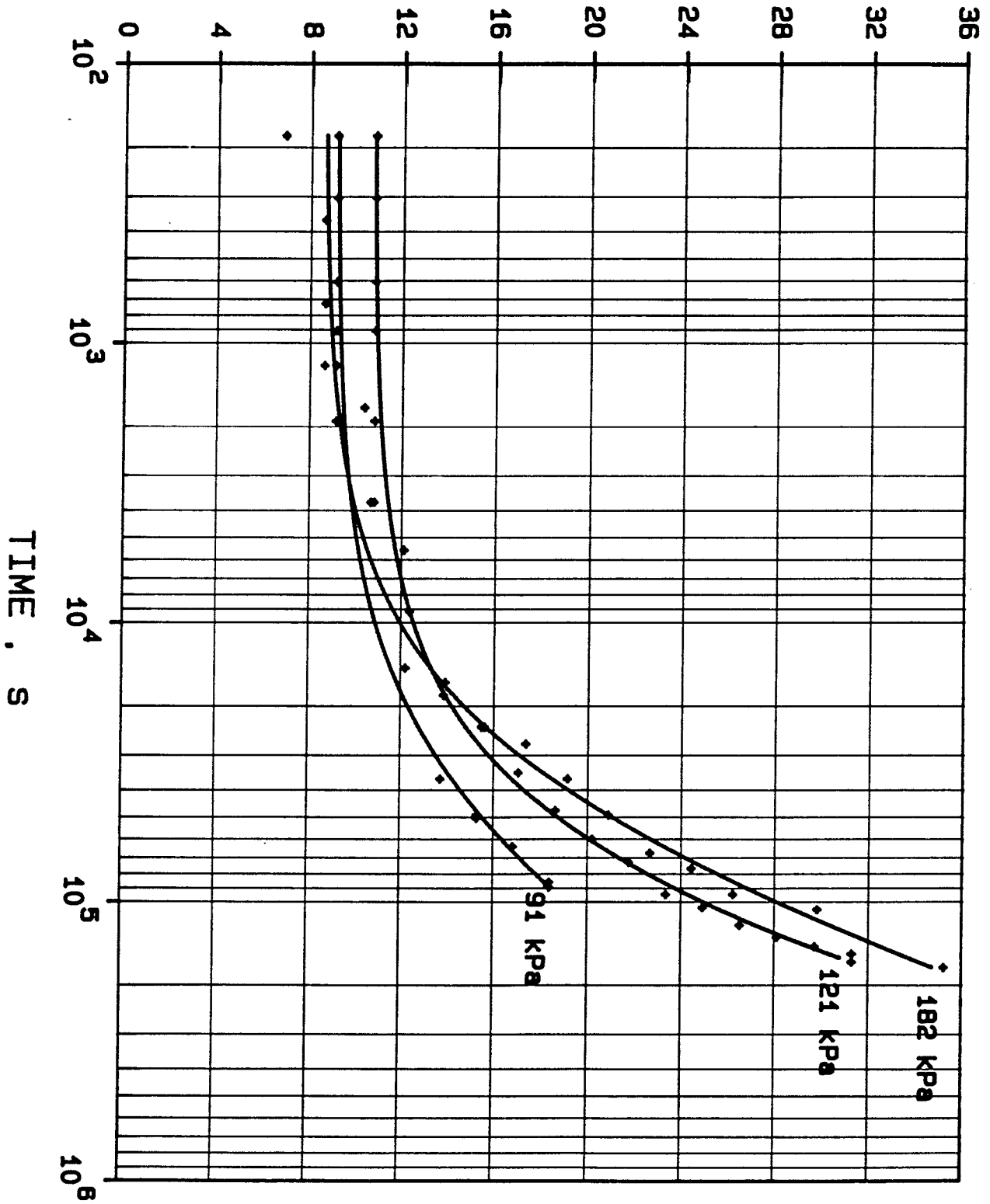
TEST C6

CORRECTED ANGULAR STRAIN * 10000

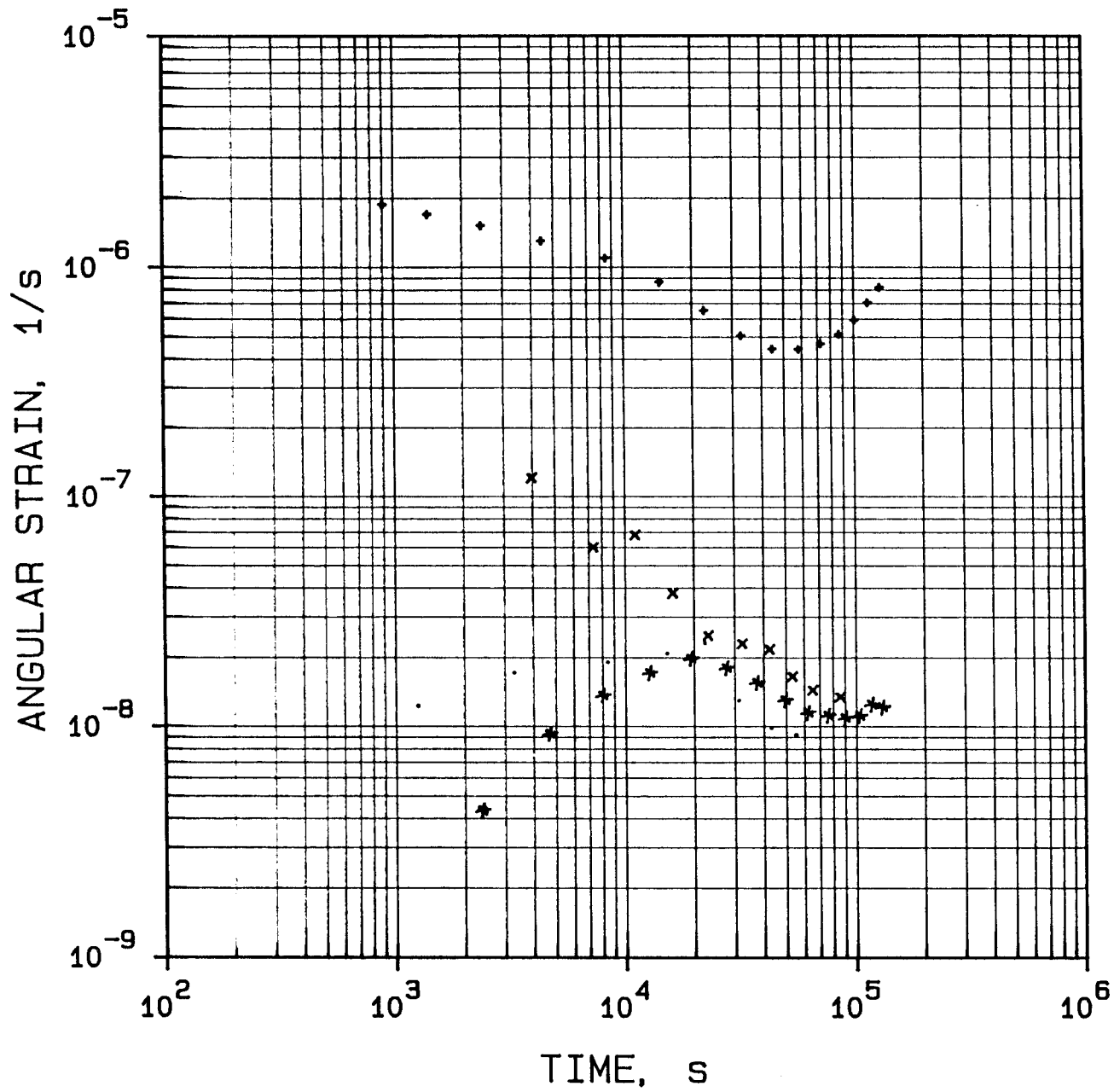


TEST C7

CORRECTED ANGULAR STRAIN * 10000

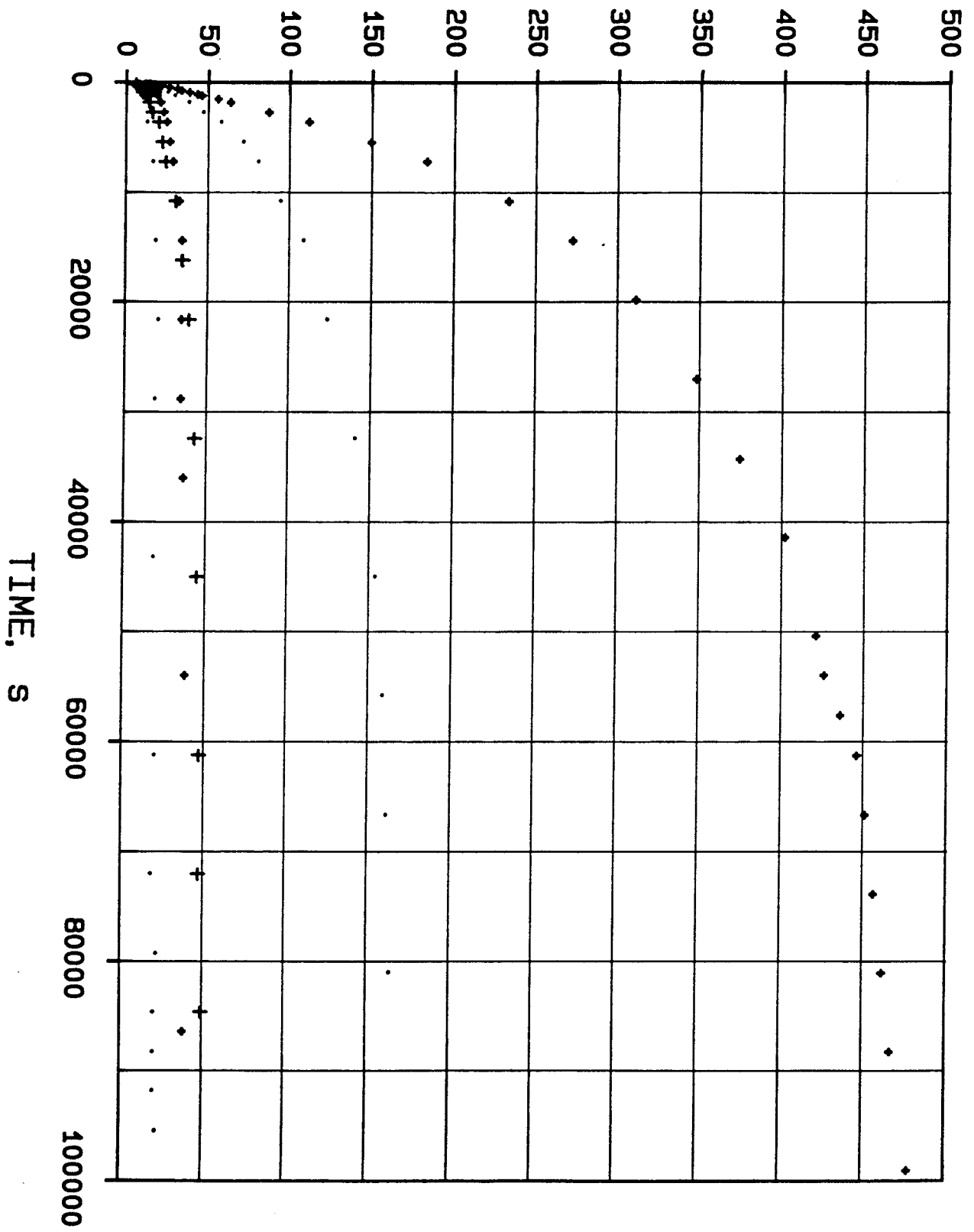


TEST C7

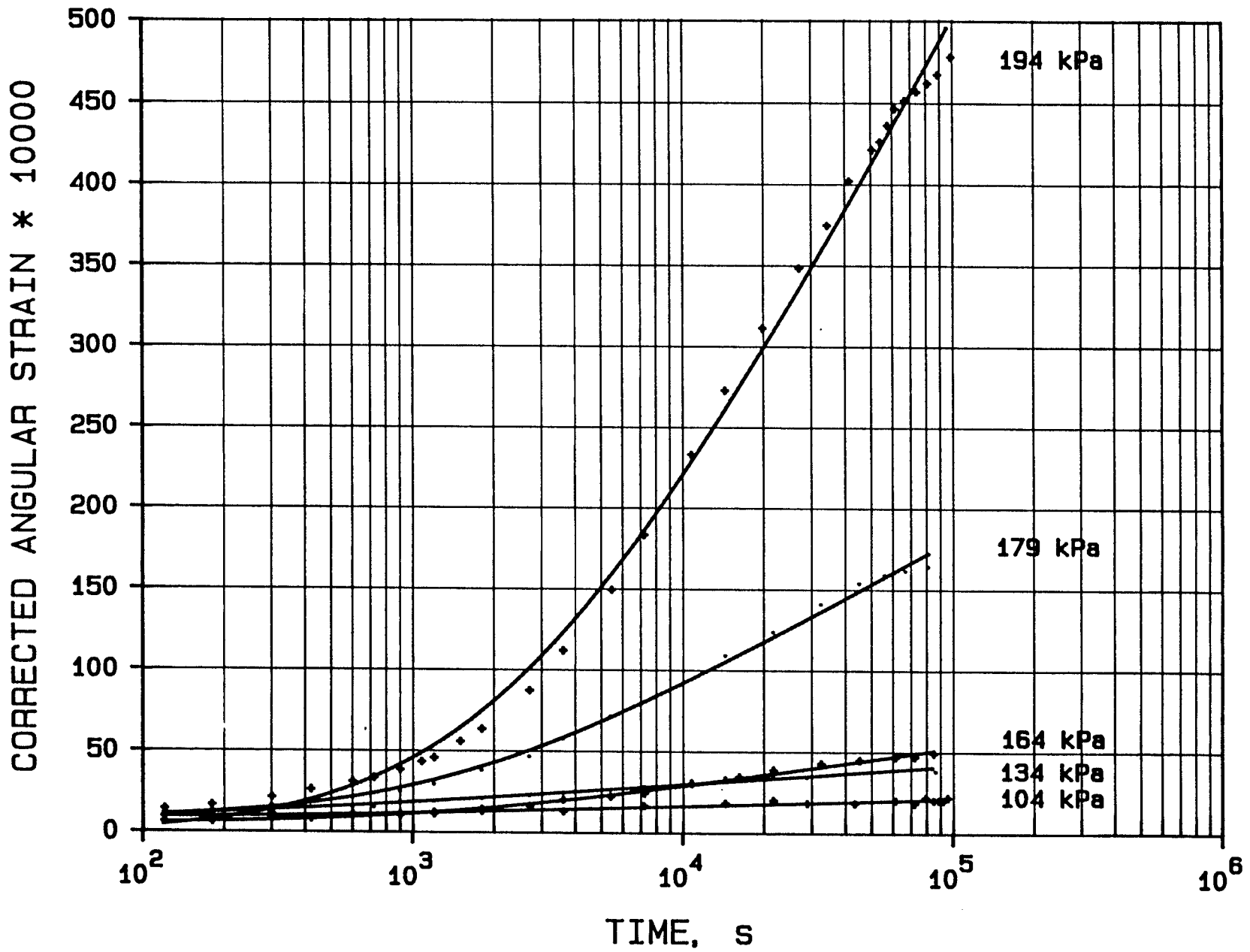


TEST C7

CORRECTED ANGULAR STRAIN * 10000

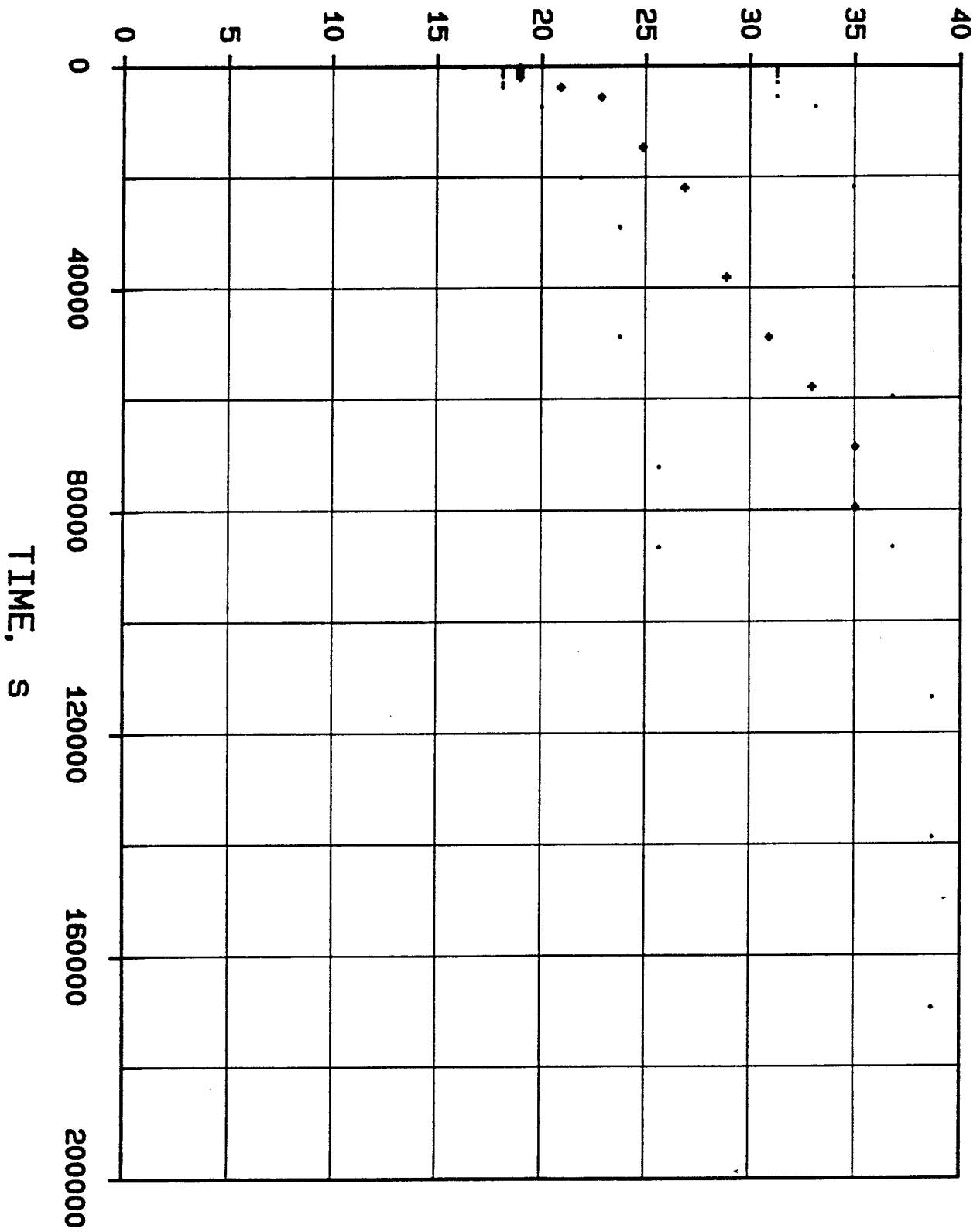


TEST C8



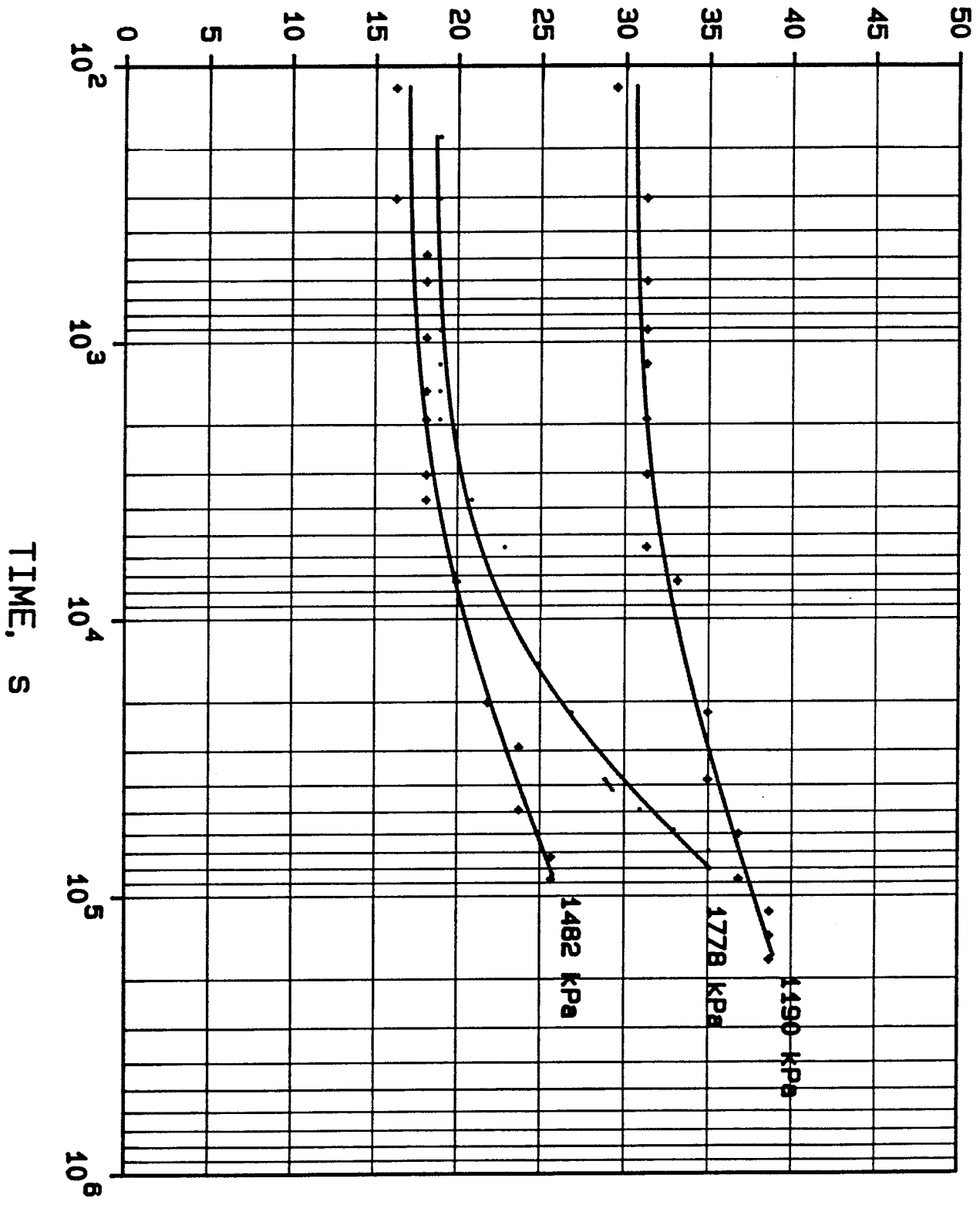
TEST C8

CORRECTED ANGULAR STRAIN * 10000



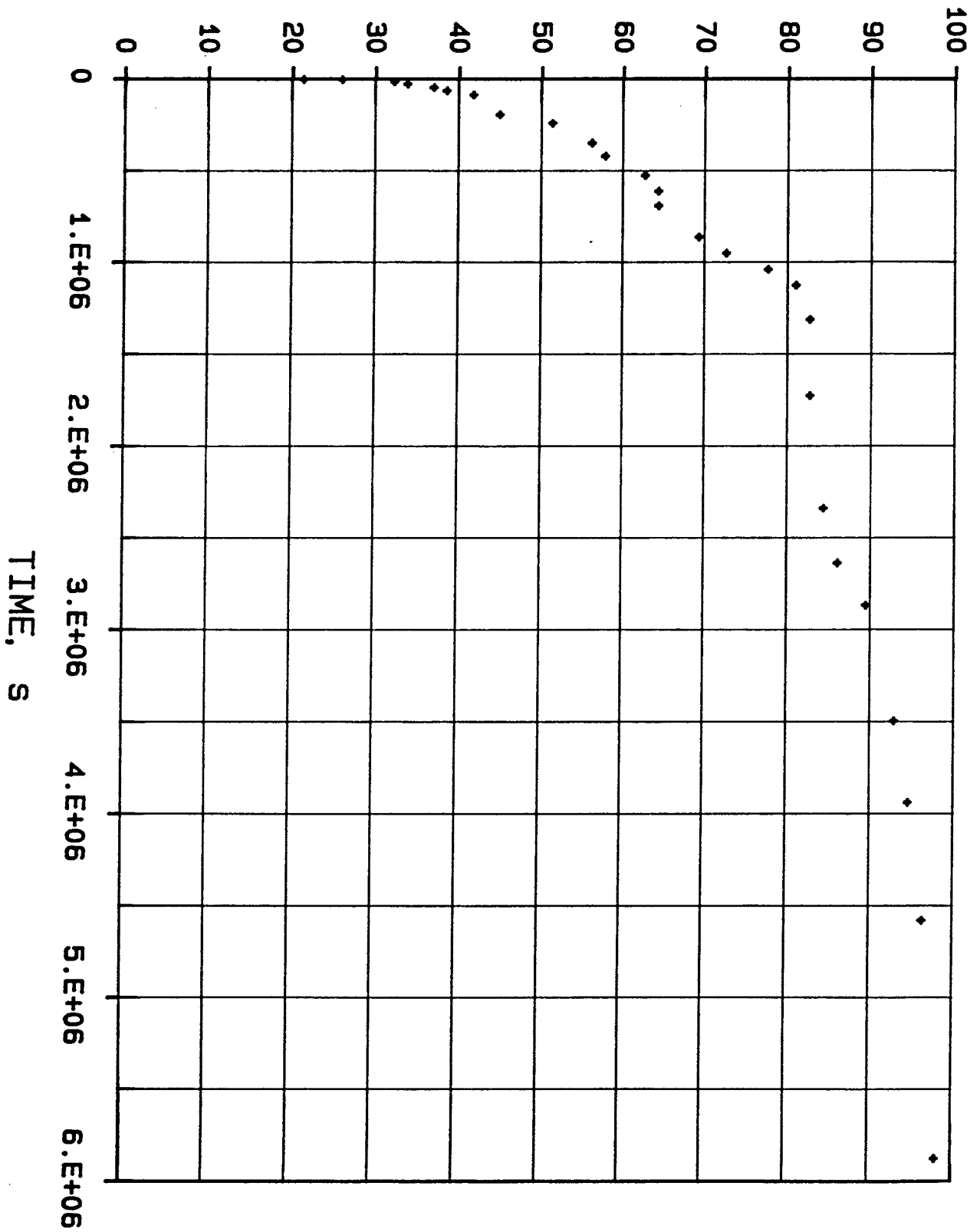
TEST C9

CORRECTED ANGULAR STRAIN * 10000



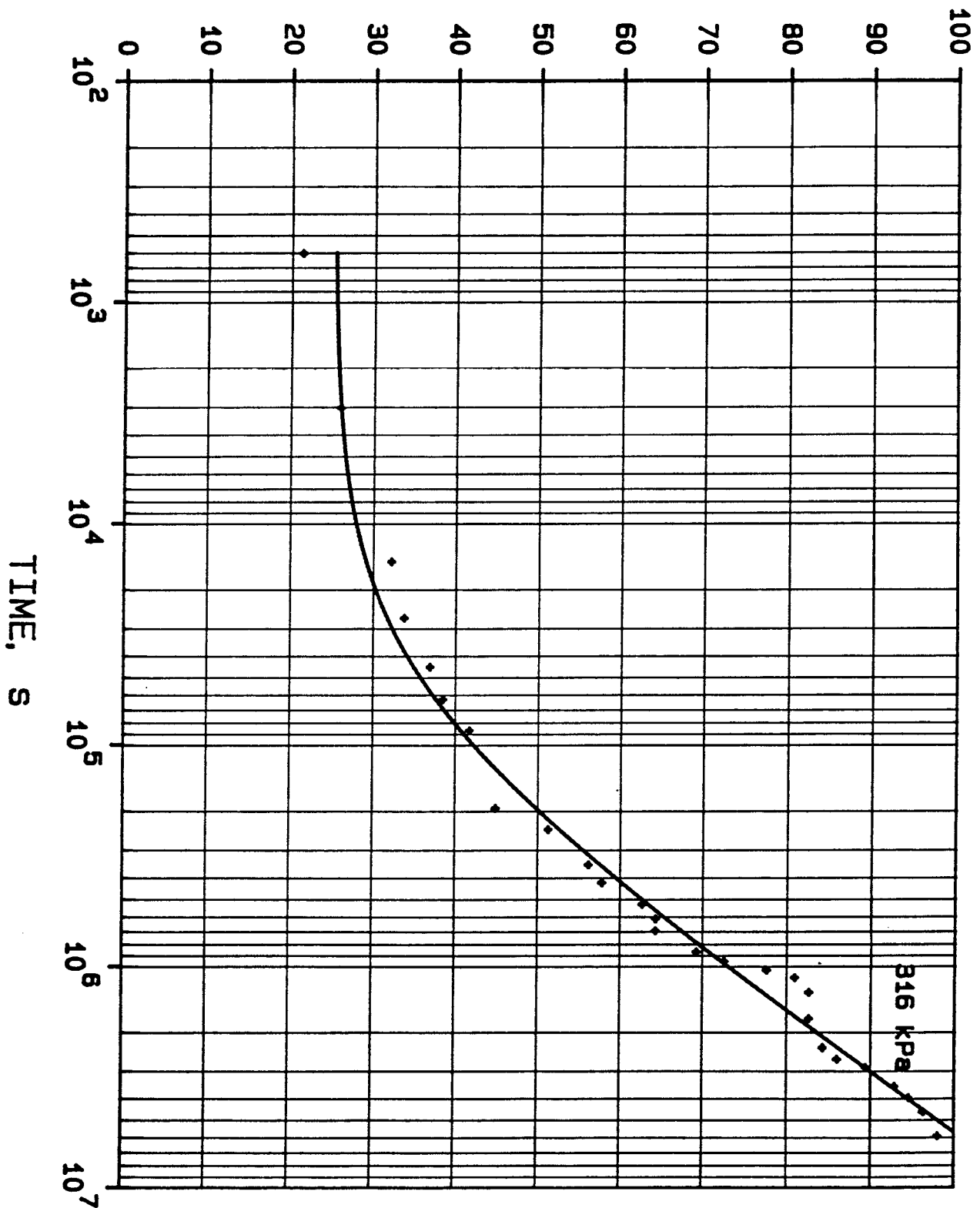
TEST C9

CORRECTED ANGULAR STRAIN * 10000

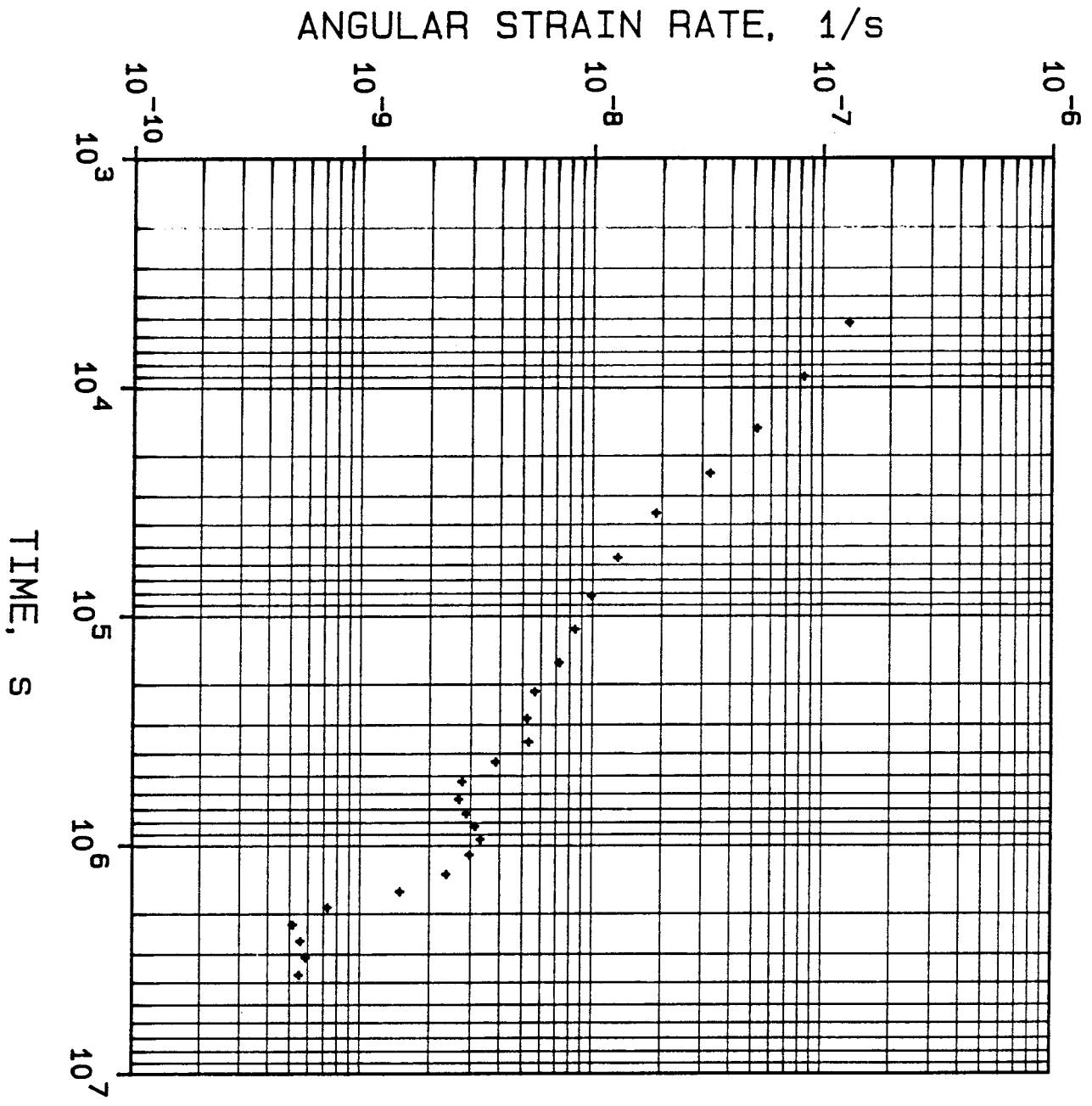


LONG TIME SHEAR BOX CREEP TEST C 10

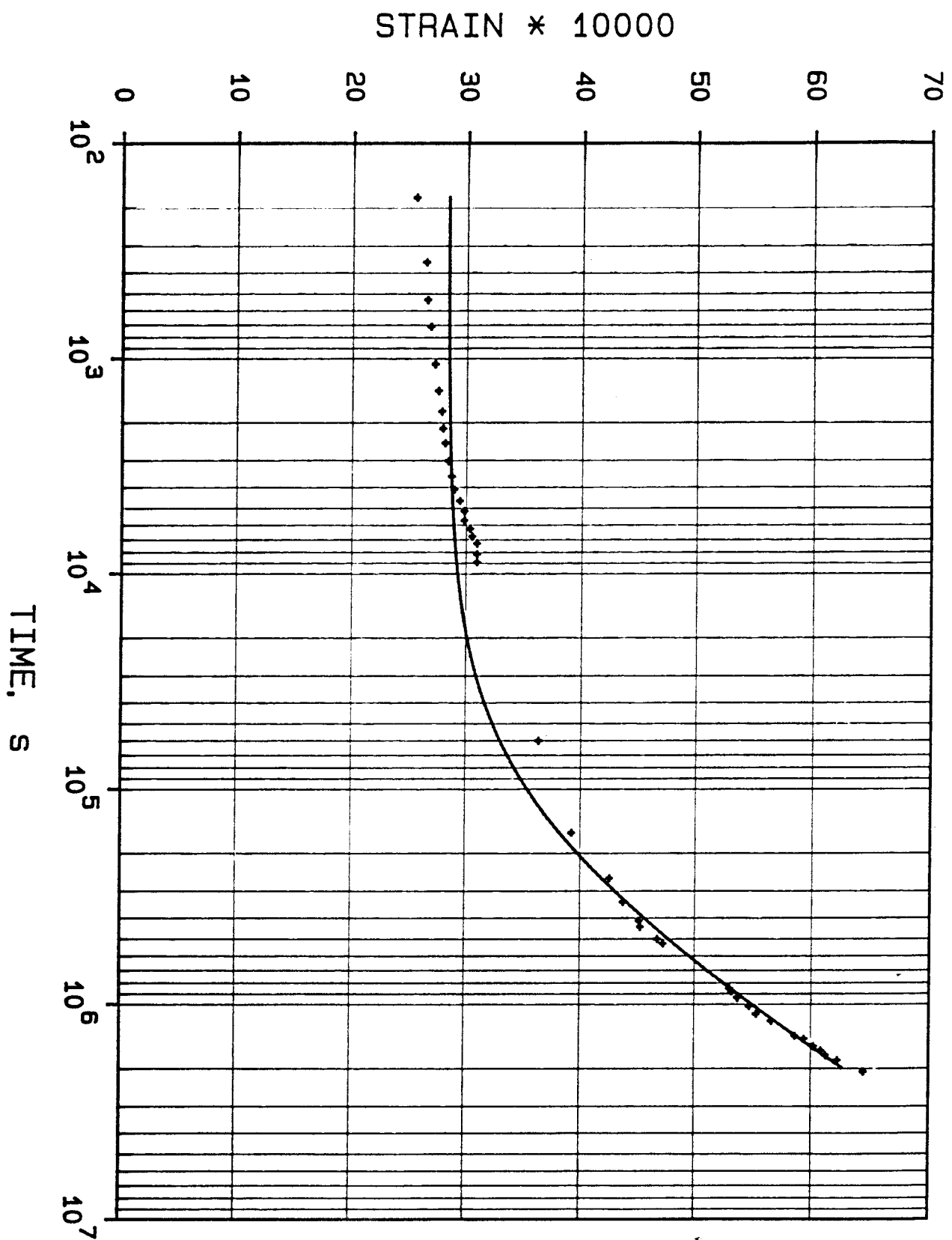
CORRECTED ANGULAR STRAIN * 10000



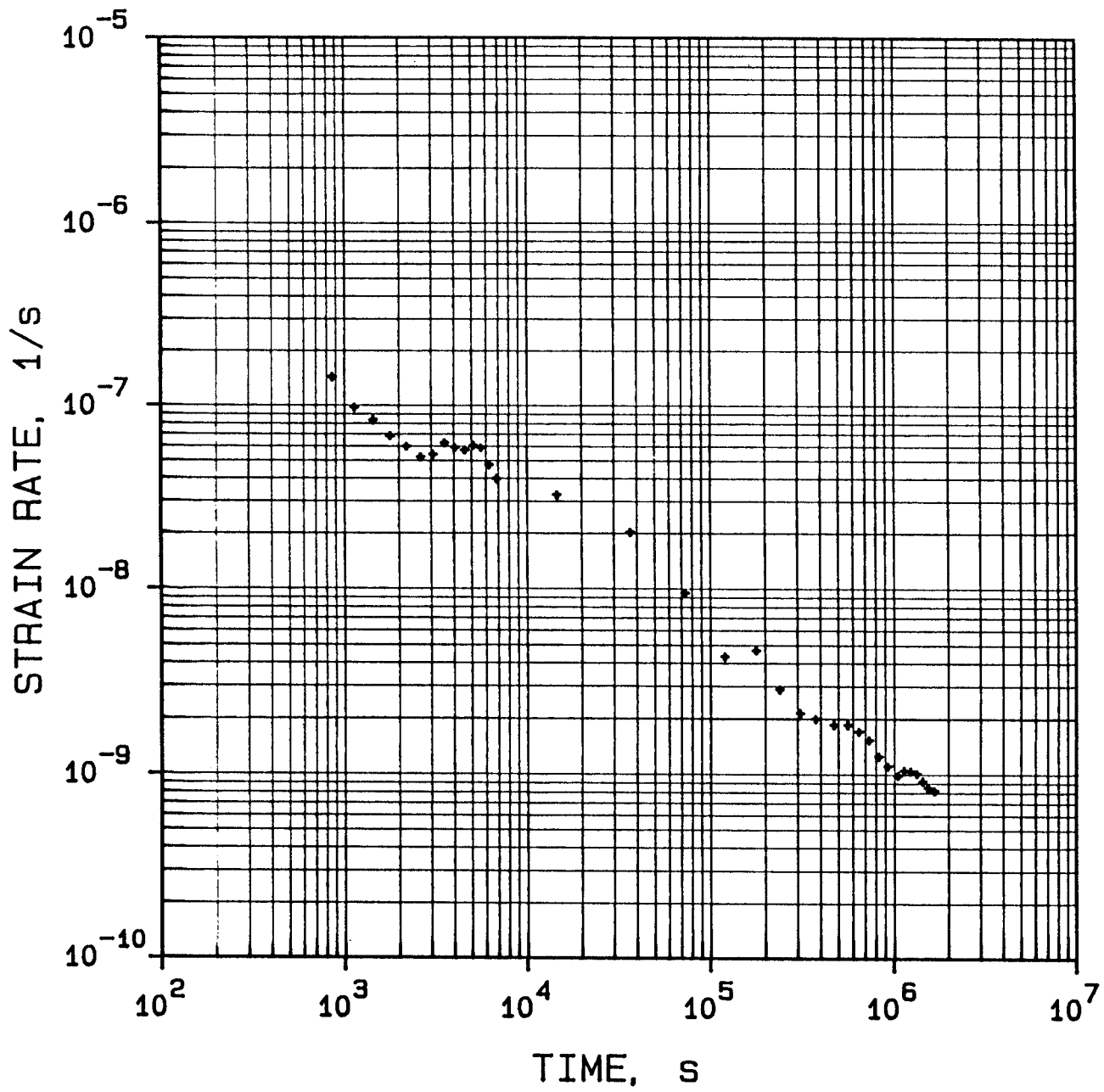
LONG TIME SHEAR BOX CREEP TEST C10



LONG TIME SHEAR BOX CREEP TEST C10



LONG TIME TRIAXIAL CREEP TEST



LONG TIME TRIAXIAL CREEP TEST

List of SKB reports

Annual Reports

1977-78

TR 121

KBS Technical Reports 1 – 120.

Summaries. Stockholm, May 1979.

1979

TR 79-28

The KBS Annual Report 1979.

KBS Technical Reports 79-01 – 79-27.

Summaries. Stockholm, March 1980.

1980

TR 80-26

The KBS Annual Report 1980.

KBS Technical Reports 80-01 – 80-25.

Summaries. Stockholm, March 1981.

1981

TR 81-17

The KBS Annual Report 1981.

KBS Technical Reports 81-01 – 81-16.

Summaries. Stockholm, April 1982.

1982

TR 82-28

The KBS Annual Report 1982.

KBS Technical Reports 82-01 – 82-27.

Summaries. Stockholm, July 1983.

1983

TR 83-77

The KBS Annual Report 1983.

KBS Technical Reports 83-01 – 83-76

Summaries. Stockholm, June 1984.

1984

TR 85-01

Annual Research and Development Report 1984

Including Summaries of Technical Reports Issued during 1984. (Technical Reports 84-01–84-19)
Stockholm June 1985.

1985

TR 85-20

Annual Research and Development Report 1985

Including Summaries of Technical Reports Issued during 1985. (Technical Reports 85-01-85-19)
Stockholm May 1986.

1986

TR86-31

SKB Annual Report 1986

Including Summaries of Technical Reports Issued during 1986
Stockholm, May 1987

Technical Reports

1987

TR 87-01

Radar measurements performed at the Klipperås study site

Seje Carlsten, Olle Olsson, Stefan Sehlstedt,
Leif Stenberg
Swedish Geological Co, Uppsala/Luleå
February 1987

TR 87-02

Fuel rod D07/B15 from Ringhals 2 PWR: Source material for corrosion/leach tests in groundwater Fuel rod/pellet characterization program part one

Roy Forsyth, Editor
Studsvik Energiteknik AB, Nyköping
March 1987

TR 87-03

Calculations on HYDROCOIN level 1 using the GWHRT flow model

**Case 1 Transient flow of water from a
borehole penetrating a confined
aquifer**

**Case 3 Saturated-unsaturated flow
through a layered sequence of
sedimentary rocks**

**Case 4 Transient thermal convection in a
saturated medium**

Roger Thunvik, Royal Institute of Technology,
Stockholm
March 1987

TR 87-04

Calculations on HYDROCOIN level 2, case 1 using the GWHRT flow model Thermal convection and conduction around a field heat transfer experiment

Roger Thunvik
Royal Institute of Technology, Stockholm
March 1987

TR 87-05

Applications of stochastic models to solute transport in fractured rocks

Lynn W Gelhar
Massachusetts Institute of Technology
January 1987

TR 87-06

Some properties of a channeling model of fracture flow

Y W Tsang, C F Tsang, I Neretnieks
Royal Institute of Technology, Stockholm
December 1986

TR 87-07

Deep groundwater chemistry

Peter Wikberg, Karin Axelsen, Folke Fredlund
Royal Institute of Technology, Stockholm
June 1987

TR 87-08

An approach for evaluating the general and localized corrosion of carbon steel containers for nuclear waste disposal

GP March, KJ Taylor, SM Sharland, PW Tasker
Harwell Laboratory, Oxfordshire
June 1987

TR 87-09

Piping and erosion phenomena in soft clay gels

Roland Pusch, Mikael Erlström,
Lennart Börgesson
Swedish Geological Co, Lund
May 1987

TR 87-10

Outline of models of water and gas flow through smectite clay buffers

Roland Pusch, Harald Hökmark,
Lennart Börgesson
Swedish Geological Co, Lund
June 1987

TR 87-11

Modelling of crustal rock mechanics for radioactive waste storage in Fennoscandia—Problem definition

Ove Stephansson
University of Luleå
May 1987

TR 87-12

Study of groundwater colloids and their ability to transport radionuclides

Kåre Tjus* and Peter Wikberg**
*Institute for Surface Chemistry, Stockholm
**Royal Institute of Technology, Inorganic Chemistry Stockholm
March 1987

TR 87-13

Shallow reflection seismic investigation of fracture zones in the Finnsjö area method evaluation

Trine Dahl-Jensen
Jonas Lindgren
University of Uppsala, Department of Geophysics
June 1987

TR 87-14

Combined interpretation of geophysical, geological, hydrological and radar investigations in the boreholes ST1 and ST2 at the Saltsjö tunnel

Jan-Erik Andersson
Per Andersson
Seje Carlsten
Lars Falk
Olle Olsson
Allan Strähle
Swedish Geological Co, Uppsala
1987-06-30

TR 87-15

Geochemical interpretation of groundwaters from Finnsjön, Sweden

Ignasi Puigdomènech¹
Kirk Nordstrom²
¹Royal Institute of Technology, Stockholm
²U S Geological Survey, Menlo Park, California
August 23, 1987

TR 87-16

Corrosion tests on spent PWR fuel in synthetic groundwater

R S Forsyth¹ and L O Werme²
¹Studsvik Energiteknik AB, Nyköping, Sweden
²The Swedish Nuclear Fuel and Waste Management Co (SKB), Stockholm, Sweden
Stockholm, September 1987

TR 87-17

The July – September 1986 Skövde aftershock sequence

Conny Holmqvist
Rutger Wahlström
Seismological Department, Uppsala University
August 1987

TR 87-18

Calculation of gas migration in fractured rock

Roger Thunvik¹ and Carol Braester²
¹Royal Institute of Technology
Stockholm, Sweden
²Israel Institute of Technology
Haifa, Israel
September 1987

TR 87-19

Calculation of gas migration in fractured rock – a continuum approach

Carol Braester¹ and Roger Thunvik²

¹Israel Institute of Technology

Haifa, Israel

²Royal Institute of Technology

Stockholm, Sweden

September 1987

TR 87-20

Stability fields of smectites and illites as a function of temperature and chemical composition

Y Tardy, J Duplay and B Fritz

Centre de Sédimentologie et de Géochimie de la

Surface (CNRS)

Institut de Géologie Université Louis Pasteur (ULP)

1 rue Blessig, F-67084 Strasbourg, France

April 1987

TR 87-21

Hydrochemical investigations in crystalline bedrock in relation to existing hydraulic conditions: Klipperås test-site, Småland, Southern Sweden

John Smellie¹

Nils-Åke Larsson¹

Peter Wikberg³

Ignasi Puigdomènech⁴

Eva-Lena Tullborg²

¹Swedish Geological Company, Uppsala

²Swedish Geological Company, Göteborg

³Royal Institute of Technology, Stockholm

⁴Studsvik Energiteknik AB, Nyköping

September 1987

TR 87-22

Radionuclide sorption on granitic drill core material

Trygve E Eriksen and Birgitta Locklund

The Royal Institute of Technology

Department of Nuclear Chemistry

Stockholm

November 1987

TR 87-23

Radionuclide co-precipitation

Jordi Bruno and Amaia Sandino

The Royal Institute of Technology

Department of Inorganic Chemistry

Stockholm

December 1987

TR 87-24

Geological maps and cross-sections of Southern Sweden

Karl-Axel Kornfält¹ and Kent Larsson²

¹SGU, Lund

²Softrock Consulting, Genarp

December 1987

TR 87-25

**The Bolmen tunnel project
Evaluation of geophysical site investigation methods**

Roy Stanfors

December 1987

TR 87-26

**The Kymmen power station
TBM tunnel
Hydrogeological mapping and analysis**

Kai Palmqvist¹ and Roy Stanfors²

¹BERGAB-Berggeologiska Undersökningar AB

²Lunds University

December 1987

TR 87-27

Earthquake measurements in southern Sweden

Oct 1, 1986 – Mar 31, 1987

Ragnar Slunga

Leif Nordgren

National Defence Research Establishment

Department 2,

Stockholm

December 1987

TR 87-28

Radionuclide deposition and migration within the Gideå and Finnsjö study sites, Sweden

A study of the fallout after the Chernobyl accident

Erik Gustafsson¹, Mats Skålberg², Björn Sundblad³,

Olle Karlberg³, Eva-Lena Tullborg⁴, Thomas Ittner²,

Paul Carbol², Niklas Eriksson², Svante Lampe³

¹Swedish Geological Company, Uppsala

²Chalmers University of Technology, Göteborg

³Studsvik Energiteknik AB, Nyköping

⁴Swedish Geological Company, Göteborg

December 1987

TR 87-29

Alteration of isolating properties of dense smectite clay in repository environments as exemplified by seven pre-quaternary clays

Roland Pusch, Lennart Börgesson, Mikael Erlström

Swedish Geological Co, Lund

December 1987

TR 87-30

Water compositions in the Lake Sibbofjärden – Lake Trobbofjärden area

Karin Andersson

Studsvik Energiteknik AB, Studsvik

August 1987